The Role of Acetyl-CoA and Acetyl-CoA Synthesis Pathways in Regulation of Nuclear Acetylation

By

Anastasia Jayne Lindahl

A dissertation submitted in partial fulfillment of the requirements for the degree of

Doctor of Philosophy

(Biochemistry)

UNIVERSITY OF WISCONSIN - MADISON

2019

Date of final oral examination: 8/12/19

The dissertation is to be reviewed by the following members of the Final Oral Committee:

John M. Denu, Professor, Department of Biomolecular Chemistry
James L. Keck, Professor, Department of Biomolecular Chemistry
Melissa M. Harrison, Associate Professor, Department of Biomolecular Chemistry
Rupa Sridharan, Associate Professor, Department of Cell and Regenerative Biology

The Role of Acetyl-CoA and Acetyl-CoA synthesis pathways in regulation of nuclear acetylation

Anastasia Jayne Lindahl

Under the supervision of Professor John M. Denu

At the University of Wisconsin - Madison

Post-translational modifications of proteins control many complex biological processes, including genome expression, chromatin dynamics, metabolism, and cell division through a language of chemical modifications. Chromatin modifying enzymes have been shown to utilize a variety of metabolites as co-substrates to catalyze their respective chromatin modifications, closely linking chromatin modifications and metabolism. Improvements in mass spectrometry-based proteomics have enabled deep interrogation of these modifications inside the cell and demonstrated posttranslational modifications are wide-spread and dynamic modifications in the cell, however, many questions remain on the regulation and downstream effects. One such metabolism-linked modification of high interest is lysine acetylation. Protein acetyltransferases connect to a cell's metabolism by using a central carbon source, acetyl-CoA, as the co-substrate donor of the acetyl group. Acetyl-CoA generation within the cell is compartmentalized and synthesized through a variety of pathways since it serves as a central metabolite. Studies have found histone acetylation to be dynamically regulated by nuclear and cytoplasmic acetyl-CoA metabolism, however, the mechanism of metabolic influence on histone acetylation has been under active investigation and debate.

I developed a mass spectrometry method to quantitatively assess subcellular lysine acetylation stoichiometry as a tool to address these open questions. Using this method, I assessed chromatin acetylation stoichiometry and histone acetylation stoichiometry to examine the effects of nuclear and cytoplasmic acyl-CoA short chain synthetase family member 2 (ACSS2) on nuclear protein acetylation. We hypothesized ACSS2 plays a specific role in nuclear signaling, partially through acetylation of proteins like histones and transcription factors. To this end, I have demonstrated ACSS2 regulates protein acetylation and transcript levels of RNA processing pathways in the brain during fasting. In response to dietary stress in the liver, ACSS2 regulates transcription of metabolic pathways and acetylation of mitochondrial proteins, rather than affecting acetylation within the nucleus likely due to systemic ACSS2-dependent alterations in metabolism previously shown. These observations are the first to indicate ACSS2 has subcellular compartment and tissue-specific metabolic and signaling functions, especially through modulating nuclear protein acetylation to regulate fatty acid metabolism.

Chapter 1 introduces protein posttranslational modifications including lysine acetylation, mass spectrometry analysis of lysine acetylation, and the connections between chromatin posttranslational modifications and metabolism. Chapter 2 presents the method of site-specific subcellular compartment lysine acetylation stoichiometry analysis using data-independent acquisition (DIA) mass spectrometry. Chapter 3 assesses the role of ACSS2 on nuclear protein acetylation and connections between nuclear protein acetylation and metabolism. Conclusions, ongoing work on the regulation of nuclear protein acetylation by ACSS2 and ATP-citrate lyase (ACLY)—the two main contributing pathways to cytoplasmic and nuclear acetyl-CoA, and future directions are presented in Chapter 4.

Acknowledgments

I am extremely thankful to many people for their support throughout my Ph.D., for I would not be here without their support. I would like to thank my advisor Dr. John Denu, for his infectious passion for science and his guidance throughout my graduate career. The ability to explore my project in whatever direction it took me and incorporate my scientific interests with his full support has made this scientific journey a truly enjoyable endeavor. I am very thankful for his support, guidance, and mentorship, as well as the independence he gave me while lending his support to succeed and to fail, which have made me a better critical thinker and scientist. I am also thankful for our in-depth conversations about work and life and people, graduate school has taught me a lot about many things, including myself and what type of person I want to be in my life and in my work and John has been a great support and has challenged me to reach for more and step out of my comfort zone.

I also want to thank my thesis committee: Dr. James Keck, Dr. Rupa Sridharan and Dr. Melissa Harrison for their advice, guidance, insight throughout my graduate training and for asking the tough questions that have challenged me to be a better scientist. I am also thankful for the collaborative projects I have been a part of with John Moffett and Ma Namboodiri (Uniformed Services University of the Health Science) and Kathryn Wellen (UPenn). Interacting with a broader scientific community has truly enriched my research.

I would like to thank the current and former members of the Denu Lab: Kristin Dittenhafer-Reed, Wei Yu, Jess Feldman, Jin Lee, Michael Smallegan, Josue Baeza, Jing Fan, Kim Krautkramer, Zhangli Su, Beatriz Camacho, Melissa Boersma, Rush Dhillon, James Dowell, Eric Armstrong, Ann Denu, Mark Klein, Wallace Lui, Amy Qin, Spencer Haws, Alexis Lawton, Sydney Thomas, Lily Miller, Laura Borth, Logan Wright, Robert Miner, and Slava

Kuznietsov for being wonderful labmates and friends. It has always been a pleasure to come into lab and do great science and have great conversations. There are several people I especially would like to thank. Ann is a central cog to the Denu lab, her advice, listening ear, and bright disposition always brings joy into lab and make it a supportive environment. I would like to thank Zhangli, Melissa, James, and Josh for the training they provided early in my graduate career and the great discussions we have had throughout my time in graduate school. I am also thankful to Alexis Lawton, Laura Borth, Sydney Thomas, Lily Miller, Amy Qin, and Emma Goguen for their wonderful friendship inside and outside of the lab, our dinners out, musicals, and ladies nights have always been a source of great friendship and joy to me.

I am thankful for the many friendships I have developed during my time in Madison, including those at Christ Presbyterian Church. The 2030's group and youth group have truly given me a sense of home here in Madison that I would be lost without. I would like to especially thank the youth at CPC - Autumn, Ben, Rowan, Josie, Alyssa, Sam, Braedon, Carolyn, Ellie, Kendra, Nate, Chris, Allison, JP, Dane, Levity, Jose, Manolo, Nana, Janat, Neena, Nadiya, Trinity, and the youth leader Abe who have been a bright spot in my week every Wednesday and Sunday for the last 5 years. I also would like to especially thank my yearmates in IPiB, Megan Dowdle, Stephanie Maciuba, Haley Brown, Alex Justen, Karl Wetterhorn, Markus Nevil, and Tyler Stanage who I know will be life-long friends. I am also thankful to Katie, Nicole, Alexis, and Kaivalya who helped me co-found the Brilliant and Diverse Graduate Research Scholars (BADGRS) a graduate student and postdoc peer mentoring support network - our work together has been a great joy to me.

I am extremely grateful to my family for their love and support throughout my life and graduate career. I would like to thank my parents, Anne and Roger, for their unconditional love

and support, and instilling in me both curiosity and determination. I would also like to thank my siblings Betsy and Alex who have been my life-long best friends and a steady rock of support. I am also thankful for those my family has added along the way, my brother-in-law Brett, and my niece and nephew Lillian and Conrad, for the support and joy they have brought me. Over the course of my graduate career I have learned how to be a good scientist, Auntie, and godmother.

I am also very thankful for the opportunity to attend the University of Wisconsin - Madison for my Ph.D. Learning in this place, about its history and vision, have instilled in me a passion for research and the community, the role of a public university in public life, and the tenants of the Wisconsin Idea.

TABLE OF CONTENTS

List of Figures

CHAPTER 1: AN INTRODUCTION TO PROTEIN POSTTRANSLATIONAL MODIFICATIONS, MASS SPECTROMETRY ANALYSIS OF LYSINE ACETYLATION, CHROMATIN MODIFICATIONS, AND METABOLISM

This chapter is presented in three parts. The first part will introduce posttranslational lysine acetylation. The second will discuss Mass Spectrometry techniques enabling the in-depth study of lysine acetylation in physiologically relevant systems. The third part will discuss the relationship between metabolism and posttranslational modifications, focusing on metabolite co-substrates and the role these molecules play in the nucleus.

1.1 Posttranslational Lysine Acetylation

1.1.1 Posttranslational Modifications

The human proteome is expanded far in complexity beyond the human genome ***(1)***. This complexity arises from forms of transcriptional regulation; alternative splicing, recombination, differential transcript initiation and termination and recently identified chemical modifications ***(2)***. Additionally posttranslational modifications of proteins arising from these different RNAs exponentially expand the complexity of the human proteome. Modifications to protein sequence through single nucleotide polymorphisms (SNPs), translation errors, and protein cleavage add diversity to the proteome. Additional posttranslational modifications, such as the covalent modification of amino acids such as phosphorylation of serine, threonine, and tyrosine and methylation of arginine and lysine, and acetylation of lysine dynamically expand the complexity even further. Estimation of the number of variants of proteins which exist in cells has been debated to be between ~20,000 and millions when looking at proteoforms, defined as a unique combinatorial state of posttranslational modifications (Figure 1-1) ***(3, 4)***. These posttranslational modifications regulate protein function through alterations in enzyme activity, protein localization, stability, degradation, protein-protein interactions, and protein-DNA interactions. The ability of posttranslational modifications to expand the diversity of functional units and dynamically regulate protein function makes it highly important to identify, localize, and characterize their effects to understand the functional significance of posttranslational modifications.

1.1.2 Lysine Acetylation

Posttranslational acetylation of the ε-amino group of the amino acid lysine is a reversible posttranslational modification. Protein acetyltransferases catalyze the addition of an acetyl group

and protein deacetylases catalyze its removal (Figure 1-2). In favorable chemical conditions, non-enzymatic addition of acetylation may occur ***(5–8)***.

Acetylation was first identified and characterized on histones using radiolabeled acetate to demonstrate the incorporation of an acetyl group onto histones and its effect on protein-DNA interactions by altering the melting temperature of chromatinized DNA ***(9–11)***. An ever-growing list of posttranslational modifications has been shown to modify histone proteins and regulate gene expression and genome architecture and stability ***(12–14)***.

The first characterization of enzymatic activity affected by lysine acetylation was on the acetyl-CoA synthetases ACSS1 and ACSS2 ***(15)***. Acetylation occurs on a conserved lysine within the enzyme active site serving as a catalytic base. Acetylation of this lysine inhibits catalysis, and removal of the acetylation restores enzymatic activity ***(15)***. Identification and functional characterization of lysine acetylation was a painstaking process, with only 90 acetylated proteins identified until the introduction of mass spectrometry-based proteomics as a tool was adopted by the field to study lysine acetylation ***(16)***. The first acetyl-proteomics study utilized an antibody enrichment strategy to profile lysine acetylation across the proteome and identified 388 sites ***(16)***. Since this study, many more lysine acetylation sites have been identified using proteomics altering the challenge from identification to functional characterization of the thousands of lysine acetylation sites identified ***(17–29)***.

Figure 1-1. The increasing diversity from a gene to its proteoforms.

Depicted is a single human gene and 1) translation to three mRNA isoforms via alternative splicing of RNA or the use of different promoters or translational start sites. These mRNAs are then 2) translated into proteins and can be modified through single nucleotide polymorphisms (SNPs), translation errors, and protein cleavage. These diverse proteins are further modified through 3) Site-specific posttranslational modifications to the protein products to generate diverse proteoforms (at right) the three examples of site-specific changes shown include phosphorylation (P), acetylation (Ac) and methylation (Me), respectively.

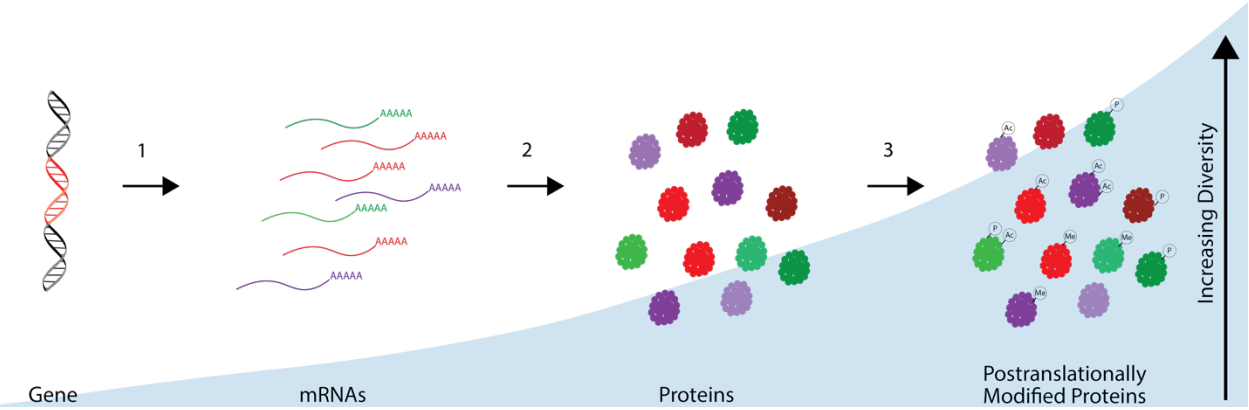

Figure 1-2. Reversible protein acetylation.

Proteins are acetylated on lysine residues by acetyltransferases using acetyl-CoA as the acetyl-donor. Acetylation is removed by histone deacetylases (HDACs) or Sirtuin NAD+-dependent deacetylases.

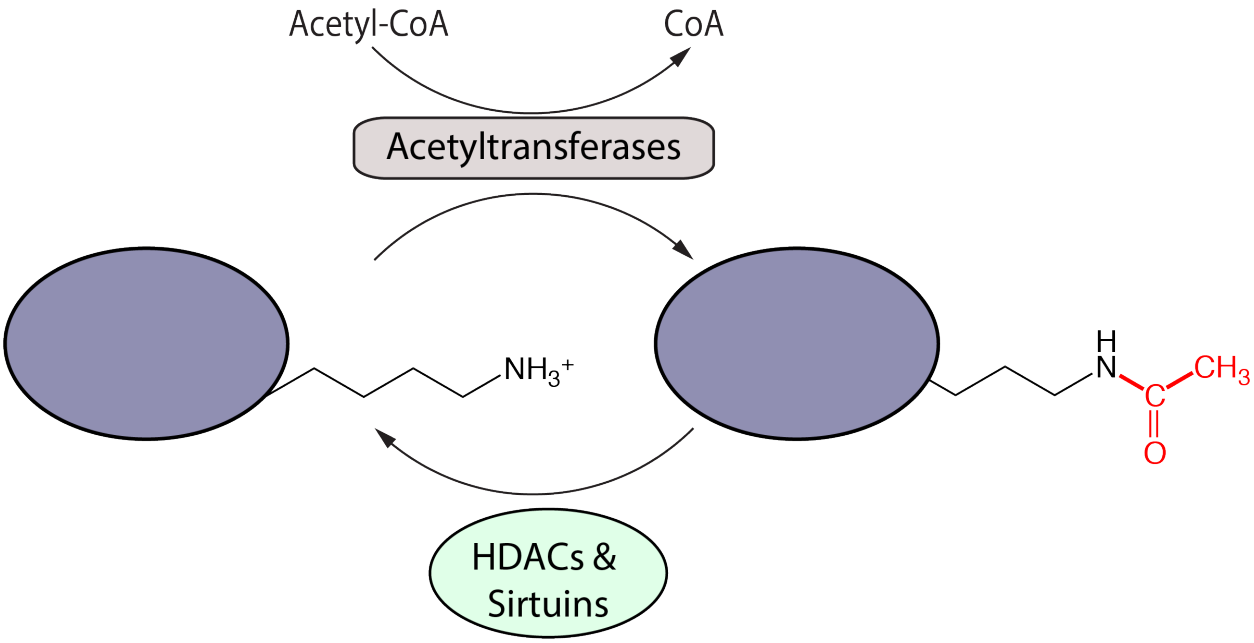

1.2 Lysine Acetylation and Mass Spectrometry

1.2.1 Acetyl-enrichment based proteomics

High mass accuracy mass spectrometry technology enabled significant advancements in proteomics. In conjunction, advancements in fragmentation techniques enabled large scale identification of posttranslational modifications and accurate localization of the modification across a proteome ***(1, 30–32)***.

Pan anti-acetyl antibody enrichment of acetylated peptides from a whole proteome led to the broad identification of lysine acetylation sites (Figure 1-4). Early studies identified 388 sites, and wider adoption of the acetyl-enrichment strategy led to an exponential identification of acetylation sites across the proteome (Figure 1-4) ***(16)***. These studies expanded our understanding of the widespread nature of lysine acetylation, rivaling phosphorylation in scope ***(33)***. These early studies identified acetylation in the mitochondria as a widespread modification with possible regulatory effects. Other studies across model organisms and systems from *E. coli*, yeast, and *C. elegans* to human tissue culture and mouse tissues demonstrated the evolutionary conserved nature of acetylation ***(34–37)***. In mice, over 30% of known mitochondrial proteins have been found to be acetylated and most of the proteins are clustered in pathways of mitochondrial metabolism such as fatty acid oxidation, oxidative phosphorylation, and the TCA cycle ***(38–40)***. The focus on mitochondrial metabolism and acetylation has left many gaps in our knowledge of the regulation and function of acetylation in other subcellular compartments.

Acetyl-enrichment strategies have enabled widespread identification of lysine acetylation and led to questions about its regulatory function. However, acetyl-enrichment has drawbacks to understanding the function of acetylation. Acetyl-enrichment removes non acetylated peptides from a sample, removing the protein quantity information regarding the rest of the proteome.

Enrichment has drawbacks for two reasons, the first -- quantification of acetylation shows relative fold change rather than stoichiometric occupancy, and second -- lowering the sequence coverage reduces the ability to quantify proteome changes in the same sample. In the context of dynamic acetylation site occupancy, both of these pieces of information are important to understanding the dynamics of acetylation. Relative quantification limits dynamic measurements to reporting fold change of acetylation between samples and limits the ability to interpret the functional significance. Acetylation stoichiometry changes from 1% to 5% would be observed as a 5-fold difference and equally prioritized for biochemical functional characterization with acetylation stoichiometry change of 10 % to 50 % which is also a 5-fold difference (Figure 1-6). Using stoichiometry quantification provides a different conclusion of which of the two sites has functional significance. In addition, relative quantification using acetyl-enrichment creates challenges deconvoluting changes in acetylation due to alteration in acetylation occupancy or protein abundance. These challenges to functionally characterizing changes in acetylation using acetyl-enrichment based proteomics has been partially addressed by combining the approach with Stable Isotope Labeling of Amino acids in Cell culture (SILAC) ***(41, 42)***. SILAC addresses these gaps, however, the introduction of metabolically labeled amino acids limits the systems in which this technique can be applied.

1.2.2 Stoichiometric Quantification of Lysine Acetylation

1.2.2.1 Data-Dependent Acquisition Mass Spectrometry Approaches

Stoichiometry based lysine acetylation quantification negotiates many of the challenges identified above. Chemical labeling with isotopically labeled acetic anhydride in a chemical derivatization method creates peptides of identical sequence for stoichiometric quantification by determining the ratio of light (endogenous) acetylation to the total of heavy (exogenous label)

and light (endogenous) acetylation (Figure 1-6) ***(43–45)***. Shotgun proteomics, a bottom-up data-dependent approach, is then employed to measure the amount of light and heavy acetylated peptides. In data-dependent acquisition (DDA) mass spectrometry, an initial survey scan of precursor masses (MS1 scan) is taken to determine the m/z of the peptides in the mixture and the top number of precursor ions are selected for fragmentation and a second scan (MS2 scan) (Figure 1-7). Fragment level information necessary for peptide identification is taken stochastically in a data-dependent manner. Approaches to improve depth of sequence coverage include dynamic exclusion during precursor selection which excludes precursor ions recently fragmented within a time window to avoid repetitive selection of highly abundant precursor ions. Increases in the speed of mass detector cycling times, prefiltering of masses, longer chromatography gradients, and offline prefractionation of samples have also been employed to increase the depth of coverage ***(46)***. Even so, DDA approaches are inherently stochastic and result in missing values across samples ***(47)***. This leads to challenges when using proteomics to probe biological questions across a large range of samples, conditions, or time points since a peptide or protein may be detected only in a subset of the samples of interest. In the case of acetylation stoichiometry, this poses an obstacle to consistently measuring both labels of a peptide since each heavy and light precursor must be selected for fragmentation independently. This hurdle can be overcome by selecting MS1 peaks for quantification based upon the mass shift pattern matching the isotopic label if both peptides are not fragmented and identified. However, the overlap of the MS1 precursor ion peaks results in interference, overestimation of the light precursor ion, and overestimation of acetylation stoichiometry ***(42)***.

1.2.2.2 Data-Independent Mass Spectrometry Approaches

Utilizing data-independent acquisition (DIA) based quantification overcomes the challenges of DDA based acetylation stoichiometry for more accurate determination of stoichiometry with fewer missing values ***(48, 49)***. DIA, also called SWATH (Sequential Window Acquisition of all Theoretical Mass Spectra), differs from DDA in that the initial MS1 survey scan of precursor ions is followed by sequential fragmentation and MS2 scans of all precursors within m/z ranges called windows ***(50–52)***. Therefore, MS2 fragment level data is collected for all peptides present within the MS1 survey scan (Figure 1-7). The challenge with DIA lies in the deconvolution of the MS2 fragment level data. DIA data is computationally deconvoluted into peptides using a spectral library, a reference library of MS1 precursor scans and their unique MS2 fragment data, to match MS1 precursor ions in a survey scan and assigning the MS2 fragments to a peptide-based on the spectral library. Using DIA to measure acetylation stoichiometry helps capture the MS2 fragment data for both labels of a given peptide ***(45, 53)***. Using MS2 based quantification also reduces interference between the heavy and light labels ensuring more accurate quantification. Spectral library sequence coverage is one of the factors limiting possible coverage within a DIA experiment. Therefore, good depth of sequence coverage in the spectral library is essential. Offline prefractionation reduces sample complexity allowing for a higher proportion of selection and fragmentation of precursors present in each MS1 scan.

Quantification of lysine acetylation using DIA also requires good coverage and is limited by cycling time of the mass detector for the survey scan and the sequential window MS2 fragment scans ***(45)***. Early studies employing DIA used offline prefractionation to accomplish greater coverage, however, technical variance introduced significantly reduces the precision of

the technique. In addition, in the case of isotopically labeled peptides for acetylation stoichiometry, deuterated peptides experience a chromatographic shift, resulting in heavy and light peptides in different fractions and injections ***(54, 55)***. One strategy to increase coverage without offline prefractionation is to reduce mass detector cycling time by utilizing a quadrupole mass detector to continuously conduct MS1 survey scans independently of the precursor window MS2 fragment scans ***(56)***. This division of labor greatly improves the depth of coverage and is compatible with high flow chromatographic techniques without a reduction in coverage. However, the ability of this technique to resolve posttranslational modifications and isotopic labeling is unknown. Therefore, a method to deeply interrogate protein acetylation without offline prefractionation before quantification is needed.

Figure 1-3 Workflow for Proteomics Analysis of Lysine-Acetylated Proteins using acetyllysine enrichment.

Proteins are denatured and digested with trypsin. The resulting peptides are subjected to immunoaffinity purification using a pan anti-acetyllysine antibody. The isolated peptides are analyzed by HPLC/MS/MS for peptide identification and relative quantification.

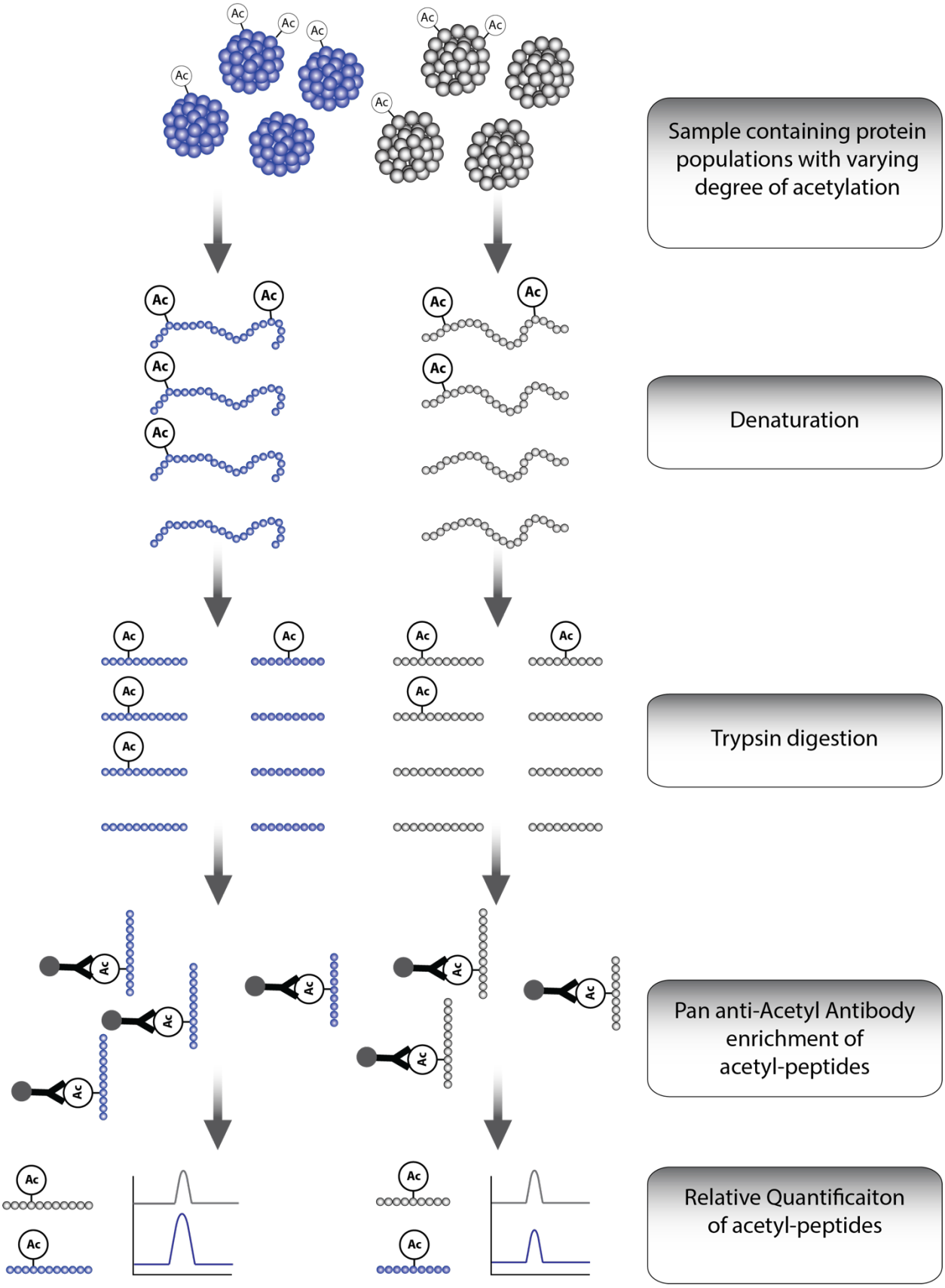
Sample containing protein populations with varying degree of acetylation
Denaturation
Trypsin digestion
Pan anti-Acetyl Antibody enrichment of acetyl-peptides
Relative Quantificaiton of acetyl-peptides

Figure 1-4. Timeline of Detected Acetylated Peptides per Publication.

The number of acetylated peptides reported per acetyl-proteome study, grouped by year. 'Identification' studies reported a list of peptides, 'quantification' studies reported change in relative abundance in an acetyl-peptide between two experimental conditions, and 'stoichiometry' studies reported ratios of acetyl-peptide to the amount of acetyl-peptide plus the unmodified corresponding peptide. Adapted from Josue Baeza ***(57)***

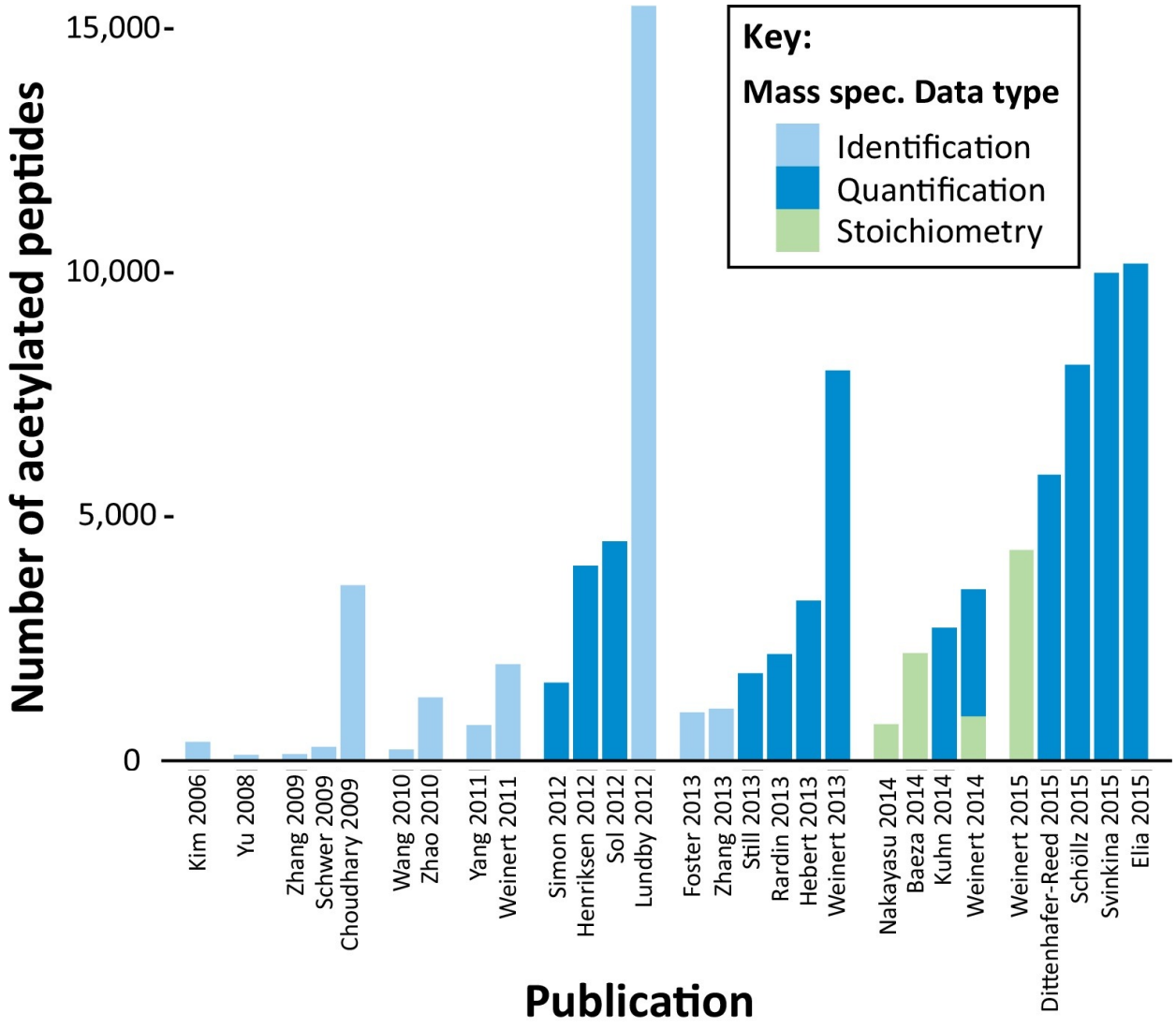

Figure 1-5. Relative quantification versus stoichiometry.

Relative quantification shows a 5-fold increase for both measure groups below between Condition A and Condition B. Stoichiometric quantification shows that the two groups measured are different, with the first changing from 1 % to 5% and the second from 10% to 50%. Adapted from Josue Baeza.

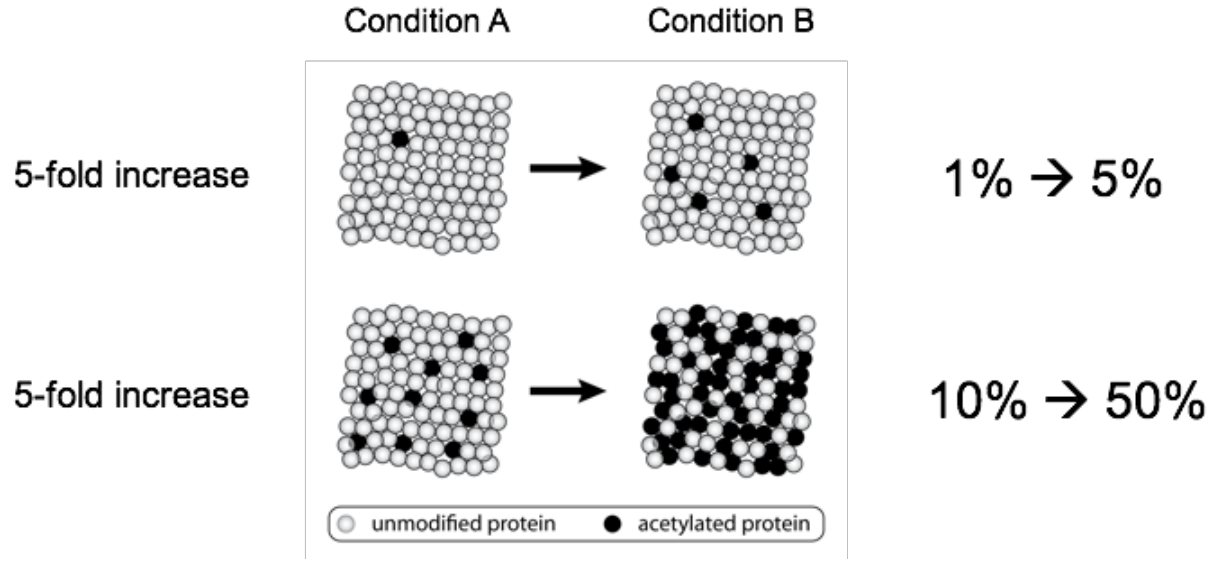

Figure 1-6. Diagram of method for determining direct acetylation stoichiometry.

Extracted protein was denatured, chemically acetylated using isotopic acetic anhydride followed by trypsin digestion. Peptides were analyzed by LC-MS/MS and quantified to determine site-specific stoichiometry. Adapted from ***(58)***.

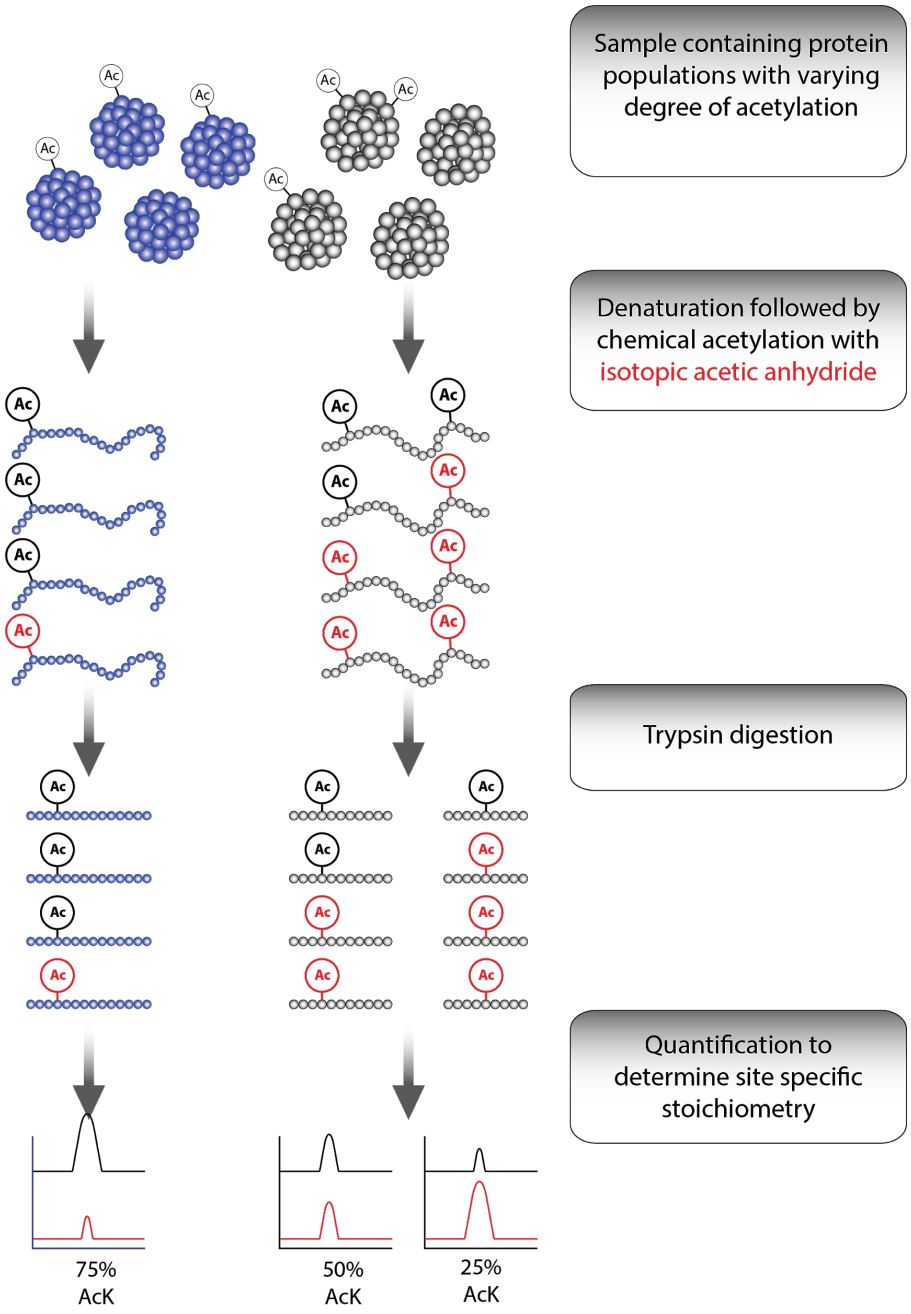

Figure 1-7. Mass spectrometry based proteomics acquisition methods.

A schematic of peptide isolation, fragmentation, and analysis by a mass spectrometer working in data-dependent acquisition (DDA), multiple reaction monitoring (MRM), or data-independent acquisition (DIA) modes. In DDA and MRM, single precursor ions are isolated form the MS1 precursor scan, fragmented, and analyzed in an MS2 scan by the mass spectrometer. In DDA mode, the precursor ions are chosen by the instrument on the basis of abundance. In MRM the precursor ions to be analyzed are defined by the user. In DIA all precursor ions within a selected mass range also called a window (from MS1 precursor scan) are isolated, fragmented, and analyzed in a single MS2 scan. Adapted from Hu A. et al ***(59)***.

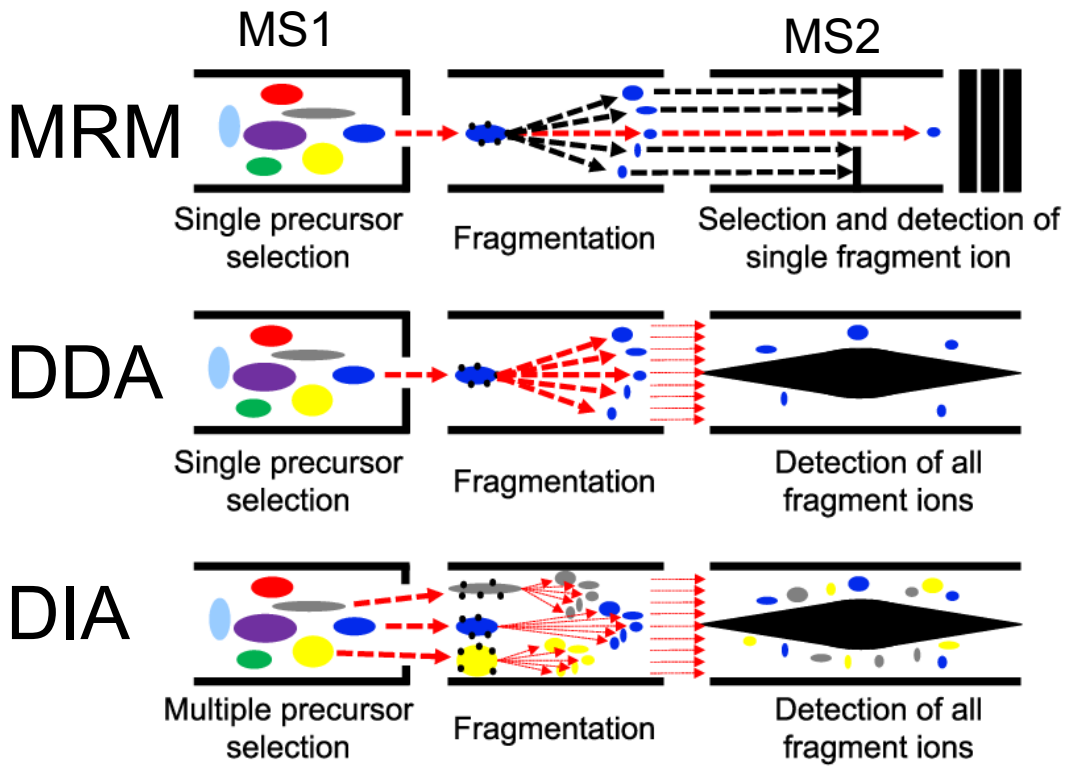

1.3 Chromatin modifications and Metabolism

1.3.1 Histone Posttranslational Modifications and Chromatin Structure

Posttranslational modifications control complex cellular processes, including the well-studied regulation of gene expression and genomic architecture by histone posttranslational modifications. DNA in the nucleus is wrapped around octamers of histone proteins to form the nucleosome, the core particle of chromatin (Figure 1-8) ***(60, 61)***. Nucleosomes are then packed into higher-order structures to create chromatin domains. These domains are regulated by posttranslational modifications on the flexible basic N-terminal tails of histone proteins, which can be extensively modified (Figure 1-8) ***(14, 60)***. Modifications span from well-characterized phosphorylation, acetylation, and methylation, to newly identified modifications such as crotonylation and other more exotic acylations (Figure 1-9) ***(12, 62–65)***. The higher-order packaging of chromatin is broadly divided into two domains of chromatin, heterochromatin, or heavily compacted inactive chromatin, and euchromatin, or active open chromatin permissive to transcription (Figure 1-10) ***(66)***. These two domains are regulated by a complex language of chemical modifications commonly referred to as the "histone code" ***(67, 68)***. The histone code is created and maintained by classes of proteins called writers, readers, and erasers to catalyze modifications, recruit protein complexes to specific modifications, and remove modifications respectively (Figure 1-8) ***(69)***. To create this complex language called the histone code and give rise to different domains in chromatin, histone can be combinatorially modified ***(70, 71)***.

1.3.2 Chromatin modifying enzymes and their metabolic co-substrates

Methylation is not solely an activating or repressive modification but rather its effect on chromatin is site-dependent ***(72, 73)***. Furthermore, methylation can occur on two residues, arginine and lysine, and multiple rounds of methylation can occur on both these residues

resulting in mono-, di-, or in the case of lysine tri-methylation. This added complexity of methylation enables methylation to have a complex set of effects on gene expression and chromatin structure. Methylation of histones acts as a binding site for reader proteins to recruit protein complexes rather than directly modifying the charge of their basic residues and electrostatic interaction with the DNA phosphate backbone. The addition of methyl groups to lysine and arginine residues is catalyzed by histone methyltransferases (HMTs) using S-adenosylmethionine (S-AdoMet, or SAM). Histone methyltransferases are divided into subgroups. Arginine methyltransferases are class I protein methyltransferases (PRMTs) which share a common seven-stranded β-sheet structure. There have been 9 PRMTs characterized to date, with many of them localizing to both the cytoplasm and nucleus of cells and have substrates in both compartments. The SET family of methyltransferases, class II, target lysine residues, and contain a SET catalytic domain ***(74)***. These proteins are broken up further into families, based upon the first 3 SET proteins identified in Drosophila, Suppressor of variegation 3-9 (Su(var)3-9) ***(75)***, the Polycomb group protein enhancer of zeste (E(z)) ***(76)***, and the Trithorax-group chromatin regulator Trithorax (Trx) ***(77)***. In humans, there are now seven families of SET domain proteins that have been identified. In addition to the SET families, DOT1L, a non-SET domain-containing lysine methyltransferase was found to methylate lysine 79 of H3 ***(77, 78)***. Many questions on the regulation, recruitment, and enzymatic processivity of these HMTs are under active investigation.

The effect of lysine methylation depends strongly on the site within the histone tail, as well as the context of surrounding modifications. Heterochromatin is often characterized by H3K9 trimethylation, a modification catalyzed by multiple HMTs and bound by heterochromatin protein 1 (HP1) ***(79)***. The other commonly known heterochromatic histone methylation

modification is H3K27 trimethylation, which is catalyzed by Polycomb Repressive Complex (PRC2), the complex containing the mammalian homolog of E(z), EZH2. PRC2 also reads H3K27 trimethylation, working to spread heterochromatin until reaching an inhibiting euchromatic modification ***(80)***. Active methylation modifications include trimethylation of H3K4 at gene promoters by MLL1-4 and H3K36 dimethylation within gene bodies ***(81–83)***.

Histone demethylation is removed by a class of protein called lysine demethylases (KMDs) that fall within two groups. The first is the flavin-dependent amine oxidase LSD1, which demethylates mono- or dimethylated H3K4 and H3K9 via a redox process ***(84)***. The second is the JmJC domain-driven demethylase (JMJD) family, which uses -ketoglutarate in an iron-dependent mechanism to release succinate and formaldehyde. There are 27 JMJD proteins, many of which target the H3 tail for demethylation ***(85)***. These proteins cluster into four distinct groups based upon C-terminal domains giving rise to differing recruitment and substrate specificity.

Histone acetylation is associated with open active chromatin, euchromatin, and is permissive to gene expression by RNA polymerase ***(66, 86)***. Histone acetylation acts by neutralizing the charge of the basic lysine and reducing electrostatic interactions between histone proteins and the DNA ***(87)***. This allows for easier eviction of histones and sliding of histones along chromatin, two mechanisms utilized by the RNA polymerase complex to facilitate transcription through chromatinized DNA ***(66)***. Histone acetylation is catalyzed by a class of enzymes called histone acetyltransferases (HATs). The first of these enzymes to be characterized was GCN5, a GNAT HAT family member, which acetylates lysine 9, 14, and 36 on Histone 3 (H3K9, K14, K16) and can participate in multiple complexes ***(86, 88)***. There are two additional families of HATs, the MYST and p300 families ***(88)***. The p300 family HATs contains p300 and

CBP, which are thought to participate in numerous complexes and have broad substrate specificity beyond histone proteins ***(89)***.

Repression of genes occurs through multiple histone posttranslational modifications working in concert, one of which is the removal of acetylation by histone deacetylases (HDACs) ***(90)***. There are two main types of HDACs, classical HDACs which use a zinc-dependent catalytic mechanism, and silent information regulator 2 deacetylases (sir2 or sirtuin), a class of NAD+-dependent deacetylases ***(91–93)***. Classical HDACs, class I and II, are localized to the nucleus and target primarily histones, however, HDAC6 is a cytoplasmic enzyme that has other substrates. On the other hand, sirtuins are distributed throughout the cell, with SIRT 1 and 2 in the cytoplasm and nucleus, 3 through 5 located in the mitochondria, and 6 and 7 primarily localized to the nucleus and target histones for deacetylation ***(91, 94, 95)***.

The search for writers, readers, and erasers of more exotic histone modifications is ongoing. More unusual acylations are thought to function similarly to acetylation and be regulated by overlapping proteins. The HATS p300/CBP have a very low Km for acetyl-CoA, and likely prefer it as their co-substrate, however in specific cellular contexts it may be outcompeted by other acyl-CoAs and transfer other groups such as propionyl and butyryl demonstrated *in vitro* and hydroxyisobutyryl *in vivo* ***(63, 96)***. However, some of these modifications may have unique writer, reader, and eraser proteins, such as the AF9 YEATS domain, which has a higher affinity for lysine crotonylation that acetylation ***(97)***.

1.3.3 Metabolic influences on histone posttranslational modifications

Histone lysine methyltransferases contain a single class of proteins, which utilize SAM as a methyl donor. Methyl donor metabolism has been shown to influence histone methylation (Figure 1-12). In mouse embryonic stem cells threonine metabolism provides a large portion of

the glycine and acetyl-CoA used to synthesize SAM, and restriction of threonine resulted in quantitative reduction of histone methylation, specifically H3K4 methylation ***(98)***. Other studies in cancer cells demonstrated a dose-dependent response to reduction of methionine, as well as a reduction of methyl-donor metabolites such as betaine and dimethylglycine ***(99)***. In yeast, cells with excess SAM from reduced phospholipid methylation upregulate the methylation of histones, particularly H3K36, as a methyl sink ***(100, 101)***.

Histone demethylases have 2 classes, separated by different mechanisms and co-substrates to perform oxidative demethylation. One class utilizes FAD and the other uses Fe(II) and α-ketoglutarate (Figure 1-11). Studies have shown histone demethylases, dependent upon small molecule metabolites as co-substrates, are responsive to alterations in cellular metabolism, specifically with regard to iron concentration and concentrations of TCA cycle intermediates ***(102, 103)***. Mutations in critical TCA cycle enzymes such as Isocitrate Dehydrogenase (IDH) have been shown to alter histone methylation through the production of the oncometabolite 2-hydroxyglutarate (2HG), which inhibits the activity of α-ketoglutarate dependent histone demethylases (Figure 1-13) ***(104, 105)***.

Both major classes of histone deacetylases have links to metabolism. Classic HDACs release acetate as part of their catalytic mechanism and are inhibited by butyrate (Figure 1-12) ***(106)***. In mice and cells, it has been demonstrated metabolism under fasting conditions can inhibit HDAC activity and upregulate histone acetylation and gene expression at specific genes of the fasting response (Figure 1-13) ***(107)***. Sources of butyrate or β-hydroxybutyrate are bacterial fermentation by the gut microbiota and ketone body synthesis, respectively. Sirtuins are NAD+-dependent deacetylates, which is a central co-factor in redox metabolism across the cell. The metabolic state of the cell can shift redox balance and promote or limit the availability of

NAD+ for sirtuin mediated deacetylation (Figure 1-11). In addition, the product of sirtuin mediated deacetylation, nicotinamide, can inhibit sirtuin function at high levels and is often used as an inhibitor in cell culture experiments.

Histone acetyltransferases are directly connected to metabolism in the cell by using a central carbon source, acetyl-CoA, as the co-substrate donor of the acetyl group. Acetyl-CoA is generated within the cell through a variety of pathways since it serves as a central metabolite. Cytoplasmic and nuclear acetyl-CoA is synthesized by two primary pathways, ATP citrate lyase (ACLY) and acyl-CoA short chain synthetase family member 2 (ACSS2). ACLY cleaves citrate exported from the mitochondria into oxaloacetate and acetyl-CoA and ACSS2 synthesizes acetyl-CoA from acetate and CoA (Figure 1-11). Two models of the influence of acetyl-CoA synthesis on nuclear protein, particularly histone, acetylation have been purposed. The first is a global concentration-dependent model, with synthesis of acetyl-CoA contributing to a diffuse global pool of acetyl-CoA and influencing changes in acetylation through changes in acetyl-CoA pool levels (Figure 1-12A). The second is a more local or targeted mechanism where acetyl-CoA synthesis influences local concentrations of acetyl-CoA to alter local HAT enzyme activity (Figure 1-12B). Early investigations into these two models have given conflicting results and not utilized physiologically relevant metabolic conditions. In cells, ACLY is the main contributor to cytoplasmic and nuclear acetyl-CoA pools in a glucose-dependent manner contributing globally to both lipogenesis and histone acetylation across all histone sites ***(108)***. ACLY translocates to the nucleus upon phosphorylation of S455 by the kinase AKT ***(109)***. In contrast to the global concentration-dependent model of ACLY influencing acetylation in high glucose conditions in tissue culture, phosphorylation and nuclear recruitment of ACLY is required for acetylation of histones locally at double stranded breaks and targeted nuclear recruitment of BRCA1 for

double-stranded break repair in a mouse model ***(110)***. ACLY has been demonstrated to serve as a glucose to acetate fuel switch, which may be in part due to locally targeted acetylation of proteins ***(112)***. In the absence of or with catalytically inactive ACLY, ACSS2 is upregulated and preferentially recruited to the nucleus for acetyl-CoA synthesis for lipid synthesis and global histone acetylation (Figure 1-12A). In cancer cell lines and cells under hypoxia which favor acetate metabolism, ACSS2 plays an important role in acetyl-CoA synthesis and histone acetylation in a global manner ***(113, 114)***. In contrast to ACSS2 globally regulating acetylation under glucose-limiting and hypoxic conditions, CBP regulates the acetylation of the transcription factor HIF2α in a targeted ACSS2-dependent manner ***(115)***. Additionally, ACSS2 was found to be important in bulk acetate recycling in cancer cell lines for lipogenesis as well as global histone acetylation levels ***(116)***. In an ACLY-deficient tissue culture system, histone acetylation levels were acetate dose-dependent across multiple histone sites on H3 suggesting control of acetylation through a global mechanism ***(112)***. In contrast, ACSS2-dependent acetylation of H3K9 in mouse hippocampus was targeted to both specific lysine sites on histones and gene loci and had effects on learning and memory in mice ***(117)***. Substrate for ACLY-dependent generation of acetyl-CoA is generated through glycolysis. In contrast, sources of acetate are diverse. Free acetate is generated from deacetylation, fermentation of fiber by the gut microbiota, acetate in the diet, and recently it was shown that keto acid dehydrogenation of pyruvate produces acetate in cells and mice ***(118)***.

The close link between acetylation and metabolism has been extensively demonstrated in the mitochondria and investigations have begun looking at other subcellular compartments. Acetyl-CoA generation is compartment throughout the cell, with fatty acid oxidation, glycolysis, and the TCA cycle generating acetyl-CoA in the mitochondria ***(24, 39)***. ACLY and ACSS2

synthesize acetyl-CoA in the nucleus and cytoplasm and are similarly responsive to metabolism as described above. The effects of metabolism by these pathways on histone acetylation has been heavily studied, however recent proteomics studies indicate acetylation in the nucleus extends far beyond histones and is enzyme regulated ***(119, 120)***. Early metabolic labeling experiment in cells of glucose and acetate to profile contributions of ACLY and ACSS2 did not adequately address challenges to studying ACSS2 in glucose rich tissue culture conditions, concluding acetate-driven acetylation was limited ***(119)***. ACSS2 is involved in fatty acid synthesis under glucose-limited conditions and particularly systemic fatty acid metabolism in an organism ***(121)***. In cell culture, ACSS2 is not a large contributor to acetyl-CoA synthesis, therefore the scope of these studies was limited ***(108, 119)***. Studies into the effects of metabolism on nuclear acetylation have not used physiologically metabolic perturbations nor systems such as an animal model under fasting necessary to interrogate ACLY and ACSS2 regulation of nuclear protein acetylation.

1.3.3 On understanding the regulation of nuclear protein acetylation by acetyl-CoA synthesis pathways

Prior to the work described in the following chapters, many questions regarding the mechanism of regulation of nuclear acetylation by acetyl-CoA synthesis pathways remain. Previous studies offer conflicting data on whether acetyl-CoA synthesis pathways influence nuclear acetylation in a global concentration-dependent or targeted local manner. Chapter 2 will address the gaps in existing methods to address these questions in a mouse model and describe method development undertaken to have the tools necessary. These question of global versus targeted influence on nuclear acetylation by ACSS2 will be addressed in a physiologically relevant metabolic perturbation in a mouse model in Chapters 3. This study shows ACSS2-dependent acetylation is controlled in a targeted and tissue-specific manner to coordinate a metabolic response to fasting conditions. Conclusion from these studies, ongoing work ,and future directions to elucidate molecular mechanism of targeted control of acetylation by acetyl-CoA synthesis pathways will be discussed in Chapter 4.

Figure 1-8. The structure of chromatin.

A histone octamer is depicted with modifications to the N-terminal histone tails (boxed in grey). The octamer is shown wrapped by DNA as a nucleosome and higher order packaging, including the highly compacted mitotic chromosome. Adapted from Zhangli Su.

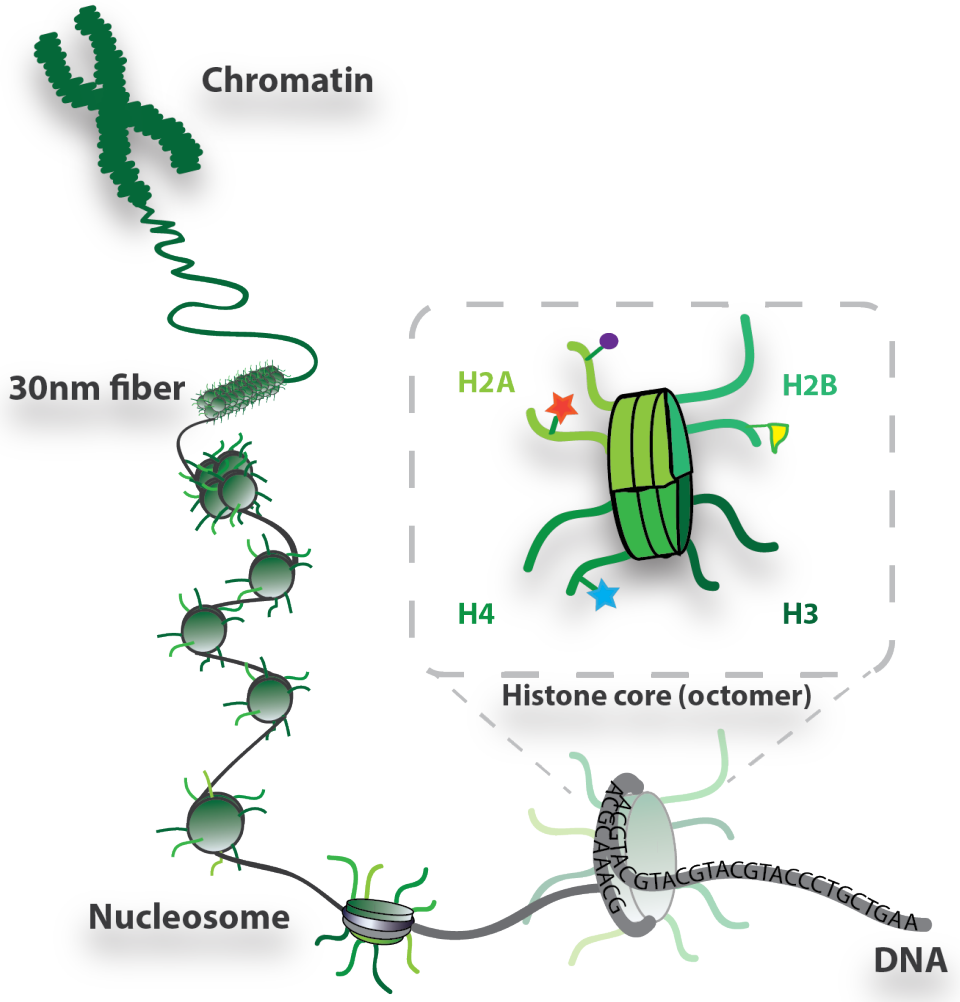

Figure 1-9. Posttranslational modification of chromatin.

The N-terminal histone tail of Histone 3 is extended with its sequence showing various acetylation and methylation modifications. Reader, writer, and eraser domains and proteins are acting upon the histone tails. Adapted from Zhangli Su.

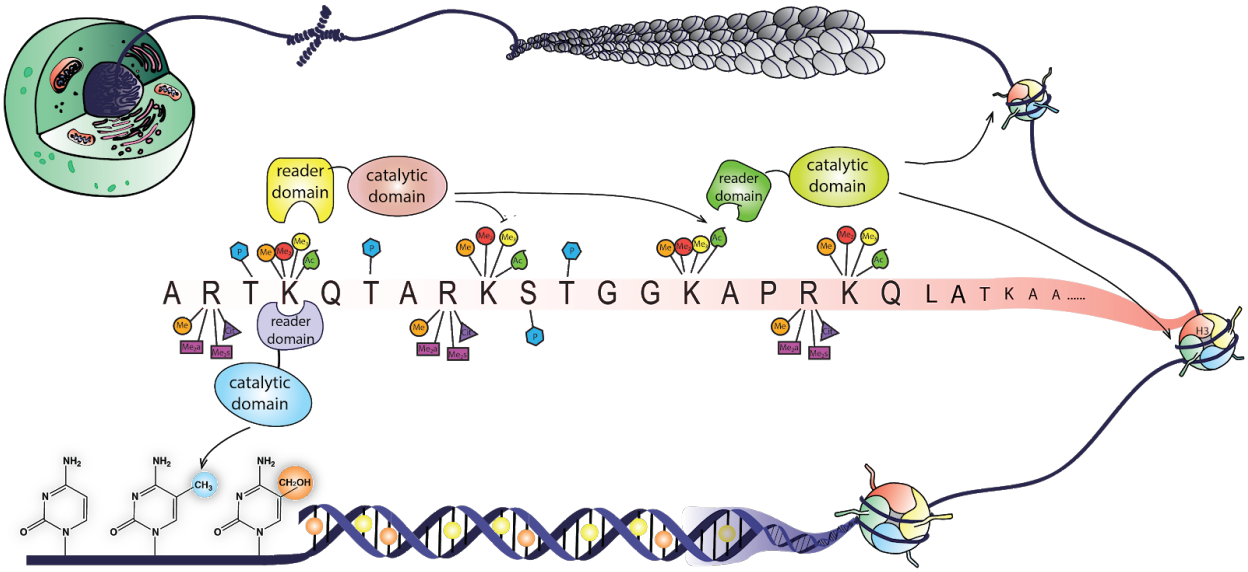

Figure 1-10. Histone acetylation opens chromatin for active transcription.

Histone acetyltransferases and deacetylases open chromatin to activate transcription and close chromatin to repress transcription by acetylation and deacetylation of histones tails respectively, adapted from Jessica Feldman.

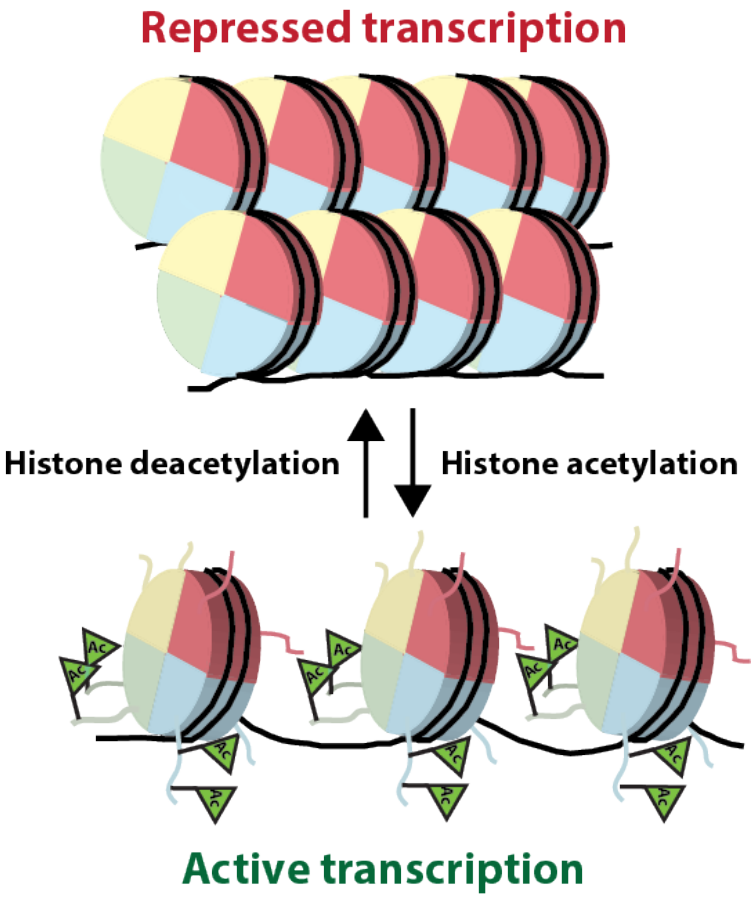

Figure 1-11. Histone code writers require metabolites as co-substrates to write epigenetic marks.

Metabolism is tightly connected with histone posttranslational modifications. Addition and removal of histone acetylation and methylation are catalyzed by several classes of enzymes commonly referred to as histone code writers and erases, require metabolite co-substrates or these metabolites act as activators/inhibitors. The reactions shown are color-coded by enzyme classes with the involved metabolites as substrates connected by solid arrows, and metabolites as activators and inhibitors shown by dash lines. Simplified metabolic pathways are shown in blue arrows with the enzymes ACSS2 and ACLY associated to their appropriate metabolic pathway to generate acetyl-CoA for histone acetylation as a co-substrate of histone acetyltransferases, adapted from Jing Fan ***(122)***.

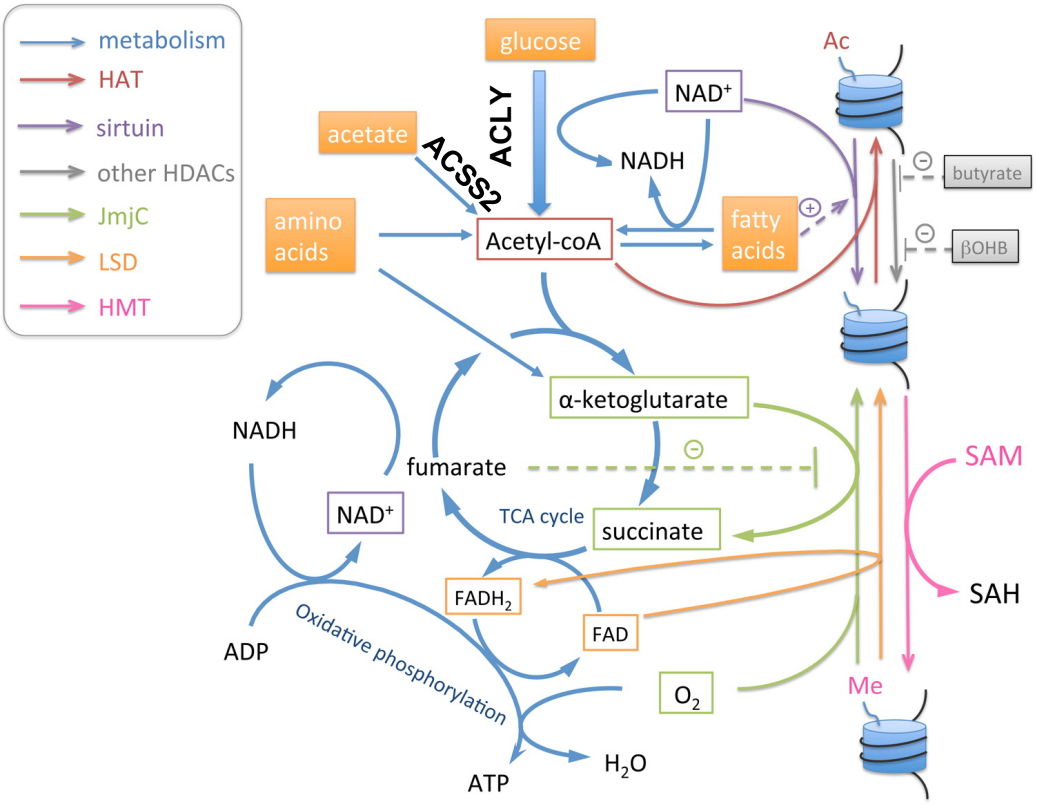
metabolism
HAT
sirtuin
other HDACs
JmjC
LSD
HMT
glucose
ACLY
acetate
ACSS2
amino acids
Acetyl-coA
NAD+
NADH
fatty acids
Ac
butyrate
βOHB
α-ketoglutarate
NADH
fumarate
NAD+
TCA cycle
succinate
FADH2
FAD
ADP
Oxidative phosphorylation
ATP
O2
H2O
SAM
SAH
Me

Figure 1-12. Histone acetylation may be mediated by global or local production of acetyl-CoA.

A) Nuclear acetyl-CoA producers acyl-CoA synthetase short-chain family member 2 (ACSS2) and ATP-citrate lyase (ACLY) create a pool of acetyl-CoA that non-specifically is used by Histone acetyltransferases (HATs) to perform protein acetylation reactions in the nucleus. **B)** Acetyl-CoA is generated locally in by a complex of proteins (in this case ACSS2) that links the production of acetyl-CoA with a HAT to locally acetylate specific histone targets. AcCoA, acetyl-CoA; CoA, coenzyme A.

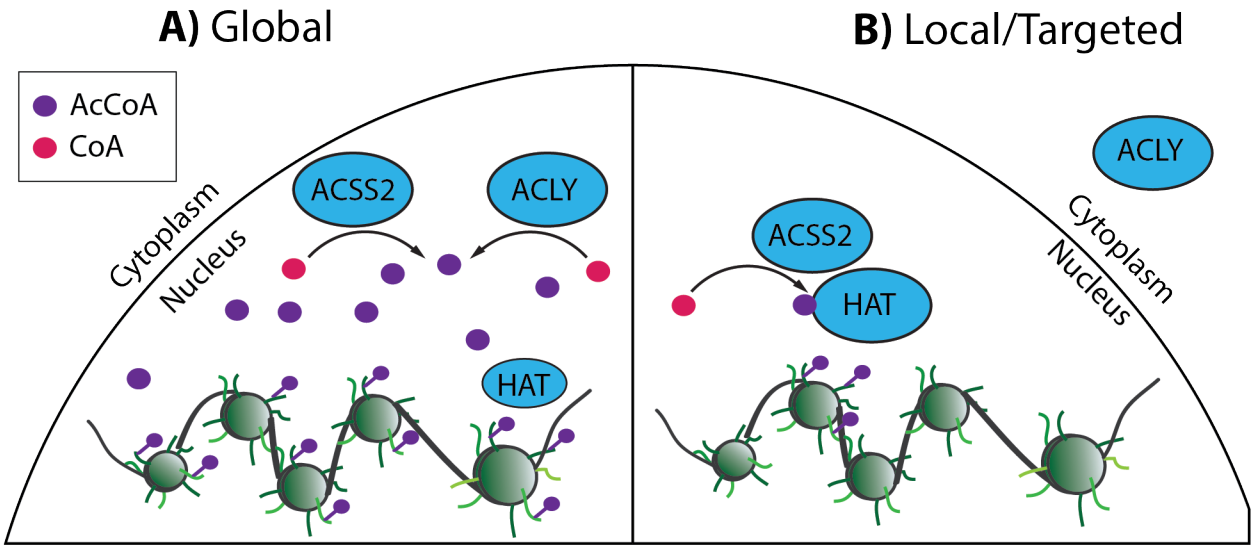

1.4 References

1. Jensen ON (2004) Modification-specific proteomics: characterization of post-translational modifications by mass spectrometry. Curr Opin Chem Biol 8:33–41

2. Nachtergaele S and He C (2017) The emerging biology of RNA post-transcriptional modifications. RNA Biol 14:156–163

3. Aebersold R, Agar JN, Amster IJ, et al (2018) How many human proteoforms are there? Nat Chem Biol 14:206–214

4. Smith LM, Kelleher NL, and Consortium for Top Down Proteomics (2013) Proteoform: a single term describing protein complexity. Nat Methods 10:186–187

5. Wagner GR and Hirschey MD (2014) Nonenzymatic protein acylation as a carbon stress regulated by sirtuin deacylases. Mol Cell 54:5–16

6. Simic Z, Weiwad M, Schierhorn A, et al (2015), The ε-Amino Group of Protein Lysine Residues Is Highly Susceptible to Nonenzymatic Acylation by Several Physiological Acyl-CoA Thioesters, http://dx.doi.org/10.1002/cbic.201500364

7. Paik WK, Pearson D, Lee HW, et al (1970) Nonenzymatic acetylation of histones with acetyl-CoA. Biochim Biophys Acta 213:513–522

8. Wagner GR and Payne RM (2013) Widespread and enzyme-independent Nε-acetylation and Nε-succinylation of proteins in the chemical conditions of the mitochondrial matrix. J Biol Chem 288:29036–29045

9. Allfrey VG, Faulkner R, and Mirsky AE (1964) ACETYLATION AND METHYLATION OF HISTONES AND THEIR POSSIBLE ROLE IN THE REGULATION OF RNA SYNTHESIS. Proc Natl Acad Sci U S A 51:786–794

10. Allfrey VG and Mirsky AE (1964), Structural Modifications of Histones and their

Possible Role in the Regulation of RNA Synthesis, http://dx.doi.org/10.1126/science.144.3618.559

11. Phillips D (1963), The presence of acetyl groups in histones, http://dx.doi.org/10.1042/bj0870258

12. Strahl BD and Allis CD (2000) The language of covalent histone modifications. Nature 403:41–45

13. Sarma K and Reinberg D (2005) Histone variants meet their match. Nat Rev Mol Cell Biol 6:139–149

14. Bannister AJ and Kouzarides T (2011), Regulation of chromatin by histone modifications, http://dx.doi.org/10.1038/cr.2011.22

15. Hallows WC, Lee S, and Denu JM (2006) Sirtuins deacetylate and activate mammalian acetyl-CoA synthetases. Proc Natl Acad Sci U S A 103:10230–10235

16. Kim SC, Sprung R, Chen Y, et al (2006) Substrate and functional diversity of lysine acetylation revealed by a proteomics survey. Mol Cell 23:607–618

17. Kim SC, Sprung R, Chen Y, et al (2006) Substrate and functional diversity of lysine acetylation revealed by a proteomics survey. Mol Cell 23:607–618

18. Yu BJ, Kim JA, Moon JH, et al (2008) The diversity of lysine-acetylated proteins in Escherichia coli. J Microbiol Biotechnol 18:1529–1536

19. Zhang J, Sprung R, Pei J, et al (2009) Lysine acetylation is a highly abundant and evolutionarily conserved modification in Escherichia coli. Mol Cell Proteomics 8:215–225

20. Schwer B, Eckersdorff M, Li Y, et al (2009) Calorie restriction alters mitochondrial protein acetylation. Aging Cell 8:604–606

21. Choudhary C, Kumar C, Gnad F, et al (2009) Lysine Acetylation Targets Protein

Complexes and Co-Regulates Major Cellular Functions. Science 325:834–840

22. Wang Q, Zhang Y, Yang C, et al (2010) Acetylation of metabolic enzymes coordinates carbon source utilization and metabolic flux. Science 327:1004–1007

23. Zhao S, Xu W, Jiang W, et al (2010) Regulation of Cellular Metabolism by Protein Lysine Acetylation. Science 327:1000–1004

24. Yang L, Vaitheesvaran B, Hartil K, et al (2011) The fasted/fed mouse metabolic acetylome: N6-acetylation differences suggest acetylation coordinates organ-specific fuel switching. J Proteome Res 10:4134–4149

25. Weinert BT, Wagner SA, Horn H, et al (2011) Proteome-wide mapping of the Drosophila acetylome demonstrates a high degree of conservation of lysine acetylation. Sci Signal 4:ra48

26. Simon GM, Cheng J, and Gordon JI (2012) Quantitative assessment of the impact of the gut microbiota on lysine epsilon-acetylation of host proteins using gnotobiotic mice. Proc Natl Acad Sci U S A 109:11133–11138

27. Henriksen P, Wagner SA, Weinert BT, et al (2012) Proteome-wide analysis of lysine acetylation suggests its broad regulatory scope in Saccharomyces cerevisiae. Mol Cell Proteomics 11:1510–1522

28. Lundby A, Lage K, Weinert BT, et al (2012) Proteomic analysis of lysine acetylation sites in rat tissues reveals organ specificity and subcellular patterns. Cell Rep 2:419–431

29. Foster DB, Liu T, Rucker J, et al (2013) The cardiac acetyl-lysine proteome. PLoS One 8:e67513

30. Olsen JV and Mann M (2013) Status of large-scale analysis of post-translational modifications by mass spectrometry. Mol Cell Proteomics 12:3444–3452

31. Lin D, Tabb DL, and Yates JR (2003), Large-scale protein identification using mass

spectrometry, http://dx.doi.org/10.1016/s1570-9639(02)00546-0

32. Han X, Aslanian A, and Yates JR 3rd (2008) Mass spectrometry for proteomics. Curr Opin Chem Biol 12:483–490

33. Kouzarides T (2000) Acetylation: a regulatory modification to rival phosphorylation? EMBO J 19:1176–1179

34. Zhang J, Sprung R, Pei J, et al (2009) Lysine acetylation is a highly abundant and evolutionarily conserved modification in Escherichia coli. Mol Cell Proteomics 8:215–225

35. Weinert BT, Wagner SA, Horn H, et al (2011) Proteome-wide mapping of the Drosophila acetylome demonstrates a high degree of conservation of lysine acetylation. Sci Signal 4:ra48

36. Henriksen P, Wagner SA, Weinert BT, et al (2012) Proteome-wide analysis of lysine acetylation suggests its broad regulatory scope in Saccharomyces cerevisiae. Mol Cell Proteomics 11:1510–1522

37. Lundby A, Lage K, Weinert BT, et al (2012) Proteomic analysis of lysine acetylation sites in rat tissues reveals organ specificity and subcellular patterns. Cell Rep 2:419–431

38. Ghanta S, Grossmann RE, and Brenner C (2013) Mitochondrial protein acetylation as a cell-intrinsic, evolutionary driver of fat storage: chemical and metabolic logic of acetyl-lysine modifications. Crit Rev Biochem Mol Biol 48:561–574

39. Dittenhafer-Reed KE, Richards AL, Fan J, et al (2015) SIRT3 mediates multi-tissue coupling for metabolic fuel switching. Cell Metab 21:637–646

40. Hebert AS, Dittenhafer-Reed KE, Yu W, et al (2013) Calorie restriction and SIRT3 trigger global reprogramming of the mitochondrial protein acetylome. Mol Cell 49:186–199

41. Steen H, Jebanathirajah JA, Springer M, et al (2005) Stable isotope-free relative and absolute quantitation of protein phosphorylation stoichiometry by MS. Proc Natl Acad Sci U S A

102:3948–3953

42. Hansen BK, Gupta R, Baldus L, et al (2019) Analysis of human acetylation stoichiometry defines mechanistic constraints on protein regulation. Nat Commun 10:1055

43. Zhou T, Chung Y-H, Chen J, et al (2016), Site-Specific Identification of Lysine Acetylation Stoichiometries in Mammalian Cells, http://dx.doi.org/10.1021/acs.jproteome.5b01097

44. Nakayasu ES, Wu S, Sydor MA, et al (2014) A method to determine lysine acetylation stoichiometries. Int J Proteomics 2014:730725

45. Meyer JG, D'Souza AK, Sorensen DJ, et al (2016), Quantification of Lysine Acetylation and Succinylation Stoichiometry in Proteins Using Mass Spectrometric Data-Independent Acquisitions (SWATH), http://dx.doi.org/10.1007/s13361-016-1476-z

46. Michalski A, Cox J, and Mann M (2011), More than 100,000 Detectable Peptide Species Elute in Single Shotgun Proteomics Runs but the Majority is Inaccessible to Data-Dependent LC−MS/MS, http://dx.doi.org/10.1021/pr101060v

47. Tabb DL, Vega-Montoto L, Rudnick PA, et al (2010) Repeatability and reproducibility in proteomic identifications by liquid chromatography-tandem mass spectrometry. J Proteome Res 9:761–776

48. Bruderer R, Bernhardt OM, Gandhi T, et al (2017) Optimization of Experimental Parameters in Data-Independent Mass Spectrometry Significantly Increases Depth and Reproducibility of Results. Mol Cell Proteomics 16:2296–2309

49. Bruderer R, Bernhardt OM, Gandhi T, et al (2015) Extending the limits of quantitative proteome profiling with data-independent acquisition and application to acetaminophen-treated three-dimensional liver microtissues. Mol Cell Proteomics 14:1400–1410

50. Gillet LC, Navarro P, Tate S, et al (2012) Targeted data extraction of the MS/MS spectra generated by data-independent acquisition: a new concept for consistent and accurate proteome analysis. Mol Cell Proteomics 11:O111.016717

51. Ludwig C, Gillet L, Rosenberger G, et al (2018) Data-independent acquisition-based SWATH-MS for quantitative proteomics: a tutorial. Mol Syst Biol 14:e8126

52. Venable JD, Dong M-Q, Wohlschlegel J, et al (2004) Automated approach for quantitative analysis of complex peptide mixtures from tandem mass spectra. Nat Methods 1:39–45

53. Baeza J, Lawton AJ, Fan J, et al Quantifying dynamic protein acetylation using quantitative stoichiometry, http://dx.doi.org/10.1101/472530

54. Iyer SS, Zhang Z-P, Kellogg GE, et al (2004) Evaluation of deuterium isotope effects in normal-phase LC-MS-MS separations using a molecular modeling approach. J Chromatogr Sci 42:383–387

55. Turowski M, Yamakawa N, Meller J, et al (2003) Deuterium isotope effects on hydrophobic interactions: the importance of dispersion interactions in the hydrophobic phase. J Am Chem Soc 125:13836–13849

56. Messner C, Demichev V, Bloomfield N, et al ScanningSWATH enables ultra-fast proteomics using high-flow chromatography and minute-scale gradients, http://dx.doi.org/10.1101/656793

57. Baeza J, Smallegan MJ, and Denu JM (2016) Mechanisms and Dynamics of Protein Acetylation in Mitochondria. Trends Biochem Sci 41:231–244

58. Baeza J, Dowell JA, Smallegan MJ, et al (2014), Stoichiometry of Site-specific Lysine Acetylation in an Entire Proteome, http://dx.doi.org/10.1074/jbc.m114.581843

59. Hu A, Noble WS, and Wolf-Yadlin A (2016) Technical advances in proteomics: new developments in data-independent acquisition. F1000Res 5

60. Luger K, Mäder AW, Richmond RK, et al (1997), Crystal structure of the nucleosome core particle at 2.8 Å resolution, http://dx.doi.org/10.1038/38444

61. Kornberg RD (1977), Structure of Chromatin, http://dx.doi.org/10.1146/annurev.bi.46.070177.004435

62. Berger SL (2007) The complex language of chromatin regulation during transcription. Nature 447:407–412

63. Chen Y, Sprung R, Tang Y, et al (2007) Lysine propionylation and butyrylation are novel post-translational modifications in histones. Mol Cell Proteomics 6:812–819

64. Tan M, Luo H, Lee S, et al (2011) Identification of 67 histone marks and histone lysine crotonylation as a new type of histone modification. Cell 146:1016–1028

65. Xie Z, Dai J, Dai L, et al (2012) Lysine succinylation and lysine malonylation in histones. Mol Cell Proteomics 11:100–107

66. Li B, Carey M, and Workman JL (2007), The Role of Chromatin during Transcription, http://dx.doi.org/10.1016/j.cell.2007.01.015

67. Linggi BE, Brandt SJ, Sun Z-W, et al (2005) Translating the histone code into leukemia. J Cell Biochem 96:938–950

68. Jenuwein T and Allis CD (2001) Translating the histone code. Science 293:1074–1080

69. Taverna SD, Li H, Ruthenburg AJ, et al (2007) How chromatin-binding modules interpret histone modifications: lessons from professional pocket pickers. Nat Struct Mol Biol 14:1025–1040

70. Wang Z and Patel DJ (2011), Combinatorial Readout of Dual Histone Modifications by

Paired Chromatin-associated Modules, http://dx.doi.org/10.1074/jbc.r111.219139

71. Gardner KE, Allis CD, and Strahl BD (2011) Operating on chromatin, a colorful language where context matters. J Mol Biol 409:36–46

72. Jenuwein T, Laible G, Dorn R, et al (1998), SET domain proteins modulate chromatin domains in eu- and heterochromatin, http://dx.doi.org/10.1007/s000180050127

73. Rea S, Eisenhaber F, O'Carroll D, et al (2000) Regulation of chromatin structure by site-specific histone H3 methyltransferases. Nature 406:593–599

74. Zhang X and Bruice TC (2008), Enzymatic mechanism and product specificity of SET-domain protein lysine methyltransferases, http://dx.doi.org/10.1073/pnas.0801788105

75. Tschiersch B, Hofmann A, Krauss V, et al (1994) The protein encoded by the Drosophila position-effect variegation suppressor gene Su(var)3-9 combines domains of antagonistic regulators of homeotic gene complexes. EMBO J 13:3822–3831

76. Jones RS and Gelbart WM (1993) The Drosophila Polycomb-group gene Enhancer of zeste contains a region with sequence similarity to trithorax. Mol Cell Biol 13:6357–6366

77. Stassen MJ, Bailey D, Nelson S, et al (1995) The Drosophila trithorax proteins contain a novel variant of the nuclear receptor type DNA binding domain and an ancient conserved motif found in other chromosomal proteins. Mech Dev 52:209–223

78. Feng Q, Wang H, Ng HH, et al (2002) Methylation of H3-lysine 79 is mediated by a new family of HMTases without a SET domain. Curr Biol 12:1052–1058

79. James TC and Elgin SC (1986) Identification of a nonhistone chromosomal protein associated with heterochromatin in Drosophila melanogaster and its gene. Mol Cell Biol 6:3862–3872

80. Margueron R and Reinberg D (2011) The Polycomb complex PRC2 and its mark in life.

Nature 469:343–349

81. Bernstein BE, Humphrey EL, Erlich RL, et al (2002) Methylation of histone H3 Lys 4 in coding regions of active genes. Proc Natl Acad Sci U S A 99:8695–8700

82. Krogan NJ, Dover J, Wood A, et al (2003) The Paf1 complex is required for histone H3 methylation by COMPASS and Dot1p: linking transcriptional elongation to histone methylation. Mol Cell 11:721–729

83. Ng HH, Robert F, Young RA, et al (2003) Targeted recruitment of Set1 histone methylase by elongating Pol II provides a localized mark and memory of recent transcriptional activity. Mol Cell 11:709–719

84. Shi Y, Lan F, Matson C, et al (2004) Histone demethylation mediated by the nuclear amine oxidase homolog LSD1. Cell 119:941–953

85. Anand R and Marmorstein R (2007) Structure and mechanism of lysine-specific demethylase enzymes. J Biol Chem 282:35425–35429

86. Brownell JE, Zhou J, Ranalli T, et al (1996) Tetrahymena histone acetyltransferase A: a homolog to yeast Gcn5p linking histone acetylation to gene activation. Cell 84:843–851

87. Shahbazian MD and Grunstein M (2007) Functions of site-specific histone acetylation and deacetylation. Annu Rev Biochem 76:75–100

88. Berndsen CE and Denu JM (2008) Catalysis and substrate selection by histone/protein lysine acetyltransferases. Curr Opin Struct Biol 18:682–689

89. Liu X, Wang L, Zhao K, et al (2008) The structural basis of protein acetylation by the p300/CBP transcriptional coactivator. Nature 451:846–850

90. Braunstein M, Rose AB, Holmes SG, et al (1993) Transcriptional silencing in yeast is associated with reduced nucleosome acetylation. Genes Dev 7:592–604

91. Frye RA (2000) Phylogenetic classification of prokaryotic and eukaryotic Sir2-like proteins. Biochem Biophys Res Commun 273:793–798

92. Taunton J, Hassig CA, and Schreiber SL (1996) A mammalian histone deacetylase related to the yeast transcriptional regulator Rpd3p. Science 272:408–411

93. Blander G and Guarente L (2004), The Sir2 Family of Protein Deacetylases, http://dx.doi.org/10.1146/annurev.biochem.73.011303.073651

94. Haigis MC and Guarente LP (2006) Mammalian sirtuins--emerging roles in physiology, aging, and calorie restriction. Genes Dev 20:2913–2921

95. Michishita E, Park JY, Burneskis JM, et al (2005), Evolutionarily Conserved and Nonconserved Cellular Localizations and Functions of Human SIRT Proteins, http://dx.doi.org/10.1091/mbc.e05-01-0033

96. Huang H, Tang S, Ji M, et al (2018) p300-Mediated Lysine 2-Hydroxyisobutyrylation Regulates Glycolysis. Mol Cell 70:984

97. Li Y, Sabari BR, Panchenko T, et al (2016) Molecular Coupling of Histone Crotonylation and Active Transcription by AF9 YEATS Domain. Mol Cell 62:181–193

98. Shyh-Chang N, Locasale JW, Lyssiotis CA, et al (2013) Influence of threonine metabolism on S-adenosylmethionine and histone methylation. Science 339:222–226

99. Mentch SJ, Mehrmohamadi M, Huang L, et al (2015) Histone Methylation Dynamics and Gene Regulation Occur through the Sensing of One-Carbon Metabolism. Cell Metab 22:861–873

100. Ye C, Sutter BM, Wang Y, et al (2019) Demethylation of the Protein Phosphatase PP2A Promotes Demethylation of Histones to Enable Their Function as a Methyl Group Sink. Mol Cell 73:1115–1126.e6

101. Ye C, Sutter BM, Wang Y, et al (2017) A Metabolic Function for Phospholipid and

Histone Methylation. Mol Cell 66:180–193.e8

102. Xiao M, Yang H, Xu W, et al (2012), Inhibition of -KG-dependent histone and DNA demethylases by fumarate and succinate that are accumulated in mutations of FH and SDH tumor suppressors, http://dx.doi.org/10.1101/gad.191056.112

103. Letouzé E, Martinelli C, Loriot C, et al (2013) SDH mutations establish a hypermethylator phenotype in paraganglioma. Cancer Cell 23:739–752

104. Lu C, Ward PS, Kapoor GS, et al (2012), IDH mutation impairs histone demethylation and results in a block to cell differentiation, http://dx.doi.org/10.1038/nature10860

105. Xu W, Yang H, Liu Y, et al (2011) Oncometabolite 2-hydroxyglutarate is a competitive inhibitor of α-ketoglutarate-dependent dioxygenases. Cancer Cell 19:17–30

106. Davie JR (2003), Inhibition of Histone Deacetylase Activity by Butyrate, http://dx.doi.org/10.1093/jn/133.7.2485s

107. Shimazu T, Hirschey MD, Newman J, et al (2013) Suppression of oxidative stress by β-hydroxybutyrate, an endogenous histone deacetylase inhibitor. Science 339:211–214

108. Wellen KE, Hatzivassiliou G, Sachdeva UM, et al (2009) ATP-citrate lyase links cellular metabolism to histone acetylation. Science 324:1076–1080

109. Berwick DC, Hers I, Heesom KJ, et al (2002) The identification of ATP-citrate lyase as a protein kinase B (Akt) substrate in primary adipocytes. J Biol Chem 277:33895–33900

110. Sivanand S, Rhoades S, Jiang Q, et al (2017) Nuclear Acetyl-CoA Production by ACLY Promotes Homologous Recombination. Mol Cell 67:252–265.e6

111. Fernandez S, Viola JM, Torres A, et al (2019) Adipocyte ACLY Facilitates Dietary Carbohydrate Handling to Maintain Metabolic Homeostasis in Females. Cell Rep 27:2772–2784.e6

112. Zhao S, Torres A, Henry RA, et al (2016) ATP-Citrate Lyase Controls a Glucose-to-Acetate Metabolic Switch. Cell Rep 17:1037–1052

113. Gao X, Lin S-H, Ren F, et al (2016) Acetate functions as an epigenetic metabolite to promote lipid synthesis under hypoxia. Nat Commun 7:11960

114. Howard BV (1977), Acetate as a carbon source for lipid synthesis in cultured cells, http://dx.doi.org/10.1016/0005-2760(77)90132-1

115. Chen R, Xu M, Nagati JS, et al (2015) The acetate/ACSS2 switch regulates HIF-2 stress signaling in the tumor cell microenvironment. PLoS One 10:e0116515

116. Bulusu V, Tumanov S, Michalopoulou E, et al (2017) Acetate Recapturing by Nuclear Acetyl-CoA Synthetase 2 Prevents Loss of Histone Acetylation during Oxygen and Serum Limitation. Cell Rep 18:647–658

117. Mews P, Donahue G, Drake AM, et al (2017) Acetyl-CoA synthetase regulates histone acetylation and hippocampal memory. Nature 546:381–386

118. Liu X, Cooper DE, Cluntun AA, et al (2018) Acetate Production from Glucose and Coupling to Mitochondrial Metabolism in Mammals. Cell 175:502–513.e13

119. Kori Y, Sidoli S, Yuan Z-F, et al (2017) Proteome-wide acetylation dynamics in human cells. Sci Rep 7:10296

120. Schölz C, Weinert BT, Wagner SA, et al (2015) Acetylation site specificities of lysine deacetylase inhibitors in human cells. Nat Biotechnol 33:415–423

121. Huang Z, Zhang M, Plec AA, et al (2018) ACSS2 promotes systemic fat storage and utilization through selective regulation of genes involved in lipid metabolism. Proc Natl Acad Sci U S A 115:E9499–E9506

122. Fan J, Krautkramer KA, Feldman JL, Denu JM. (2015) *Metabolic regulation of histone post-translational modifications*. ACS Chem. Biol. 10(1):95-108

CHAPTER 2: SITE-SPECIFIC LYSINE ACETYLATION STOICHIOMETRY ACROSS SUBCELLULAR COMPARTMENTS*

Anastasia J Lindahl, Alexis J Lawton, Josue Baeza, James A Dowell, John M Denu

Author contributions: A.J.L, J.A.D, and J.M.D designed research. A.J.L. and A.J.L performed experiments and analyzed data. A.J.L wrote the manuscript and A.J.L, J.B. J.A.D and J.M.D reviewed and edited the manuscript.

Portions of this chapter were published as a first author methods book chapter in Methods in Molecular Biology. (2019) Site-Specific Lysine Acetylation Stoichiometry Across Subcellular Compartments. Methods Mol Biol 1983:79–106

2.1 Abstract

Post-translational modifications of proteins control many complex biological processes, including genome expression, chromatin dynamics, metabolism, and cell division through a language of chemical modifications. Improvements in mass spectrometry-based proteomics have demonstrated protein acetylation is a wide-spread and dynamic modification in the cell, however many questions remain on the regulation and downstream effects, and an assessment of the overall acetylation stoichiometry is needed. In this chapter, we describe the determination of acetylation stoichiometry using data-independent acquisition mass spectrometry to expand the number of acetylation sites quantified. However, the increased depth of data-independent acquisition is limited by the spectral library used to deconvolute fragmentation spectra. We describe a powerful approach of subcellular fractionation in conjunction with offline prefractionation to increase the depth of the spectral library. This deep interrogation of subcellular compartments provides essential insights into the compartment-specific regulation and downstream functions of protein acetylation.

2.2 Introduction

Post-translational modification of proteins is a mechanism of controlling many complex biological processes, including genome expression, chromatin dynamics, metabolism, and cell division. Reversible phosphorylation was the first modification to be well studied and demonstrated to have widespread regulatory effects ***(1–3)***. Many studies have contributed to the identification of other post-translational modifications, including protein acetylation and more recently other protein acylations ***(4–16)***. Protein acetylation was first characterized on histone proteins and has been well studied in the regulation of gene expression and chromatin dynamics ***(17–20)***. More recent studies have found acetylation sites on proteins in compartments throughout the cell, investigating the functional outcomes of protein acetylation ***(15)***. Advancements in mass spectrometry-based proteomics have led the widespread identification of protein acetylation. However for the majority of the acetylation sites identified thus far, their biological effects and their mechanism of regulation of these acetylation events has remained unknown ***(4–16, 21–35)***.

Protein acetylation is a reversible enzymatic reaction, with the addition of an acetyl group on the ε-amino group of lysine residues catalyzed by a lysine acetyltransferase and the removal catalyzed by a lysine deacetylase ***(36–38)***. Lysine acetyltransferases (KATs) contain two families of proteins, the MYST and GNAT families as well as the metazoan-specific CBP/p300 histone acetyltransferases, which utilize acetyl-CoA as the acetyl donor ***(39–43)***. Lysine deacetylases have four classes, separated by different mechanisms and co-substrates to perform deacetylation ***(44–46)***. Class I, II, and IV are canonical lysine deacetylases and utilize a Zinc ion and coordinated water to hydrolyze their acetyl-lysine substrates, whereas class III are NAD^+-dependent deacetylases called sirtuins, which couple the deacetylation reaction with hydrolysis

of the NAD^+ cofactor ***(45)***. Studies have shown lysine acetyltransferases and deacetylases may be regulated by alterations in cellular metabolism. These enzymes are sensitive to changes in concentration of acetyl-CoA and NAD^+, the cellular metabolites that are used as co-substrates, and enzymatic activity may be regulated by altering the availability of co-substrates ***(9, 10, 47–56)***.

Studies investigating reversible protein acetylation have explored protein acetylation in the context of metabolism and the response to changes in concentration of the acetyl donor acetyl-CoA ***(56–58)***. Particularly, the metabolic enzyme acetyl-CoA synthetase in both bacteria and mammals was found to be acetylated on a single conserved lysine residue within its active site, rendering the enzyme inactive. The enzyme is restored to full activity through deacetylation by the sirtuin proteins, a family of conserved proteins which coordinate many pathways within metabolism ***(59–61)***. Acetylation also plays an important regulatory role in the nucleus, mitochondria, and endoplasmic reticulum, influencing protein-DNA interactions of histones and DNA to promote transcription, metabolic activity and flux within mitochondria, and protein folding and secretion in the endoplasmic reticulum ***(17, 21, 25, 62, 63)***. Proteins within the nucleus and the cytosol have been characterized as substrates of histone acetyltransferases (HATs), particularly the undiscriminating enzymes CBP and p300, which themselves are regulated by reversible acetylation ***(64–68)***. Similarly to kinase signaling cascades regulated by phosphorylation, the post-translational regulation, including the auto-acetylation, of histone modifying complexes regulates their activity on histones creating signal amplification in the nucleus ***(69, 70)***. Alternatively, within the mitochondria, no lysine acetyltransferase has been identified, with active investigation into the roles of non-enzymatic acetylation ***(71–75)***.

Currently, acetylation of proteins has been shown to regulate protein-protein interactions, protein stability, localization, and enzymatic activity. The most well-known example of protein acetylation is histone acetylation, regulating gene expression and chromatin dynamics and considered to be an epigenetic mark ***(17)***. Histone acetylation can occur on the same histone tail, different tails within the same nucleosome, or adjacent nucleosomes; giving rise to a highly complex set of substrates for recognition by histone modifying enzymes and other chromatin associated proteins ***(76–79)***. Histone acetylation regulates gene expression through a variety of mechanisms including increased specificity, affinity, localization, or release of inhibition; and leads to upregulation of gene expression ***(77, 80–83)***. Beyond histone acetylation, the function of lysine acetylation has been characterized for transcription factors, metabolic enzymes, chaperone proteins, and cytoskeletal proteins ***(9, 10, 84–89)***. However, recent studies enabled by advances in mass spectrometry-based proteomics indicate lysine acetylation occurs broadly within cells, raising questions about function and regulatory mechanisms controlling lysine acetylation throughout the cell ***(4–16)***.

Initial mass spectrometry-based proteomics results increased the number of identified acetylation sites, however such studies fell short of being able to comprehensively quantify stoichiometry of acetylation in an entire proteome. Rather than reporting relative fold change, we recently reported a data dependent acquisition (DDA) method to quantify acetylation stoichiometries, which provides additional information for interpreting biological significance ***(24)***. An example of the biological importance of understanding stoichiometry comes from the case of mitochondrial acetylation. Relative fold-change of acetylation stoichiometry characterized in response to alterations in diet were found to be large, resulting in expectations of high acetylation stoichiometry ***(90, 91)***. However, stoichiometry measurements suggested the majority of

acetylation sites within the mitochondria had very low stoichiometry with a median occupancy of ≤2% stoichiometry, with a small subset of sites having high stoichiometry ***(92, 93)***. This more in-depth information given by stoichiometry assists with interpretation of biological function, particularly the differences between high and low stoichiometry when considering how acetylation results in loss-of-function or gain-of-function. Furthermore, the observation of low stoichiometry broadly in the mitochondria raised the question whether acetylation acts independently or acts in an additive fashion across many proteins in a pathway ***(92)***.

Data dependent methods used in mass spectrometry-based proteomics are stochastic in nature. The selection of a peptide for MS/MS fragmentation is determined by its overall abundance during an MS run ***(94)***. In contrast, data independent acquisition (DIA) is a method that continuously collects fragmentation spectra from all peptides using predefined sequential mass-to-charge windows, thus increasing the quantification of light and heavy acetyl containing peptides captured in our analysis ***(95, 96)***. This analysis addresses the limitation of missing data stemming from stochastic data collection when using DDA. The DIA approach results in the increase in the identification and quantitation of lysine stoichiometry by increasing the sample depth to quantifying both non-isotopically and isotopically labeled peptides. Performing DIA analysis requires a spectral library of MS2 fragmentation spectra from DDA analysis to deconvolute the DIA MS2 spectra for identification and quantification. To increase depth of peptide coverage within the spectral library, we generated libraries utilizing orthogonal separation approaches, previously shown to increase sampling depth of DDA analysis ***(97–99)***. In this chapter, we describe methods of subcellular organelle enrichment and chemical labeling of lysine residues coupled with data-independent acquisition mass spectrometry to quantify site-specific lysine acetylation stoichiometry.

Figure 2-1. DIA acetylation stoichiometry workflow.

(A) Workflow for measuring acetylation stoichiometry from whole cell lysate. **(B)** Diagram representing DIA quantitation of precursor and fragment ions across the elution profile. Peak areas for precursor and fragment ions are quantified. **(C)** Diagram illustrating MS2 spectra for the Histone H3 peptide containing lysine K18Ac and K23Ac. The fragments b2-b3 are specific for K18 and y4-y8 are specific for K23. The fragments b6-b8 are ambiguous as they contain K18Ac and K23Ac, while the fragments y1-y3 contain no acetyl lysine information. Adapted from Josue Baeza ***(107).***

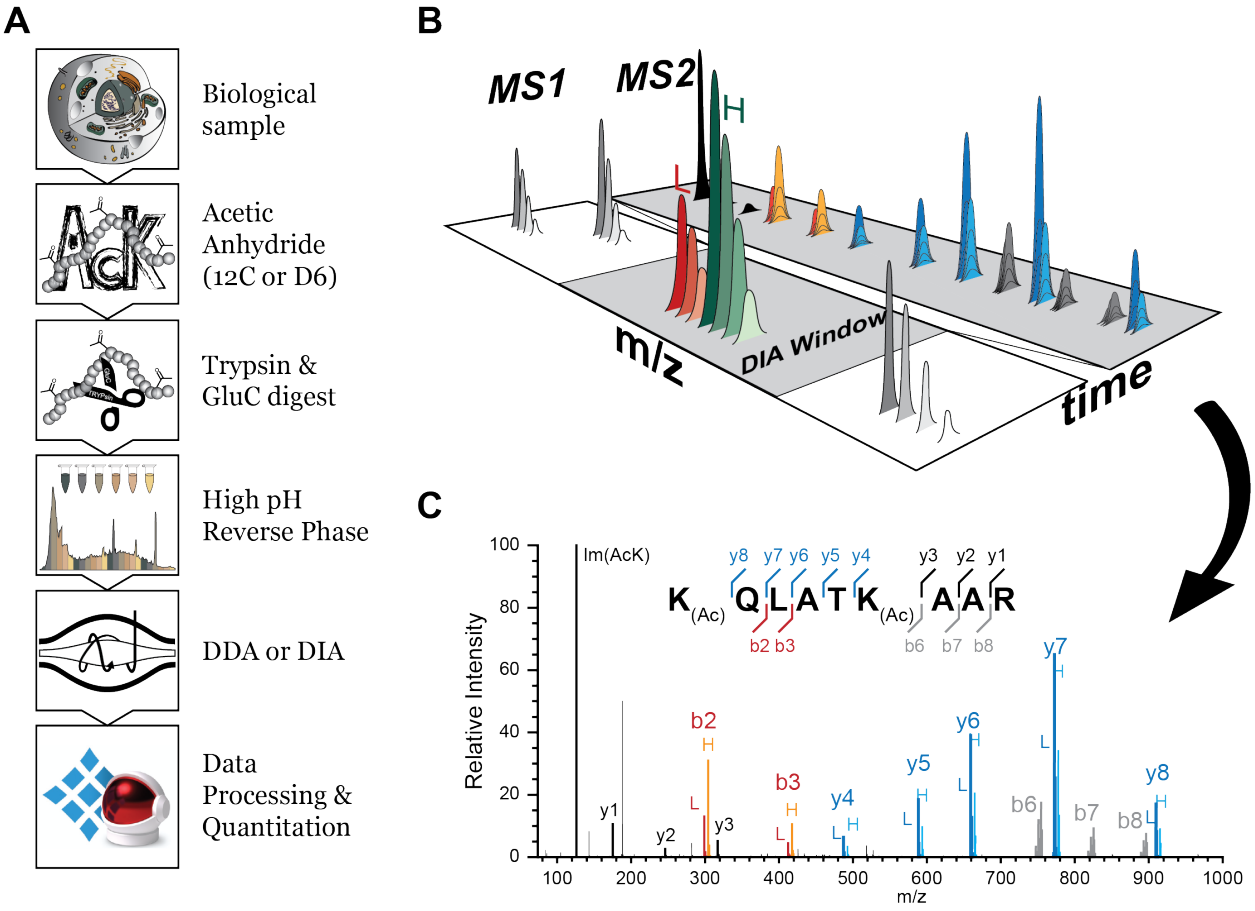

2.3 Methods

2.3.1 Methods for Sample Preparation and Subcellular Fractionation

2.3.1.1 General Experimental Design

Our DIA approach results in an increase in the identification and quantitation of lysine stoichiometry over other shotgun based methods of quantifying acetylation stoichiometry (Figure 2-2). Performing DIA analysis requires a spectral library of MS2 fragmentation spectra from DDA analysis to deconvolute MS2 spectra. Here we detail generation of spectral libraries from analysis of a non-isotopically labeled DDA analysis with *in silico* generation of the heavy acetyl-lysine label. This approach creates a library with all possible isotopically labeled peptide combinations, many of which may be too low in abundance generate experimental peptide fragmentation spectra. Utilizing the experimentally produced library with *in silico* generation of heavy deuterated label, we quantify both the light endogenous non-isotopic acetylation and the heavy deuterium labeled acetylation, derived from the *in vitro* chemical labeling reaction, to calculate site-specific stoichiometry across the proteome.

Figure 2-2. Outline of Acetylation Stoichiometry Protocol

Adapted from Josue Baeza.

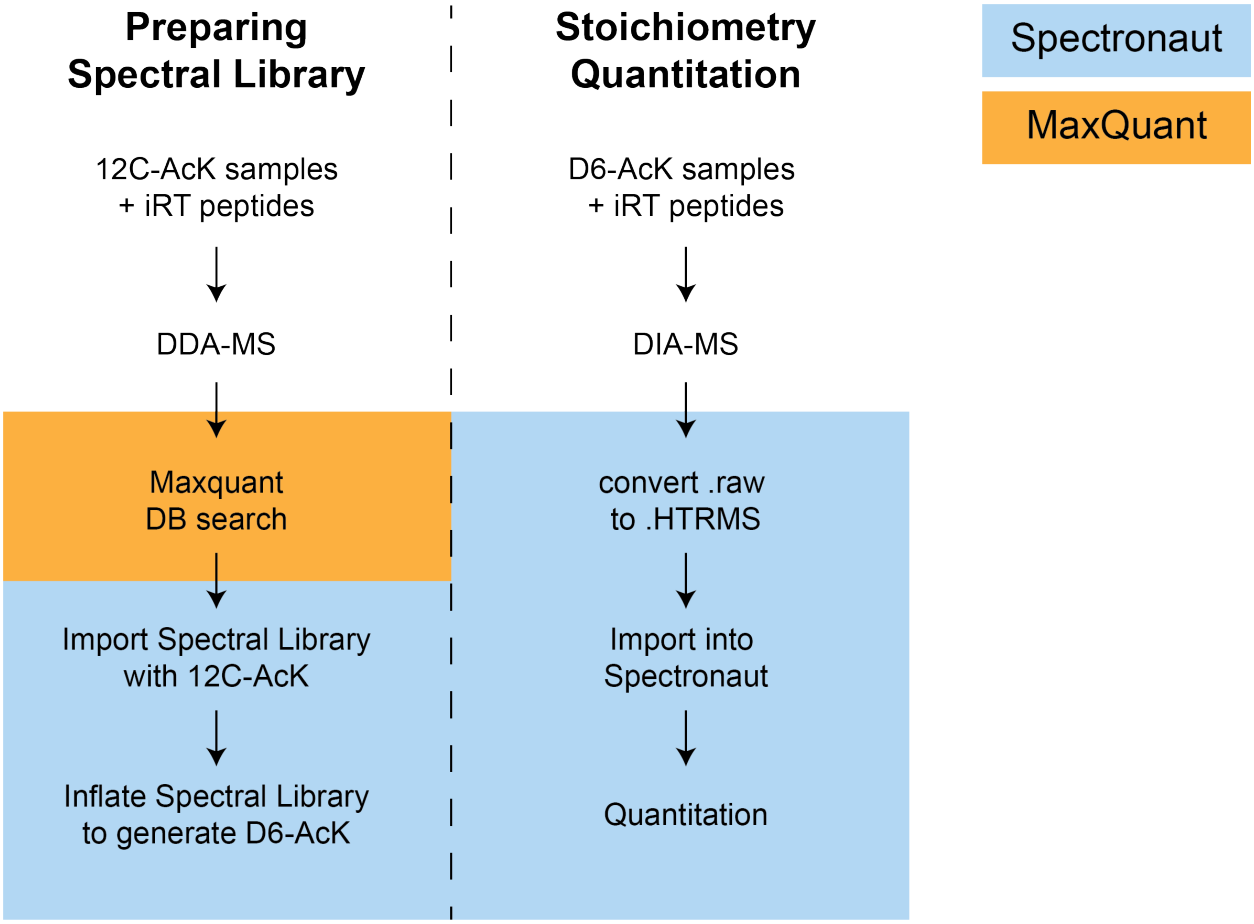

2.3.1.2 Methods for Cell Culture and Serum Stimulation

Protein post-translational modifications, such as acetylation, provide cells with an ability to rapidly modulate the activities of existing proteins within the cells, rather than through the slower processes of protein synthesis and degradation ***(100, 101)***. To adequately capture the relatively rapid process of dynamic acetylation changes in response to stimuli in cell culture, time points such as 0, 1, 2, and 4 hours will be examined. These times are longer than the rapid metabolic response, however they were shorter than previously experimentally determined average protein half-life, ideally capturing dynamic changes of protein acetylation through active acetylation and deacetylation rather than passive changes through protein synthesis or turnover ***(102)***. To examine the dynamic changes in acetylation stoichiometry, we utilized a time course to quantify the alterations of acetylation over time in response to growth factor stimulation of MCF7 cells in tissue culture. Generation of samples for the spectral library requires at least 50 μg of protein for offline prefractionation of labeled and digested peptides and subsequent LC-MS/MS analysis. As demonstrated in Figure 2-3, utilizing subcellular fractionation, focusing on chromatin protein (shown in green) and offline prefractionation (shown in light blue) to create a spectral library increased the depth of protein, peptide, and acetyl site coverage as shown by the increased identifications observed in each of these categories. Furthermore, generating a spectral library with subcellular fractionation in combination with offline prefractionation (shown in dark blue) resulted in increased depth of coverage of subcellular organelles, beyond the depth of coverage of offline prefractionation alone, with a particular increase in depth on the peptide level (Figure 3-3B).

To perform whole cell lysate analysis, a single 10 cm plate provides sufficient material for analysis. Alternatively, to perform analysis on subcellular compartments more starting

material was required, utilizing a 70 - 80% confluent 15 cm plate. This protocol has been readily adapted to performing analysis on alternate cell types, as well as mouse tissue such as brain and liver. For tissue utilizing approximately 10-15 mg of starting material for whole cell lysate and 40-50 mg for subcellular fractionation to obtain adequate yields.

Figure 2-3. Data Dependent Acquisition Spectral Library Quality and Depth Analysis. An analysis of the spectral libraries generated from a Single Injection Whole Cell Lysate (WCL), a Single Chromatin Isolation (utilizing subcellular fractionation without offline prefractionation), a Fractionated WCL utilizing offline prefractionation, Fractionated Chromatin Isolation utilizing offline prefractionation on a subcellular fractionated chromatin isolation, a Fractionated WCL utilizing offline prefractionation with a single chromatin isolation (utilizing subcellular fractionation without offline prefractionation), and the Fractionated Chromatin Isolation and Fractionated WCL utilizing together utilizing offline prefractionation, on both whole cell lysate and a subcellular fractionated chromatin sample to examine the effects of library preparation on the counts of **A)** Acetyl Sites, **B)** Acetyl Peptides, **C)** Acetyl Proteins, **D)** MS2 Fragments, **E)** Total peptides, and **F)** Total proteins.

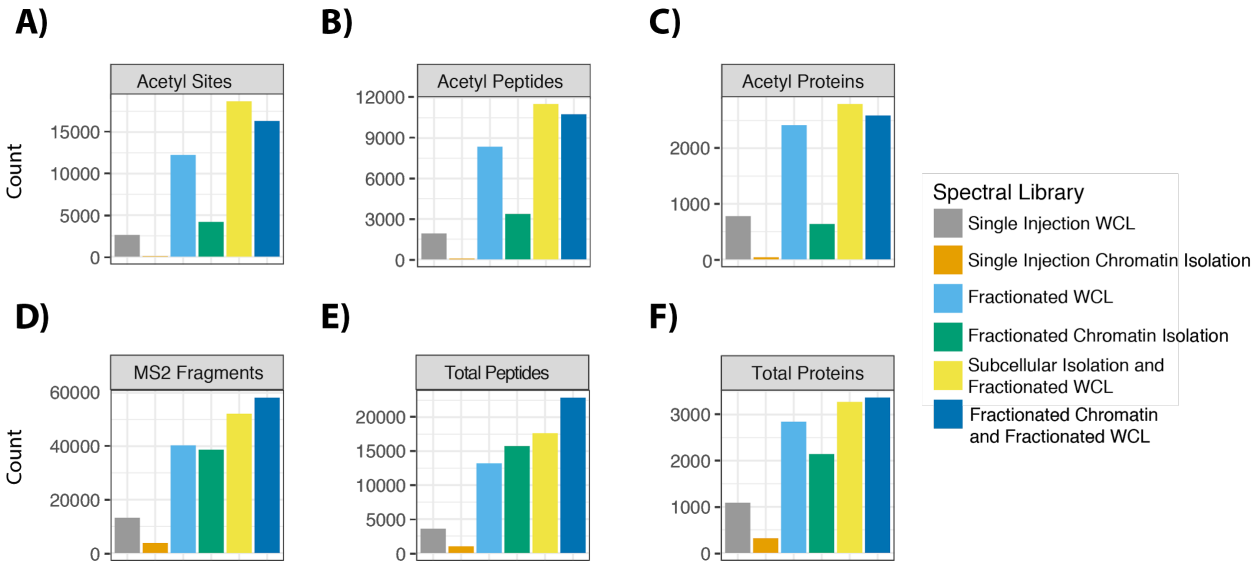

Figure 2-4. Subcellular Localization Depth and Quality Analysis of Data Dependent Acquisition Spectral Libraries.

An analysis of the spectral libraries generated from a Single Injection Whole Cell Lysate (WCL), a Single Chromatin Isolation (utilizing subcellular fractionation without offline prefractionation), a Fractionated WCL utilizing offline prefractionation, Fractionated Chromatin Isolation utilizing offline prefractionation on a subcellular fractionated chromatin isolation, a Fractionated WCL utilizing offline prefractionation with a single chromatin isolation (utilizing subcellular fractionation without offline prefractionation), and the Fractionated Chromatin Isolation and Fractionated WCL utilizing together utilizing offline prefractionation, on both whole cell lysate and a subcellular fractionated chromatin sample to examine the effects of library preparation on the counts of **A)** Proteins and **B)** Peptides in a subcellular localization specific manner.

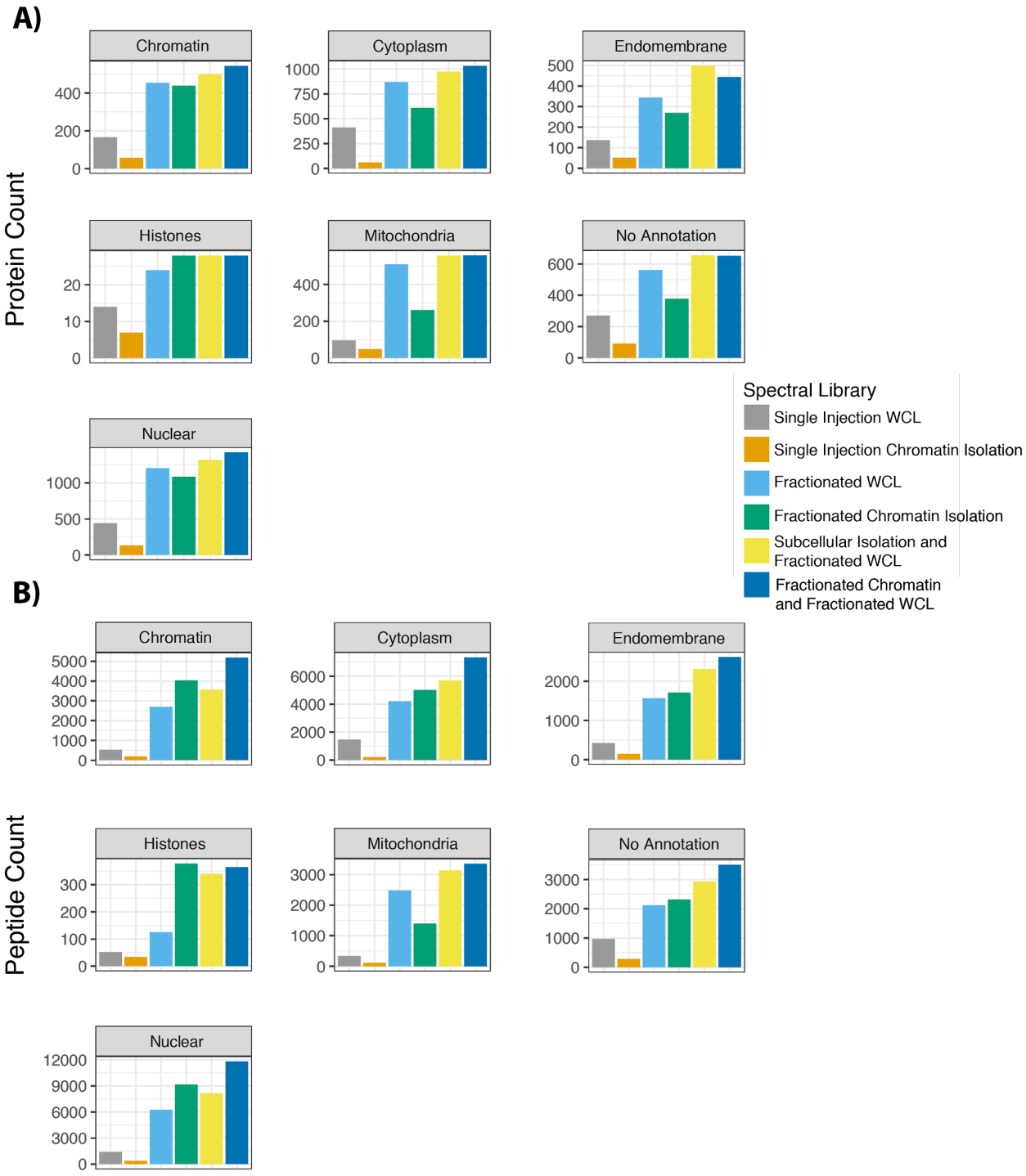
A)
Protein Count
Chromatin
Cytoplasm
Endomembrane
Histones
Mitochondria
No Annotation
Nuclear
B)
Peptide Count
Chromatin
Cytoplasm
Endomembrane
Histones
Mitochondria
No Annotation
Nuclear
Spectral Library
Single Injection WCL
Single Injection Chromatin Isolation
Fractionated WCL
Fractionated Chromatin Isolation
Subcellular Isolation and Fractionated WCL
Fractionated Chromatin and Fractionated WCL

2.3.1.3 Preparing Whole Cell Lysate (without subcellular fractionation)

1. Resuspend cell pellet in 200 mM Ammonium Bicarbonate with protease and HDAC inhibitors: 10μg/mL leupeptin, 10μg/mL aprotinin, 100 μM phenylmethanesulfonyl fluoride (PMSF), 1 mM sodium butyrate, 4 μM trichostatin A, 10 mM nicotinamide, and 1 mM DTT.
2. Lyse cells using mechanical force via sonication. Using a tip sonicator, sonicate the sample on 5 seconds on-off pulse for 30 seconds at 20 % amplitude. Avoid chemical lysis when possible for mass spectrometry sample preparation. If chemical lysis is needed for a specific sample, follow-up protein isolation with a precipitation protocol such as acetone or chloroform methanol precipitation to minimize detergent contamination of downstream analyses. For tissue samples, first homogenize the tissue sample previous to tip sonication to disrupt subcellular organelles using a dounce homogenizer with 20 strokes loose pestle and 20 strokes tight pestle. Let the samples stand on ice for 10 min to complete hypotonic lysis. For tissue analysis, filter the homogenate through a cell strainer to remove debris.
3. Measure protein concentration using a Bicinchoninic Acid assay (BCA) (Invitrogen).

2.3.1.4 Isolating Subcellular Fractions from Cell Culture or Tissue Samples

1. Performing subcellular fractionation will increase coverage of acetyl sites within a compartment of interest (Figure 2-4). Resuspend cell pellet in 800 μL of hypotonic lysis buffer (10 mM Tris-HCl, 10 mM NaCl, 3 mM $MgCl_2$ at pH 7.4) in a 1 mL dounce homogenizer. Mechanically lyse cells by homogenizing samples with 20 strokes loose pestle and 20 strokes tight pestle. Let the samples stand on ice for 10 min to complete

hypotonic lysis. For tissue analysis, filter the homogenate through a cell strainer to remove debris.

2. Centrifuge homogenate at 800 x g for 5 minutes at 4 °C to pellet crude nuclear fraction. Supernatant contains cytoplasm and mitochondria. To isolate mitochondria, centrifuge supernatant at 10,000 x g for 10 minutes at 4 °C which pellets the mitochondria, while the supernatant contains cytoplasmic proteins. Resuspend pellet with 500 µL buffer and repeat centrifugation (Figure 2-5).
3. To isolate chromatin proteins from the crude nuclear fraction, wash crude nuclear fraction with 2 mL cold lysis buffer and centrifuge at 800 x g for 5 minutes at 4 °C. Repeat wash steps again with lysis buffer and then PBS (Figure 2-5).
4. Resuspend nuclear pellet in 500 µL of nuclear lysis buffer (10 mM Tris-HCl 10 mM NaCl 3 mM $MgCl_2$ 0.2 mM EDTA at pH 7.4) with protease and histone deacetylase inhibitors added immediately before use. Incubate for 15 minutes on ice with vortexing every 5 minutes.
5. Centrifuge at 16,000 x g for 5 minutes. Pellet is chromatin with histones. Resuspend pellet with lysis buffer and centrifuge at 3000 x g and keep pellet.
6. To isolate chromatin proteins from the highly abundant histones proteins which dominate the proteins observed from the nucleus, resuspend chromatin pellet in 300 µL of 150 mM salt in the lysis buffer (10 mM Tris-HCl 3 mM $MgCl_2$ pH 7.4) with protease and histone deacetylase inhibitors added immediately before use. Let stand on ice for 15 minutes with vortexing every 5 minutes. Centrifuge at 3000 x g for 5 minutes and keep pellet for further extraction (Figure 2-3). Supernatant can be kept for gel electrophoresis if you wish.

7. Resuspend in 300 µL 450 mM salt in the lysis buffer (10 mM Tris-HCl 3 mM $MgCl_2$ pH 7.4) with protease and histone deacetylase inhibitors added immediately before use. Let stand on ice for 15 minutes with vortexing every 5 min. Centrifuge at 3000 x g for 5 min. Supernatant contains chromatin bound proteins (Figure 2-3). Keep pellet for further extraction of histones if desired, following the previously described acid extraction of histone and subsequent mass spectrometry histone post-translational modification profiling strategies ***(103, 104)***.
8. Perform a Bicinchoninic Acid assay (BCA) (Invitrogen) on each of the subcellular compartments of interest for downstream analysis to measure protein concentration.

Figure 2-5. Method of Chromatin Isolation and Salt Fractionation.

Our method utilizes sample homogenization and cell lysis to pellet nuclei, removal of the perinuclear envelope, lysis of the core nuclei, and subsequent salt washes and fractionation of pelleted chromatin.

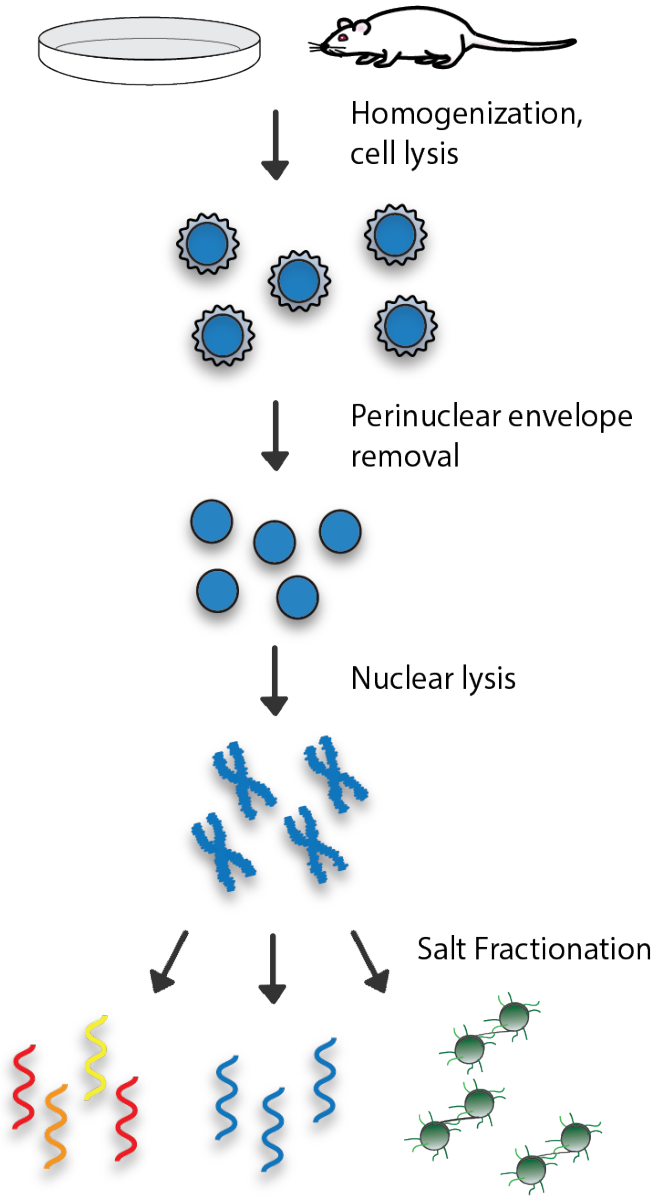

2.3.2 Sample Analysis

2.3.2.1 Chemical Acetylation

Our labeling approach leads to the acetylation of all lysines, whether non-isotopically acetylation from *in vivo* sources or deuterium labeled acetylation from our *in vitro* labeling reaction. Due to the chemical labeling approach, all lysines are modified with an acetyl group, either a non-isotopic acetyl group which is generated *in vivo* or deuterium labeled acetylation generated from the *in vitro* chemical labeling reaction. Proteolytic digestion by trypsin generates chemically identical light and heavy peptides which can be directly compared to determine the level of acetylation stoichiometry. Furthermore, the use of chemical labeling over modification enrichment strategies minimizes the amount of bias introduced to the sample preparation. It furthers the understanding of the dynamics of acetylation changes in comparison to the state of all lysines across the whole proteome, rather than only quantifying the ratio of acetylated lysines.

2.3.2.2 Acetic Anhydride Labeling and Digestion of Samples for Spectral Library

1. To prepare samples for the DDA analysis to generate the peptide spectra for the spectral library, pool protein from all of the samples for analysis. For example, when analyzing dynamic acetylation over time after serum stimulation in MCF7 cells, combine equal protein amounts of each condition (time point samples) up to 50 µg. The pooled samples should total to at least 50 µg for subsequent offline prefractionation and downstream LC-MS/MS analysis of the fractions.
2. To start with the same concentration in each of the mixed samples, dry down to 10µL using a speedvac.
3. Resuspend sample to 50 µL total volume using 8 M urea, 100 mM ammonium bicarbonate pH at 8.5 with 5 mM DTT in a 1.5 mL tube. Prepare the buffers and urea

fresh for each experiment. For subsequent labeling steps avoid buffers with free amine groups that would react with the acetic anhydride, affecting the labeling efficiency.

4. To denature the proteins place samples on Thermomixer C (Eppendorf), which has a heated lid to avoid condensation at 60 °C while mixing at 1000 RPM for 30 minutes.
5. Add 20 mM iodoacetamide to alkylate cysteine residues and incubate at 60 °C while mixing at 1000 RPM for 30 minutes on the Thermomixer C (Eppendorf).
6. To chemically acetylate unmodified lysine residues, add 2 µL of non-isotopic acetic anhydride to the samples, vortex, and incubate for 30 min, 60 °C 1000 RPM on the Thermomixer C (Eppendorf). For the spectral library samples, use non-isotopic acetic anhydride to chemically acetylate all lysine residues with the same label. In downstream processing, heavy acetylated peptide pairs will be generated *in silico.* This approach creates a spectral library with heavy and light pairs of all lysine containing peptides.
7. Add ~10 µL NH_4OH to bring the pH back up to ~8.0. Check the pH with a 0.5 µL spot on litmus paper and add more NH_4OH as necessary.
8. For complete labeling repeat the chemical labeling from steps 6 and 7, again using non-isotopically labeled acetic anhydride.
9. After the second round of chemical labeling, incubate samples at pH 8 for 20 minutes at 60 °C with 1000 RPM mixing on the Thermomixer C (Eppendorf) to hydrolyze any O-acetyl esters formed during the reaction.
10. Add 100 mM ammonium bicarbonate to bring the volume up to 200 µL to dilute the urea to a final concentration of 2 M. Trypsin digestion efficiency is reduced with urea levels above 2 M.

11. Add sequencing grade trypsin to a 1:100 ratio (trypsin:protein) and incubate from 4 hours to overnight at 37 °C mixing at 350 RPM on Thermomixer C (Eppendorf).
12. Add 100 mM ammonium bicarbonate to bring the volume up to 400 µL and the final concentration down to 1 M for the subsequent gluC digestion. GluC digestion efficiency is reduced with urea levels above 1 M.
13. Add gluC in a 1:100 (gluC:protein) ratio and incubate from 4 hours to overnight at 37 °C mixing at 350 RPM on Thermomixer C (Eppendorf). Additional digestion with GluC is necessary to digest labeled peptides to lengths amenable for LC-MS/MS analysis.
14. Quench the reaction by adding ~ 40 µL of acetic acid.

2.3.2.3 Prefractionation with High pH Reverse Phase Chromatography

A major challenge to performing stoichiometric acetyl lysine analysis is the lack of an enrichment step for lysines acetylated *in vivo.* Antibody based techniques increase acetyl lysine coverage by enriching for acetyl-peptides, thereby simplifying the complex mixture and increasing the sampling depth. Since our strategy does not involve an enrichment step, offline fractionation is used to reduce the proteomic complexity in order to increase the depth of coverage of acetyl lysine containing peptides. The advantage of this strategy is highlighted in Figure 2-3 and 2-4. To evaluate the increase in the depth of coverage within a spectral library, we examined the number of proteins, peptides, and fragment ions identified using a single sample whole cell lysate (whole cell lysate without offline prefractionation), a single sample chromatin isolation (utilizing subcellular fractionation without offline prefractionation), fractionated whole cell lysate utilizing offline prefractionation, and fractionated chromatin isolation utilizing offline prefractionation on a subcellular fractionated chromatin sample. These

approaches in combination, displayed in Figure 1, demonstrate the clear advantage in the depth of the spectral library generated using subcellular fractionation and offline prefractionation in conjunction.

1. To perform the offline prefractionation, we use high pH reverse phase (HPRP) chromatography for peptide separation. Resuspend the labeled and digested peptides in ~2mL of HPRP solvent A (100 mM Ammonium Formate pH = 10) and separate by high pH reverse phase chromatography on a Waters-C18 column (5µm, 130 Å, 250 x 2.1mm) with a Shimadzu LC-20AT HPLC system with a 60 minute gradient of two solvents, solvent A is 100 mM Ammonium formate, pH 10 and solvent B is ACN. The gradient is a 60 minute gradient, starting at 2% solvent B for 30 minutes, and then a linear gradient from 2% to 90 % solvent B with a flow rate of 400 µL/minute. Fractions of 0.7 mL are collected from 30 to 72 minutes in the gradient, with 24 collected in total. Peptides are detected by a UV detector at 280 nm.
2. Samples are dried down using the speedvac concentrator, to concentrate the fractions until they reach a small enough volume to be combined. The following HPRP fractions are combined using a concatenated strategy to form six final fractions:

1, 7, 13, 19

2, 8, 14, 20

3, 9, 15, 21

4, 10, 16, 22

5, 11, 17, 23

6, 12, 18, 24

3. These recombined 6 fractions are dried down completely and then resuspend in 100 µL of 10% acetic acid for subsequent desalting and cleanup.

2.3.2.4 Desalting Prior to MS Analysis

Sample preparation for MS analysis requires desalting of peptide samples as well as removal of hydrophilic molecules. We generate our own desalting tips for our peptide cleanup based on a previously published protocol ***(105)***. The desalting tips we make have the added benefit of being cost efficient as well as having minimal sample loss. The desalting tips are made with C-18 disks (Empore) in p200 pipette tips and act as spin columns in 1.5 mL microcentrifuge tubes.

1. The desalting tip must first be activated. To activate the C-18 disks, add ~50 µL of methanol to the desalting tip and centrifuge at 1000 x g for 1 minute.
2. To condition the desalting tip, add ~50 µL of the elution buffer, 0.5% acetic acid in 80% ACN in LC-MS grade H_2O, to the desalting tip and centrifuge at 1000 x g for 1 minute.
3. To equilibrate the desalting tip, add ~50 µL of the wash buffer, 0.5% acetic acid in LC-MS grade H_2O, to the desalting tip and centrifuge at 1000 x g for 1 minute.
4. Load the sample in the desalting tip and centrifuge at 1000 x g until the sample volume has run completely through the desalting tip. The peptides are now bound to the C-18 disks within the desalting tip.
5. Wash the sample by adding ~50 µL of the wash buffer, 0.5% acetic acid in LC-MS grade H_2O, to the desalting tip and centrifuge at 1000 x g for 1 minute.
6. Switch the desalting tip to a new tube and elute the peptides by adding ~50 µL of the elution buffer, 0.5% acetic acid in 80% ACN in LC-MS grade H_2O, to the desalting tip and centrifuge at 1000 x g for 1 minute.

7. Dry down the sample using the speedvac.
8. Prepare the samples for MS analysis by resuspending in the sample diluent of 2% ACN, 0.1% formic acid in LC-MS grade H_2O. For analysis using Spectronaut software, add the internal retention time standards required, the Biognosys iRT kit, as instructed ***(106)***.

2.3.2.5 LC-MS/MS Data Dependent Acquisition (DDA) Analysis of Spectral Library Samples

Our method to analyze site-specific lysine acetylation by mass spectrometry-based proteomics utilizes a Thermo Q-Exactive Orbitrap mass spectrometer coupled to a Dionex Ultimate 3000 RSLC nano UPLC with a Waters Atlantis reverse phase column (100 um x 150 mm). The mobile phases contain 0.1% formic acid in HPLC grade H_2O as solvent A and 0.1% formic acid in HPLC grade ACN as solvent B. The sample is eluted over a linear gradient of 2-40% B at a flow rate of 700 nL/minute over a 60 minute gradient. The peptides are introduced into the mass spectrometer by nanoelectrospray ionization. The mass spectrometer performs in positive mode with a survey scan with a 70 000 resolution, AGC of 1E6, max fill time 250 ms, and a scan range of 350-2000 m/z. The data-dependent MS/MS analysis is performed with a resolution of 17 500, AGC of 1E5, max fill time 100 ms, isolation window of 2.0 m/z and a loop count of 10. The voltage of the source is set at 2.3 kV and the capillary temperature is 250 °C ***(107)***.

2.3.2.6 Analyzing Site-Specific Acetylation Stoichiometry using Isotopic Labeling and Data-Independent Acquisition Analysis

Utilizing chemical acetylation labeling strategy for stoichiometry determination of acetyl lysine requires heavy labeling from an *in vitro* labeling reaction, as detailed in this chapter. The

isotopic label used should have a mass shift that can be easily observed in the MS2 fragmentation pattern, ideally outside of the isotopic envelope accurate determination of acetylation stoichiometry. We choose to use deuterated acetic anhydride $(CD_3CO_2)O$, for our *in vitro* labeling reaction, which results in the 3 Da mass shift at the acetylation site ***(107)***. Furthermore, to account for the overestimation of stoichiometries at a high abundance with low heavy labeling, we corrected for the natural isotopic abundance of the light acetyl peptide by subtracting the natural isotopic abundance M+3 isotopic peak from the heavy deuterated acetyl M+0 isotopic peak based upon calculations of natural isotopic abundance distribution of the fragment ion. Utilizing deuterated acetic anhydride for labeling to generate a 3 Da mass shift in conjunction with MS2 fragment based in conjunction with MS2 fragment ion based quantification of acetyl lysine stoichiometry significantly reduces the interference between the light and heavy acetylated fragment ions, increasing the accuracy and reducing the overestimation of stoichiometry determination ***(107)***. These problems were discussed and tackled by moving towards other forms of quantification of the lysine stoichiometry using the MS2 fragments. This latest step forward in methodology to quantify stoichiometry of lysine acetylation has been described here as well as by others, utilizing data-independent acquisition to increase the sampling depth of a sample and the number of acetylation sites quantified. ***(107)***

2.3.2.7 Deuterated Acetic Anhydride Labeling and Digestion of Samples

15. To start with the same concentration in each of the samples dry down using a speedvac.
16. Resuspend sample to 50 μL total volume using 8 M urea, 100 mM ammonium bicarbonate with 5 mM DTT, with the pH at 8.5 in a 1.5 mL tube. Prepare the buffers

fresh for each experiment. For subsequent labeling steps avoid buffers with free amine groups that would react with the acetic anhydride.

17. To denature the proteins place samples on Thermomixer C (Eppendorf), which has a heated lid to avoid condensation at 60 °C while mixing at 1000 RPM for 30 minutes.
18. Add 40 mM iodoacetamide to alkylate cysteine residues and incubate at 60 °C while mixing at 1000 RPM for 30 minutes on the Thermomixer C (Eppendorf).
19. To chemically acetylate unmodified lysine residues, add 2 μL of deuterated acetic anhydride to the samples, vortex, and incubate for 30 min, 60 °C, 1000 RPM on the Thermomixer C (Eppendorf).
20. Add ~10 μL NH_4OH to bring the pH back up to ~8.0. Check the pH with a 0.5 μL spot on litmus paper and add more NH_4OH as necessary.
21. For complete labeling repeat the chemical labeling from steps 6 and 7, again using deuterated acetic anhydride.
22. After the second round of chemical labeling incubate sample at pH 8 for 20 min at 60 °C with 1000 RPM mixing on the Thermomixer C (Eppendorf) to hydrolyze any O-acetyl esters formed during the reaction.
23. Add 100 mM ammonium bicarbonate to bring the volume up to 100 μL and the final concentration down to 2M.
24. Add sequencing grade trypsin to a 1:100 ratio (trypsin:protein) and incubate from 4 hours to overnight at 37 °C mixing at 350 RPM on Thermomixer C (Eppendorf). Trypsin will
25. Add 100 mM ammonium bicarbonate to bring the volume up to 200 uL and the final concentration down to 1M for the subsequent gluC digestion. GluC digestion efficiency is reduced with urea levels above 1 M.

26. Add gluC in a 1:40 (gluC:protein) ratio and incubate from 4 hours at 37 °C mixing at 350 RPM on Thermomixer C (Eppendorf). Additional digestion with GluC is necessary to digest labeled peptides to lengths amendable for LC-MS/MS analysis.
27. Quench the reaction by adding ~ 40 µL of acetic acid.

2.3.2.8 Desalting Prior to MS Analysis

Perform peptide desalting as detailed in 2.3.2.4, following steps 1-9 as written.

2.3.2.9 LC-MS/MS DIA Data Analysis

Our method to quantify acetylation stoichiometry uses a Thermo Q-Exactive Orbitrap mass spectrometer coupled to a Dionex Ultimate 3000 RSLC nano HPLC with a Waters Atlantis reverse phase column (100 um x 150mm). The mobile phases contain 0.1% formic acid in HPLC grade H_2O as solvent A and 0.1% formic acid in HPLC grade ACN as solvent B. The sample is eluted over a linear gradient of 2-40% B at a flow rate of 700 nL/minute over a 60 minute gradient. The peptides are introduced into the mass spectrometer by nanoelectrospray ionization. The mass spectrometer performs in positive mode with a survey scan with a 70,000 resolution, AGC of 1E6, max fill time 100 ms, and a scan range of 400-1000 m/z. The survey scan was followed 30 DIA scans in profile mode with a resolution of 35,000, AGC 1E6, 20 *m/z* window, and NCE of 25 to balance the frequency of b-ions, y-ions, and the number of PSMs to gain higher fragmentation coverage for MS2 quantitation, particularly important for site-specific quantitation of multiple lysine containing peptides ***(107)***. The voltage of the source is set at 2.3 kV and the capillary temperature is 250 °C .

2.4 Data Analysis and Quantification Acetylation Stoichiometry

2.4.1 Generating a Spectral Library

Analyzing acetylation stoichiometry using DIA requires a spectral library containing all combinations of light and heavy acetyl fragment ions. In this study, we use MaxQuant to perform a database search of the completely light acetylated samples to generate a spectral library followed by the subsequent in silico generation of the heavy labeled fragment ions ***(107)***. To perform DDA data analysis, we use the openly available MaxQuant software package to perform our database searches and generate our library within the Spectronaut Professionals software (Biognosys) ***(108–112)***.

1. Perform a database search in MaxQuant to identify peptides present in the DDA samples analyzed. Add the modifications for the non-isotopically labeled "Acetyl (K)" and the heavy deuterated "Acetyl D3 (K)" to the database search. The "Acetyl (K)" modification should be specified as a modification on lysines (K) be located anywhere except the C terminus of the peptide, and contains 2 carbons, 2 hydrogens, and one oxygen, which has a mass of 42 Da. The "Acetyl D3 (K)" modification should be specified as a modification on lysines (K) be located anywhere except the C terminus of the peptide, and contains 2 carbons, 3 deuterium, one oxygen, and the loss of one hydrogen, which has mass of 45 Da. Assign "Acetyl (K)" and "Oxidation (M)" modifications as variable modification through the sample with "Carbamidomethyl (C)" as a fixed modification ***(108–112)***. Allow for up to 5 modifications and 5 missed cleavages by Trypsin and GluC due to the acetyl labeling blocking all lysine digestion sites within the peptide.
2. For the FASTA file used, you will need to configure a file that contains the internal retention time standard peptides if utilizing the Biognosys iRT kit by adding the

Biognosys iRT sequence to the proteome of the organism of interest. In our case, we added the Biognosys iRT sequence to the human SwissProt sequences FASTA file ***(106)***.

3. To prepare a library in Spectronaut (Biognosys), generate the library from the MaxQuant output utilizing the same modified FASTA file as a protein database. This will generate the spectral library file of the non-isotopically labeled acetyl peptide spectral library.
4. To add the deuterated heavy acetyl label *in silico*, export the library file for subsequent analysis.
5. Load the library file into the Spectronaut Library Modifier, and select the modification you would like to add, in this case "Acetyl D3 (K)" and which modification it pairs with, the "Acetyl (K)", from the existing library. Export the *in silico* inflated spectral library file .
6. Import the *in silico* inflated library file into Spectronaut (Biognosys) to utilize the inflated library for downstream analysis.
7. Alternatively to using Spectronaut (Biognosys), the open source Skyline proteomics software can be used to generate a spectral library and analyze DIA data. In the case of Skyline, the heavy label can be generated within the modification settings, by adding the isotope label of deuterium to the "Acetyl (K)" modification settings ***(113)***.

2.4.2. Analyzing DIA Mass Spectrometry Data

2.4.2.1 Analysis of the raw DIA sample analysis

1. Add raw files of the deuterated acetic anhydride labeled samples acquired with the DIA sample analysis.

2. Pair the samples with the inflated spectral library to be used for the search, identification and quantification of the peptides.
3. Set the identification Q-value cut off at 0.1 and utilize the earlier generated FASTA file, containing the iRT sequence if using Spectronaut (Biognosys).
4. Export the report, including the modified peptide sequence, the unmodified peptide sequence, the fragment ion sequence, and the peak area of the fragment ions to quantify the acetyl stoichiometry for lysine containing peptides. Also include data quality measures, such as the peptide identification Q value for later filtering by data quality.

2.4.2.2 Quantification of Site-Specific Acetyl Lysine Stoichiometry

The quantification of site-specific lysine acetyl stoichiometry DIA analysis quantifies stoichiometry of MS2 fragments, rather than a MS1 based approach. This allows for site specificity within a peptide containing multiple lysines; calculating the stoichiometry of fragments from each lysine independently, rather than an overall average of the peptide ***(107)***. MS2 fragment quantification overcomes interference and bias with MS1 quantification that can result in an overestimation of the acetyl stoichiometry at many low abundant and acetyl occupancy sites. We perform our stoichiometry analysis utilizing R version 3.3.3 (2017-03-06) "Another Canoe" and R studio version 1.0.1316. The analysis described here can be performed in many data analysis programs or software available.

1. Filter the data by MS2 fragments containing a single lysine for site-specific quantification. Fragments containing multiple lysines will not provide site-specific information on lysine acetylation label stoichiometry.
2. Filter the data by the presence of both the heavy and light label to have both values for subsequent stoichiometry calculations. For the analysis of offline prefractionated DIA

data, filter by the presence of both the heavy and light label before summing the values across any fractions of a single biological sample.

3. Filter by peptide identification quality, we require a Q score of the peptide identification for one of the two labeled forms, heavy or light, of the acetyl lysine containing peptide.
4. Perform isotopic envelope corrections on the heavy labeled peak by using the BRAIN package in R ***(114)***. This package calculates the M+3 peak of the light peak using the fragment ion sequence and natural isotopic distributions, which then is subtracted from the heavy M+0 peak to determine the abundance of the heavy peak. This calculation corrects for the overlap between the natural abundance of peptides containing 3 naturally occurring heavy atoms and the peak area assigned to the M+0 peak from the labeled heavy acetylated peptide. The isotopic correction is particularly important for reducing the overestimation of high stoichiometry lysine acetylation sites ***(107)***.
5. Sum the area of the MS2 peaks of the y and b fragment ions of each lysine from the light and heavy labels separately to determine the total peak area of the heavy and light acetylated lysine.
6. Calculate the stoichiometry of the summed MS2 peaks for each lysine by dividing the total non-isotopically labeled peak area by the total peak area of both labels of the fragments.
7. Using the FASTA file, assign the residue number of the lysine site within the fragments. This is important for multiply acetylated peptides which have unique sets of MS2 fragment for the C and N proximal lysine residues.

2.4.2.3 Statistics and Determining Significant Changes in Acetyl Stoichiometries

Calculating statistical significance of acetyl stoichiometry changes in dynamic systems poses a challenge to interpreting acetyl stoichiometry alterations due to the nature of correcting for multiple testing across samples as well as the dynamics along the time course. We go about tackling this issue by performing ANOVA analysis instead of single pairwise interactions between 2 time points.

1. Calculate the mean stoichiometry for each lysine within the proteome observed.
2. Calculate the linear model to perform one way repeated measures analysis of variance (ANOVA), which performs the comparison of three or more means within-subject variables. If performing comparisons between multiple groups rather than a time course, a t-test for two samples or sets of paired samples would be appropriate with a multiple testing correction depending on the experimental design. If performing between the means of more than two groups, a one way ANOVA or a mixed ANOVA may be more appropriate.

2.4.2.4 Analyzing Global Trends in Site-Specific Acetylation Stoichiometry Proteomics Data

One of the major challenges to understanding posttranslational modification dynamics of non-histone chromatin-associated proteins has been effective purification of chromatin-associated proteins. Histone proteins are highly abundant in the nucleus and make up the basic unit of chromatin, therefore separation of histones from other chromatin-associated proteins is necessary for detection of lower abundant chromatin-associated proteins and their modification states. Furthermore, the outer membrane of the nuclear envelope is contiguous with the endoplasmic reticulum of the cell, leading to high levels of contamination from other cellular

compartments. This study aims to develop a chromatin purification method to remove the perinuclear membrane from the nucleus to reduce contamination from other cellular compartments and use salt fractionation to separate chromatin-associated proteins from histone proteins.

Our method utilizes four main steps, sample homogenization and cell lysis to pellet nuclei, washing of the nucleus, lysis of the core nuclei, and subsequent salt washes and fractionation of pelleted chromatin depicted in Figure 2-5. Salt fractionation using 450 mM NaCl from isolated chromatin after removal of the perinuclear envelope results in the greatest enrichment from chromatin-associated proteins as seen in Figure 2-6A and B. Both in the number of proteins identified and much more greatly in their abundance. Salt fractionation from chromatin without clean-up of the nucleus also shows significant improvement over early methods of performing total protein extraction from chromatin. In addition, subsequent acid extraction (Fig 2-6D, 2E) of the chromatin pellet after salt fractionation yields a more highly enriched histone fraction.

Salt fractionation using 450 mM NaCl from isolated chromatin results in the greatest enrichment from acetylated peptides from chromatin-associated proteins as seen in Figure 2-6C and D and shows significant improvement over early methods of performing total protein extraction from chromatin. In addition, we were able to quantify the posttranslational modification from the subsequent acid extraction of the chromatin pellet after salt fractionation, which yielded a more highly enriched histone fraction.

In this chapter we have used subcellular fractionation with chemical labeling of lysine residues coupled withto data-independent acquisition mass spectrometry-based proteomics to quantify lysine acetylation stoichiometry. The subcellular localization distribution within the

spectral libraries demonstrated the increase in coverage provided by both the subcellular isolation and offline prefractionation, as well as the two methods in conjunction (Figure 2-4). Offline prefractionation (light blue) resulted in approximately double the numbers of proteins identified throughout the compartment as compared to a single whole cell lysate DDA spectral library (grey), and a similar increase in the number of peptides identified. The subcellular isolation followed a similar pattern, with the spectral library of the offline prefractionated chromatin isolation (green) resulting in double the protein and peptide identifications of the single sample of the chromatin isolation (orange) (Figure 2-3). The two separation techniques used in conjunction expanded the spectral library even further, increasing protein and peptides identifications three-fold above a single whole cell lysate DDA spectral library. For analysis of subcellular compartment isolation and its impact on increasing the coverage of lysine sites, we analyzed subcellular localization based upon evidence in annotated databases, such as UniProt (Figure 2-8 and 2-9A). The greatest increase in compartment-specific identifications in the spectral library was seen in the chromatin isolation in combination with offline prefractionation, increasing the percent of nuclear proteins, peptides, and acetyl peptides identified to approximately 50% of the library (Figure 2-8A and B). The combination of subcellular compartment isolation and offline prefractionation significantly increases spectral library coverage and enables deep interrogation of compartment-specific acetylation stoichiometry as shown in Figure 4, which highlights the subcellular functions captured in our chromatin isolation and offline prefractionation approach (Figure 2-9A and C).

Increasing depth of the spectral library results in increased proteins, peptides, and acetyl peptides deconvoluted from the DIA MS2 spectra, as shown in Figure 5. Analysis of the acetylation stoichiometry of a single injection of whole cell lysate without offline

prefractionation resulted in 25 % coverage of the acetylation site stoichiometry when compared to offline prefractionation DIA analysis. However, depth of coverage in a single DIA sample was greatly improved by subcellular compartment isolation, with the depth of coverage within isolated chromatin being comparable to chromatin acetylation sites quantified in an offline prefractionation of a whole cell lysate (Figure 2-8C and D). Furthermore, the increased depth of the spectral library in conjunction with subcellular isolation prior to DIA analysis resulted in the increase in the number of acetylation site stoichiometries quantified. The reasons for this increase were two-fold, with the increase in the spectral library depth resulting in the identification and quantification of more fragment ions, including those from peptides of much lower abundance. This is shown by the distribution of the Log_{10} fragment ion peak area in Figure 2-10. In addition, the reduction in sample complexity by subcellular isolation increased the likelihood of observing both the non-isotopic and isotopically labeled acetyl fragment ions to calculate acetylation stoichiometry.

The global distribution of acetylation stoichiometry within a whole cell lysate measurements yielded a median of approximately 2% (Figure 2-10A). Our method of subcellular compartment isolation demonstrates important differences, with resolution capable of revealing the higher acetylation stoichiometry proteins occurring within the isolated mitochondria and nucleus ***(24, 115)*** (Figure 2-11B). Calculation of site-specific stoichiometry from a whole cell lysate reflect the combination of stoichiometries of a protein across subcellular compartments. However, our subcellular fractionation method captures the dynamic stoichiometries of a protein across different subcellular compartments, which may be independently regulated (Figure 2-12).

Figure 2-6. Percent Protein Identification and Quantity from Methods of Chromatin Protein Isolation by compartment.

A) The percent of Proteins identified from Chromatin Isolation protein extraction, Nuclear Isolation followed by Salt Fractionation of pelleted chromatin, and Perinuclear clean-up followed by Salt Fractionation of pelleted chromatin. **B)** The percent protein quantity based upon LFQ intensities, **C)** The percent of acetylated peptides identified, **D)** and the raw number of acetyl peptides per compartment for each method of chromatin isolation. Compartments are not mutually exclusive.

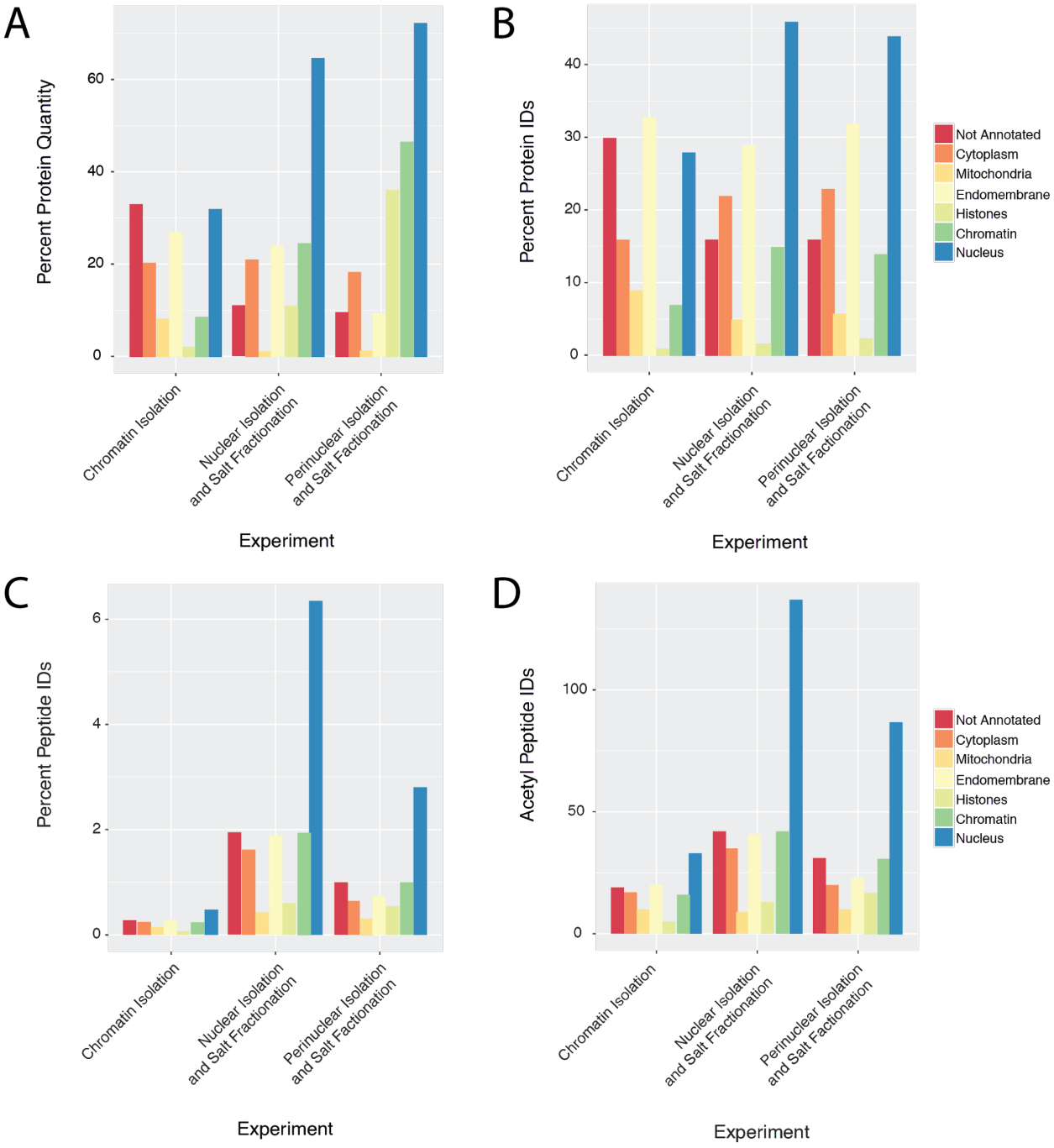
A
Percent Protein Quantity
0
20
40
60
Chromatin Isolation
Nuclear Isolation and Salt Fractionation
Perinuclear Isolation and Salt Factionation
Experiment
B
Percent Protein IDs
0
10
20
30
40
Chromatin Isolation
Nuclear Isolation and Salt Fractionation
Perinuclear Isolation and Salt Factionation
Experiment
Not Annotated
Cytoplasm
Mitochondria
Endomembrane
Histones
Chromatin
Nucleus
C
Percent Peptide IDs
0
2
4
6
Chromatin Isolation
Nuclear Isolation and Salt Fractionation
Perinuclear Isolation and Salt Factionation
Experiment
D
Acetyl Peptide IDs
0
50
100
Chromatin Isolation
Nuclear Isolation and Salt Fractionation
Perinuclear Isolation and Salt Factionation
Experiment
Not Annotated
Cytoplasm
Mitochondria
Endomembrane
Histones
Chromatin
Nucleus

Figure 2-7. Enrichment of Non-Histone Chromatin Associated Proteins Using Salt Fractionation.

Proteins are clustered based upon their percent quantity out of the total protein quantified using LFQ intensities.Samples are from Chromatin Isolation protein extraction, Nuclear Isolation followed by Salt Fractionation of pelleted chromatin, and Perinuclear clean-up followed by Salt Fractionation of pelleted chromatin.

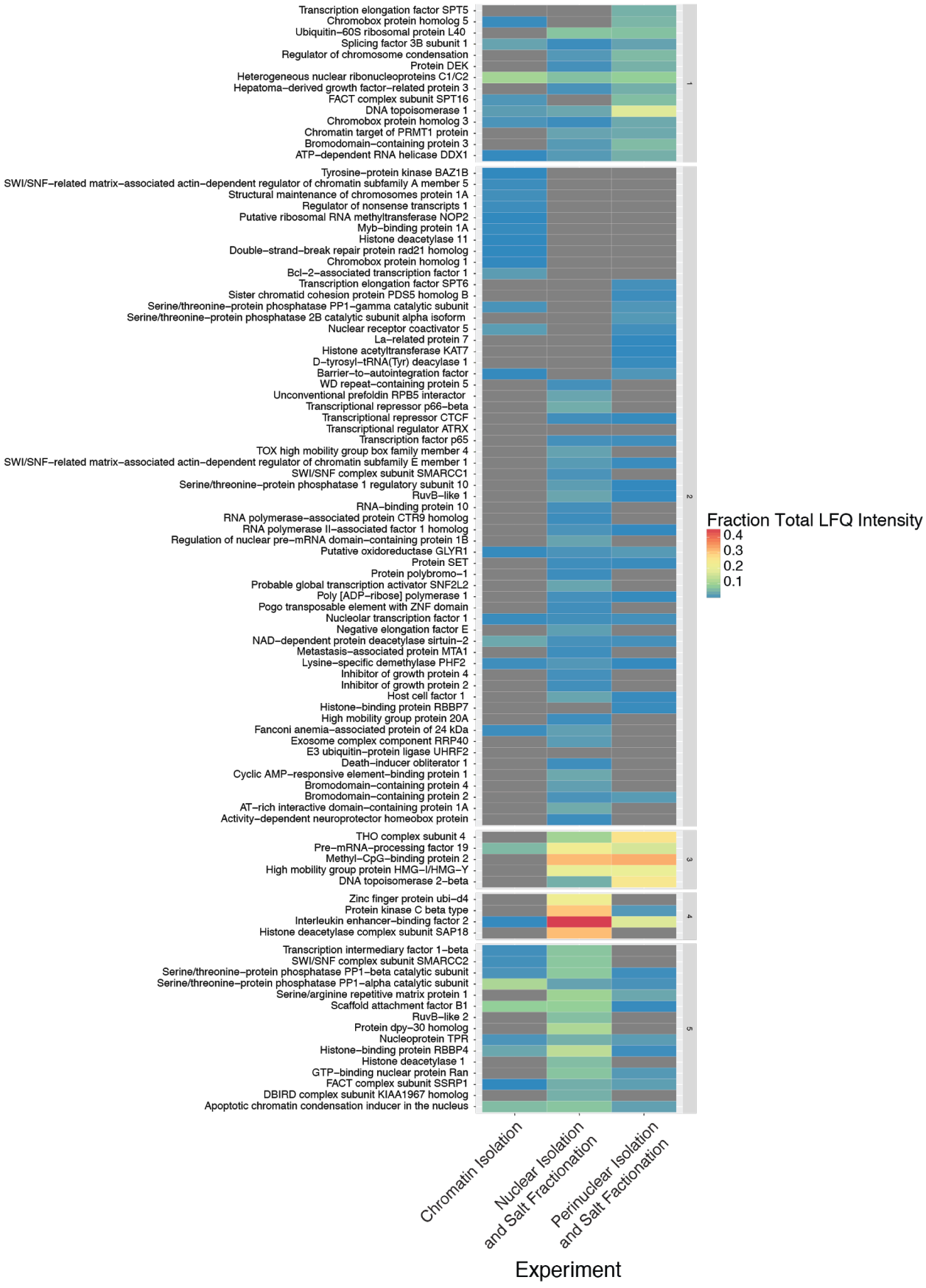
Transcription elongation factor SPT5
Chromobox protein homolog 5
Ubiquitin–60S ribosomal protein L40
Splicing factor 3B subunit 1
Regulator of chromosome condensation
Protein DEK
Heterogeneous nuclear ribonucleoproteins C1/C2
Hepatoma–derived growth factor–related protein 3
FACT complex subunit SPT16
DNA topoisomerase 1
Chromobox protein homolog 3
Chromatin target of PRMT1 protein
Bromodomain–containing protein 3
ATP–dependent RNA helicase DDX1
Tyrosine–protein kinase BAZ1B
SWI/SNF–related matrix–associated actin–dependent regulator of chromatin subfamily A member 5
Structural maintenance of chromosomes protein 1A
Regulator of nonsense transcripts 1
Putative ribosomal RNA methyltransferase NOP2
Myb–binding protein 1A
Histone deacetylase 11
Double–strand–break repair protein rad21 homolog
Chromobox protein homolog 1
Bcl–2–associated transcription factor 1
Transcription elongation factor SPT6
Sister chromatid cohesion protein PDS5 homolog B
Serine/threonine–protein phosphatase PP1–gamma catalytic subunit
Serine/threonine–protein phosphatase 2B catalytic subunit alpha isoform
Nuclear receptor coactivator 5
La–related protein 7
Histone acetyltransferase KAT7
D–tyrosyl–tRNA(Tyr) deacylase 1
Barrier–to–autointegration factor
WD repeat–containing protein 5
Unconventional prefoldin RPB5 interactor
Transcriptional repressor p66–beta
Transcriptional repressor CTCF
Transcriptional regulator ATRX
Transcription factor p65
TOX high mobility group box family member 4
SWI/SNF–related matrix–associated actin–dependent regulator of chromatin subfamily E member 1
SWI/SNF complex subunit SMARCC1
Serine/threonine–protein phosphatase 1 regulatory subunit 10
RuvB–like 1
RNA–binding protein 10
RNA polymerase–associated protein CTR9 homolog
RNA polymerase II–associated factor 1 homolog
Regulation of nuclear pre–mRNA domain–containing protein 1B
Putative oxidoreductase GLYR1
Protein SET
Protein polybromo–1
Probable global transcription activator SNF2L2
Poly [ADP–ribose] polymerase 1
Pogo transposable element with ZNF domain
Nucleolar transcription factor 1
Negative elongation factor E
NAD–dependent protein deacetylase sirtuin–2
Metastasis–associated protein MTA1
Lysine–specific demethylase PHF2
Inhibitor of growth protein 4
Inhibitor of growth protein 2
Host cell factor 1
Histone–binding protein RBBP7
High mobility group protein 20A
Fanconi anemia–associated protein of 24 kDa
Exosome complex component RRP40
E3 ubiquitin–protein ligase UHRF2
Death–inducer obliterator 1
Cyclic AMP–responsive element–binding protein 1
Bromodomain–containing protein 4
Bromodomain–containing protein 2
AT–rich interactive domain–containing protein 1A
Activity–dependent neuroprotector homeobox protein
THO complex subunit 4
Pre–mRNA–processing factor 19
Methyl–CpG–binding protein 2
High mobility group protein HMG–I/HMG–Y
DNA topoisomerase 2–beta
Zinc finger protein ubi–d4
Protein kinase C beta type
Interleukin enhancer–binding factor 2
Histone deacetylase complex subunit SAP18
Transcription intermediary factor 1–beta
SWI/SNF complex subunit SMARCC2
Serine/threonine–protein phosphatase PP1–beta catalytic subunit
Serine/threonine–protein phosphatase PP1–alpha catalytic subunit
Serine/arginine repetitive matrix protein 1
Scaffold attachment factor B1
RuvB–like 2
Protein dpy–30 homolog
Nucleoprotein TPR
Histone–binding protein RBBP4
Histone deacetylase 1
GTP–binding nuclear protein Ran
FACT complex subunit SSRP1
DBIRD complex subunit KIAA1967 homolog
Apoptotic chromatin condensation inducer in the nucleus
1
2
3
4
5
Fraction Total LFQ Intensity
0.4
0.3
0.2
0.1
Chromatin Isolation
Nuclear Isolation and Salt Fractionation
Perinuclear Isolation and Salt Factionation
Experiment

Figure 2-8. Subcellular Localization Identification and Abundances of Spectral Libraries and DIA sample Analysis.

A) Percent of Proteins identified in spectral libraries by subcellular localization and **B)** and Percent of peptides identified in spectral libraries by subcellular localization of the spectral libraries generated from a Single Injection Whole Cell Lysate (WCL), a Single Chromatin Isolation (utilizing subcellular fractionation without offline prefractionation), a Fractionated WCL utilizing offline prefractionation, Fractionated Chromatin Isolation utilizing offline prefractionation on a subcellular fractionated chromatin isolation, a Fractionated WCL utilizing offline prefractionation with a single chromatin isolation (utilizing subcellular fractionation without offline prefractionation), and the Fractionated Chromatin Isolation and Fractionated WCL utilizing together utilizing offline prefractionation, on both whole cell lysate and a subcellular fractionated chromatin sample. **C)** Percent of acetylated peptides identified from analysis of DIA samples from an offline prefractionated WCL, a single injection WCL sample, a mitochondrial isolation, and a chromatin isolation by subcellular compartment **D)** Percent of acetylated peptide abundance of DIA samples from an offline prefractionated WCL, a single injection WCL sample, a mitochondrial isolation, and a chromatin isolation by subcellular compartment.

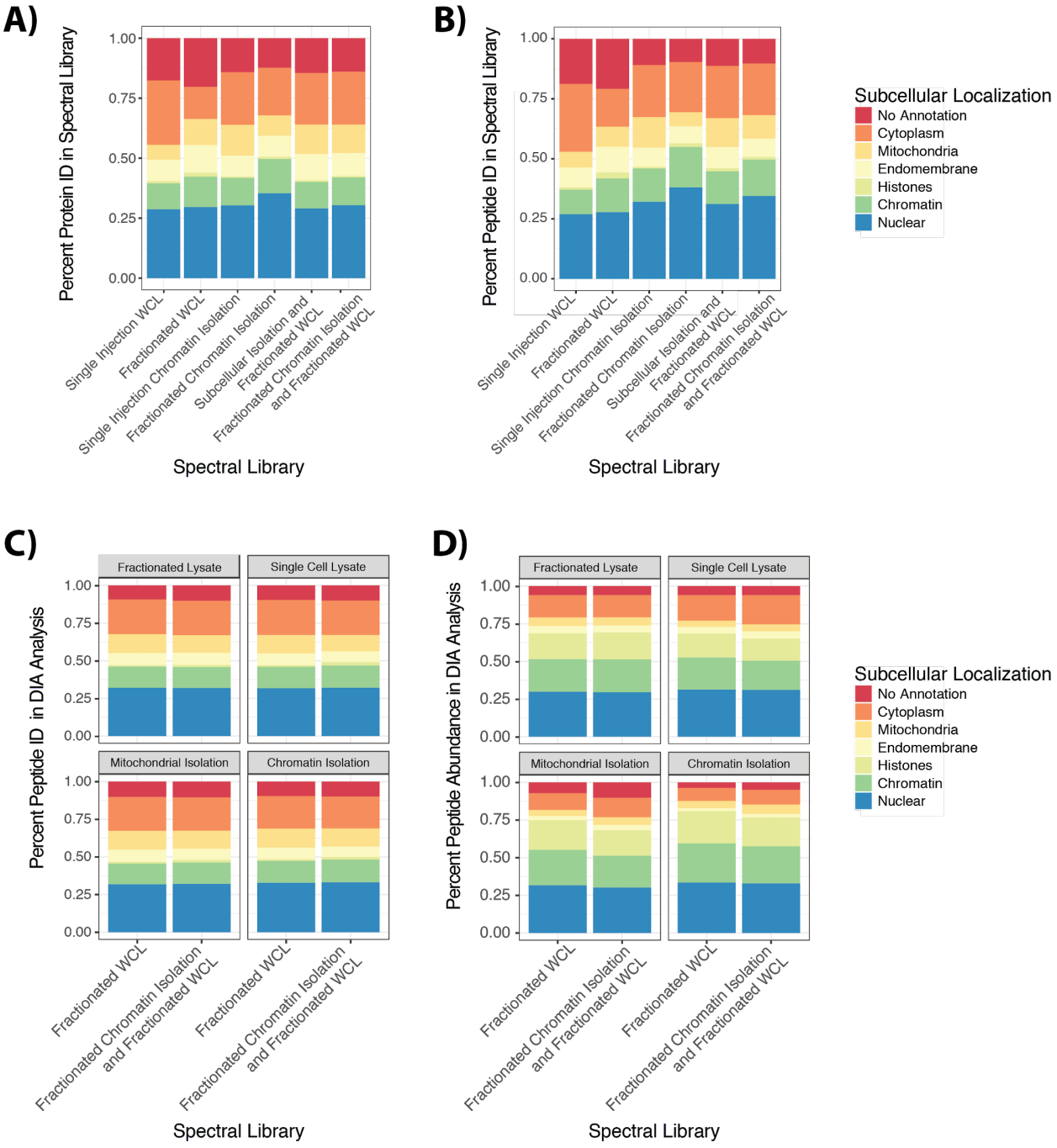
A)
Percent Protein ID in Spectral Library
1.00
0.75
0.50
0.25
0.00
Single Injection WCL
Fractionated WCL
Single Injection Chromatin Isolation
Fractionated Chromatin Isolation
Subcellular Isolation and Fractionated WCL
Fractionated Chromatin Isolation and Fractionated WCL
Spectral Library
B)
Percent Peptide ID in Spectral Library
1.00
0.75
0.50
0.25
0.00
Single Injection WCL
Fractionated WCL
Single Injection Chromatin Isolation
Fractionated Chromatin Isolation
Subcellular Isolation and Fractionated WCL
Fractionated Chromatin Isolation and Fractionated WCL
Spectral Library
Subcellular Localization
No Annotation
Cytoplasm
Mitochondria
Endomembrane
Histones
Chromatin
Nuclear
C)
Percent Peptide ID in DIA Analysis
Fractionated Lysate
Single Cell Lysate
Mitochondrial Isolation
Chromatin Isolation
1.00
0.75
0.50
0.25
0.00
Fractionated WCL
Fractionated Chromatin Isolation and Fractionated WCL
Spectral Library
D)
Percent Peptide Abundance in DIA Analysis
Fractionated Lysate
Single Cell Lysate
Mitochondrial Isolation
Chromatin Isolation
1.00
0.75
0.50
0.25
0.00
Fractionated WCL
Fractionated Chromatin Isolation and Fractionated WCL
Spectral Library
Subcellular Localization
No Annotation
Cytoplasm
Mitochondria
Endomembrane
Histones
Chromatin
Nuclear

Figure 2-9. Analysis of overlapping and unique features of subcellular localization in spectral libraries.

A) The overlap of the annotated subcellular localization of proteins as obtained by UniProt demonstrating the overlap of proteins across compartments and the existence of a single protein across compartments. **B)** An analysis of the overlap of peptide identifications of spectral libraries generated from a Single Injection Whole Cell Lysate (WCL), a Single Chromatin Isolation (utilizing subcellular fractionation without offline prefractionation), a Fractionated WCL utilizing offline prefractionation, and Fractionated Chromatin Isolation utilizing offline prefractionation on a subcellular fractionated chromatin sample, **C)** DAVID analysis of the unique KEGG pathway enrichment and significance of the enrichment of peptides from subcellular chromatin isolation in comparison to the offline prefractionation WCL and fractionated chromatin isolation spectral library.

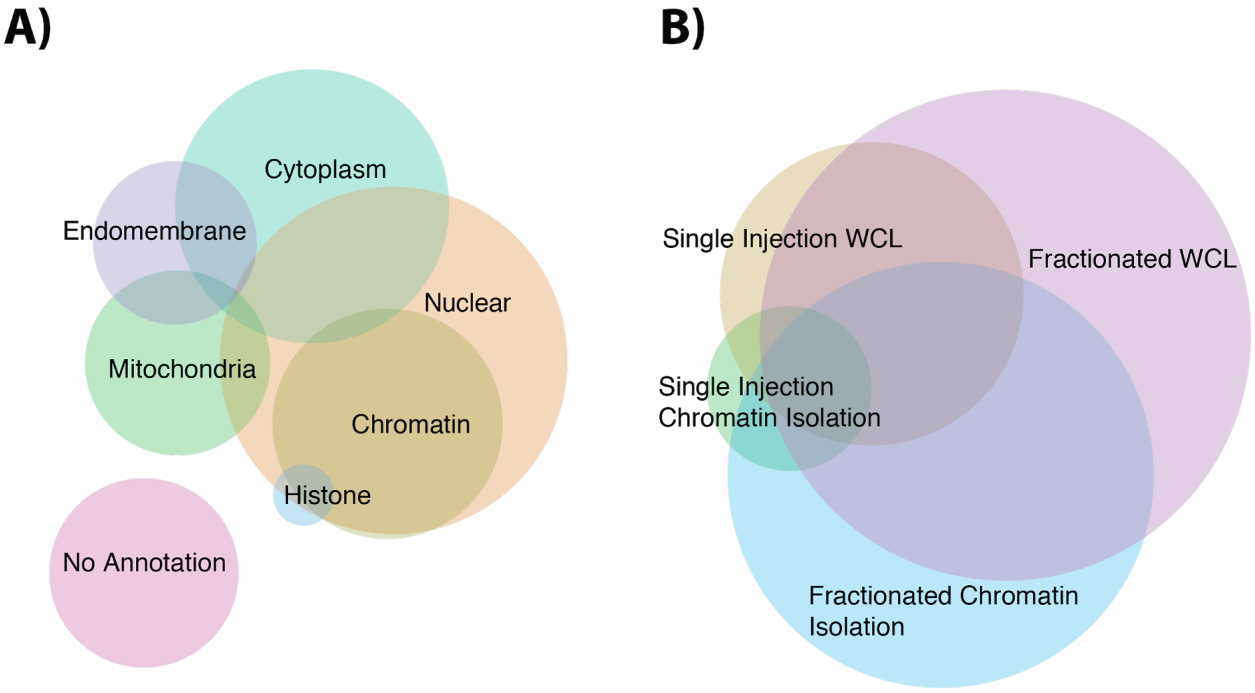
A)
Cytoplasm
Endomembrane
Nuclear
Mitochondria
Chromatin
Histone
No Annotation
B)
Single Injection WCL
Fractionated WCL
Single Injection
Chromatin Isolation
Fractionated Chromatin
Isolation

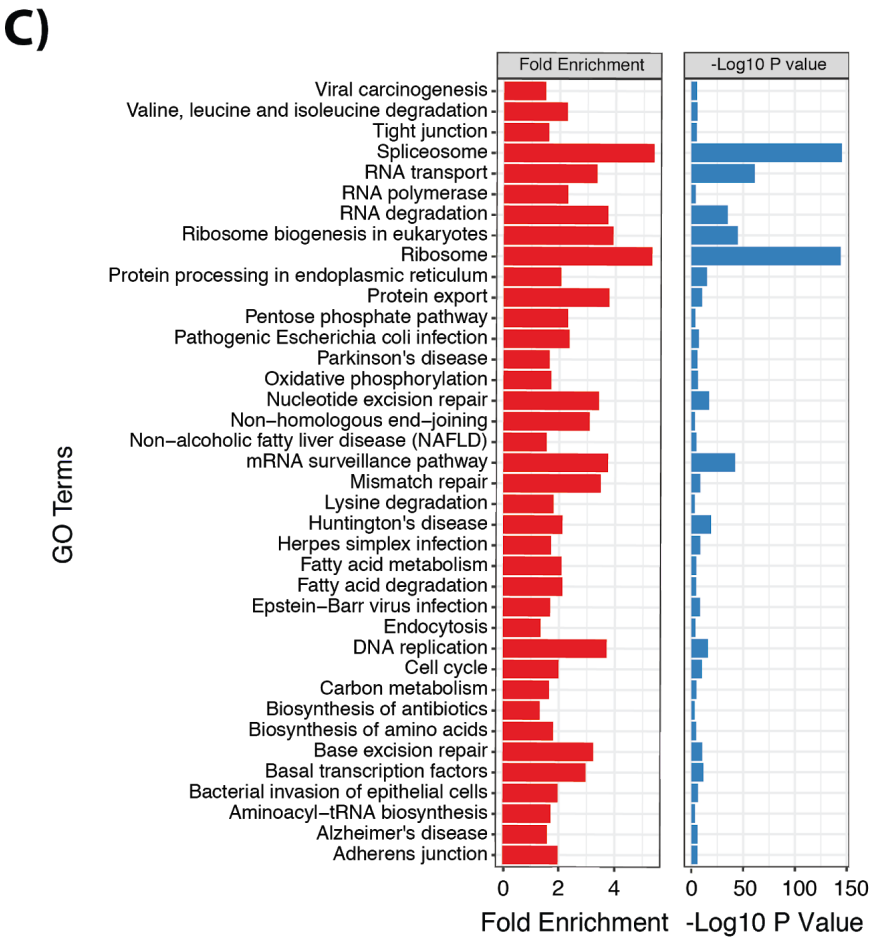
C)
Fold Enrichment
-Log10 P value
GO Terms
Viral carcinogenesis
Valine, leucine and isoleucine degradation
Tight junction
Spliceosome
RNA transport
RNA polymerase
RNA degradation
Ribosome biogenesis in eukaryotes
Ribosome
Protein processing in endoplasmic reticulum
Protein export
Pentose phosphate pathway
Pathogenic Escherichia coli infection
Parkinson's disease
Oxidative phosphorylation
Nucleotide excision repair
Non–homologous end–joining
Non–alcoholic fatty liver disease (NAFLD)
mRNA surveillance pathway
Mismatch repair
Lysine degradation
Huntington's disease
Herpes simplex infection
Fatty acid metabolism
Fatty acid degradation
Epstein–Barr virus infection
Endocytosis
DNA replication
Cell cycle
Carbon metabolism
Biosynthesis of antibiotics
Biosynthesis of amino acids
Base excision repair
Basal transcription factors
Bacterial invasion of epithelial cells
Aminoacyl–tRNA biosynthesis
Alzheimer's disease
Adherens junction
0
2
4
0
50
100
150
Fold Enrichment
-Log10 P Value

Figure 2-10. Subcellular Fractionation Increases Depth Similar to Offline Prefractionation with Lower Peptide Abundance.

A) The difference in unique peptides identified, unique lysine (K) containing peptides, and unique peptides with quantified stoichiometry in the DIA analysis of Offline Prefractionated Whole Cell Lysate (WCL, red), Subcellular Mitochondrial Isolation (green), and Subcellular Nuclear Isolation (blue) using the Fractionated WCL Fractionation spectral library and the Subcellular Fractionation with Offline WCL Fractionation spectral library demonstrating similar levels of acetylation stoichiometry coverage. **B)** The distribution of the log10 peak area of MS2 fragments from acetyl-lysine containing peptides with determined stoichiometry showed the mean peak area of peptides from the single DIA analysis of subcellular isolation quantifies a similar depth of lysine acetylation sites captured with offline prefractionation.

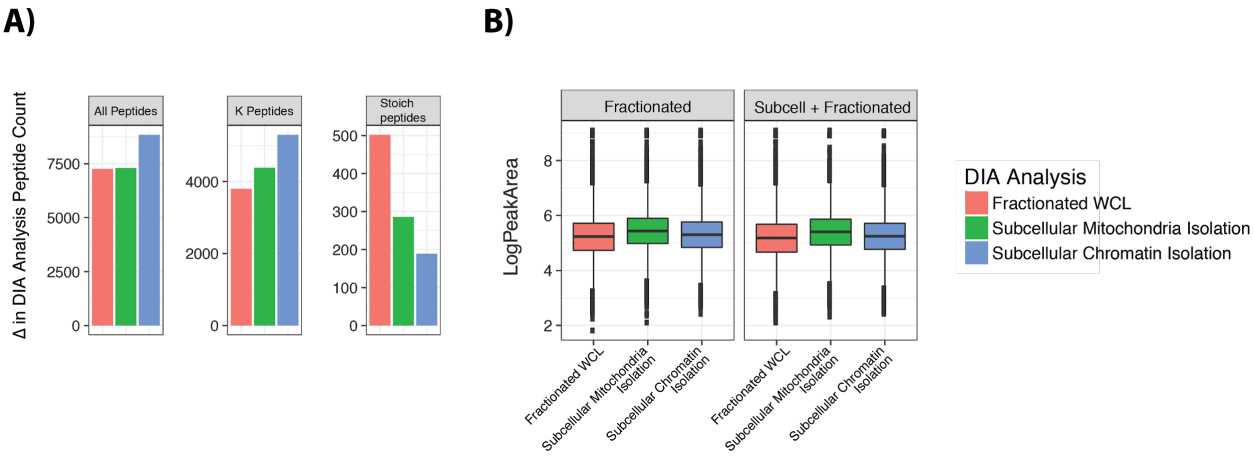

Figure 2-11. Analysis of Global Lysine Acetylation Stoichiometry by Spectral Library. **A)** Density plot of the relative distribution of lysine acetylation stoichiometry of DIA samples from an offline prefractionated whole cell lysate (WCL, pink), a single injection WCL (green), a mitochondrial isolation (blue), and a chromatin isolation (purple). The median stoichiometry in these samples is 2% and the distribution was not highly variable, area under the curve normalized across samples. **B)** Histogram of the absolute distribution of mean lysine site acetylation stoichiometry of DIA analysis from an offline prefractionated WCL, a Single Injection WCL sample, and a chromatin isolation across a time course experiment demonstrates the similar distribution of acetylation stoichiometries **C)** Density plot of the relative distribution of lysine acetylation stoichiometry by subcellular localization of DIA samples from an offline

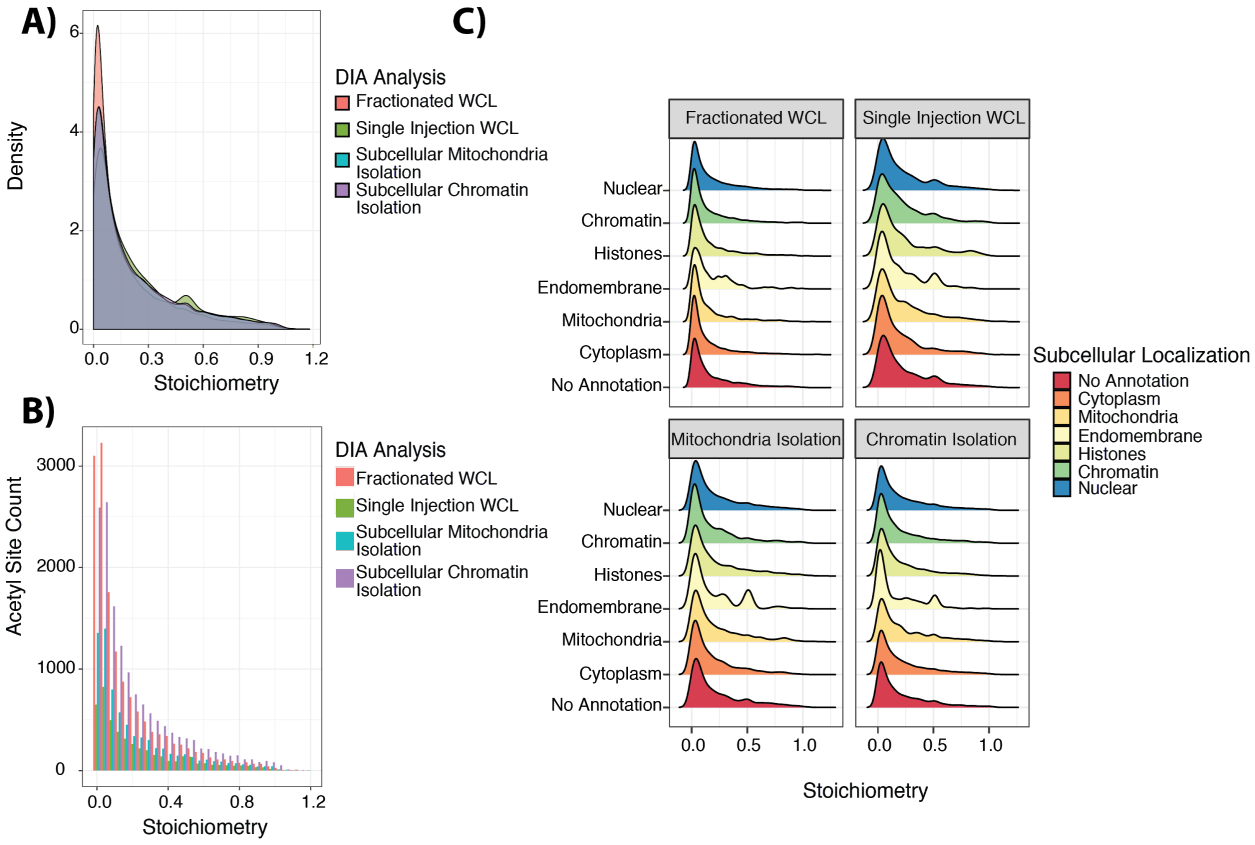

Figure 2-12. DIA Analysis of Subcellular Fractions Reveals Subcellular Compartment Specific Patterns of Lysine Acetylation Stoichiometry.

A) Density plot of the relative distribution of lysine acetylation stoichiometry of nuclear localized lysine acetylation sites from DIA samples from an offline prefractionated whole cell lysate (WCL, pink), a single injection WCL sample (green), and a chromatin isolation (blue). **B)** Density plot of the relative distribution of lysine acetylation stoichiometry of mitochondria localized lysine acetylation sites from DIA samples from an offline prefractionated WCL (pink), a single injection WCL sample (green), and a mitochondrial isolation (blue). **C)** Venn Diagram of overlap and unique nuclear lysine acetylation sites from DIA samples from an offline prefractionated whole cell lysate (brown), a single injection WCL sample (purple), and a chromatin isolation (green). **D)** Venn Diagram of overlap and unique mitochondria lysine acetylation sites from DIA samples from an offline prefractionated WCL (brown), a single injection WCL sample (green), and a mitochondrial isolation (purple). **E)** Density plot of the relative distribution of lysine acetylation stoichiometry of unique nuclear lysine acetylation sites from DIA samples from an offline prefractionated WCL (pink), a single injection WCL sample (green), and a chromatin isolation (blue). **F)** Density plot of the relative distribution of lysine acetylation stoichiometry of unique mitochondria localized acetylation sites from DIA samples from an offline prefractionated WCL (pink), a single injection WCL sample (green), and a mitochondrial isolation (blue).

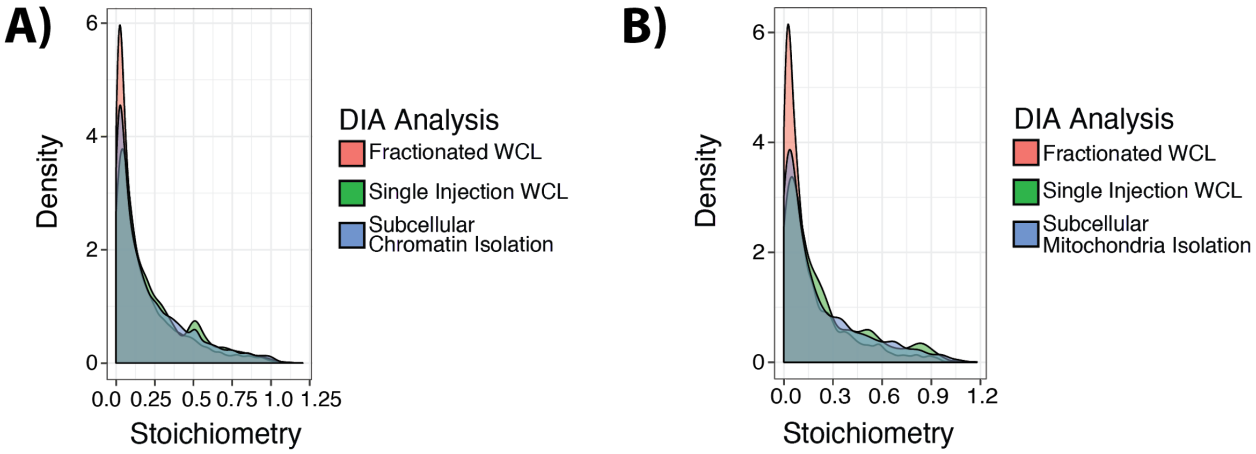
A)
Density
Stoichiometry
0.0 0.25 0.5 0.75 1.0 1.25
DIA Analysis
Fractionated WCL
Single Injection WCL
Subcellular Chromatin Isolation

B)
Density
Stoichiometry
0.0 0.3 0.6 0.9 1.2
DIA Analysis
Fractionated WCL
Single Injection WCL
Subcellular Mitochondria Isolation

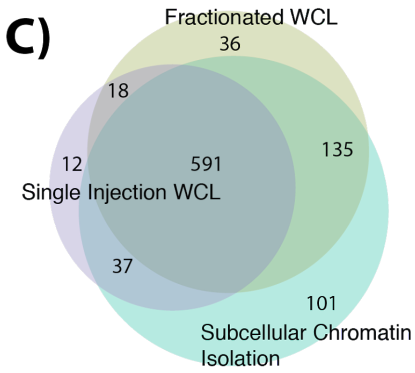
C)
Fractionated WCL
36
18
135
12
591
Single Injection WCL
37
101
Subcellular Chromatin Isolation

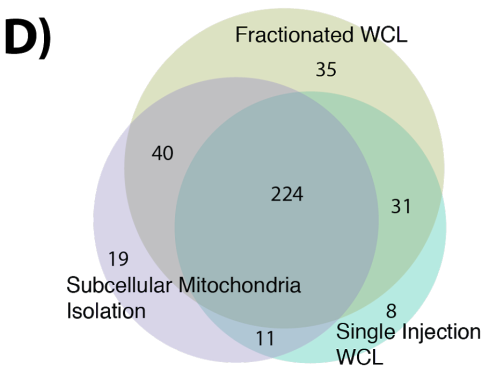
D)
Fractionated WCL
35
40
224
31
19
Subcellular Mitochondria Isolation
11
8
Single Injection WCL

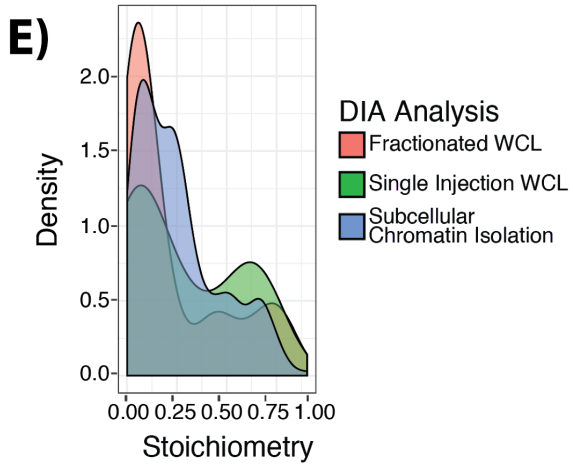
E)
Density
Stoichiometry
0.00 0.25 0.50 0.75 1.00
DIA Analysis
Fractionated WCL
Single Injection WCL
Subcellular Chromatin Isolation

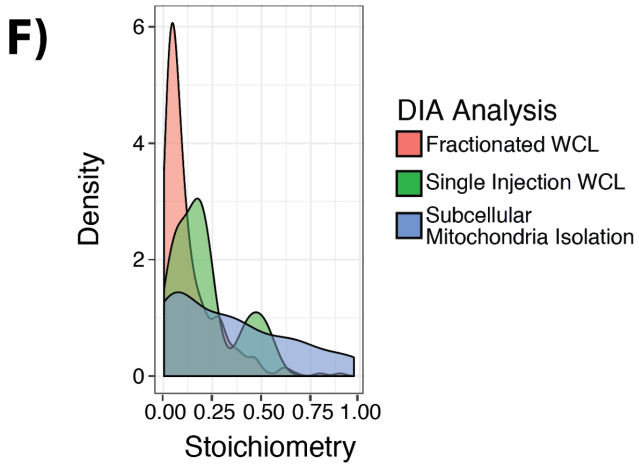
F)
Density
Stoichiometry
0.00 0.25 0.50 0.75 1.00
DIA Analysis
Fractionated WCL
Single Injection WCL
Subcellular Mitochondria Isolation

B)

2.5 Discussion and Perspective

We have discussed methods to utilize chemical labeling of lysine residues coupled with data-independent acquisition mass spectrometry-based proteomics to quantify lysine acetylation stoichiometry, increasing the sampling depth and the number of acetylation sites captured. Furthermore, the methods describing subcellular organelle enrichment and its impact on increasing the coverage of lysine sites of a specific organelle, provided a useful tool for in-depth studies to investigate the impacts of different factors on lysine acetylation dynamics in specific organelles. This approach provides a useful tool for examining the differences in the regulation of lysine acetylation within cellular organelles, in particular the differences between enzymatic and nonenzymatic acetylation in the nucleus, cytoplasm, and mitochondria. Our approach has further demonstrated that subcellular fractionation gives an increase in sampling depth of a specific organelle over orthogonal separation approaches of a whole cell lysate alone. Finally, we have demonstrated the utility for a deep spectral library for DIA sample analysis. With a deep spectral library, offline prefractionation of the experimental samples was not necessary when performing final DIA analysis. The main bottleneck in the depth of peptide identification is the generation of the spectral library. Furthermore, the technical error has been decreased from the reduced handling of samples without the offline prefractionation on DIA sample analysis.

Mass spectrometry-based proteomics approaches for identifying and quantifying lysine acetylation have undergone many improvements within the last decade, now enabling comprehensively quantification of acetylation stoichiometry in an entire proteome ***(24)***. Initial proteomics studies used antibody based enrichment strategies, which largely expanded the acetylation sites identified ***(4, 12)***. Quantification of these sites was undertaken by combining enrichment based methods with SILAC labeling for relative quantification of acetylation ***(13, 14,***

28). These studies began to profile the dynamic nature of lysine acetylation, however they were limited to systems where SILAC was readily usable. Furthermore, questions remained about the stoichiometry of lysine acetylation, as relative quantification can indicate how much acetylation of a site has increased or decreased. Because enrichment strategies removed non-acetylated peptides from the sample analyzed, these ratios do not reflect the total peptide abundance. The first undertaking of quantifying lysine acetylation with tandem mass tags (TMTs) revealed more information about the complex dynamics of mitochondrial protein acetylation in response to diet ***(21, 25, 116)***. Recently, we and others have reported a data dependent acquisition (DDA) method to determine stoichiometric quantification rather than relative fold changes, however this method had limits based upon the use of MS1 quantification, and lowly abundant modification was more susceptible to signal interference and bias ***(24, 75, 117, 118)***. These problems were discussed and addressed by using the MS2 fragments. The latest step forward, described here as well as by others, utilizes data-independent acquisition to increase the peptides identified and the number of acetylation sites quantified ***(75, 115)***. In this chapter, we have expanded the coverage of this method to subcellular organelles, resulting in considerably deeper coverage of the acetyl stoichiometry of these organelles, allowing for more detailed investigations of the dynamics and regulation of acetyl lysine stoichiometry, which is functionally compartmentalized within the cell. This method may be more broadly applied to other lysine acyl modifications ***(115)***. Recent studies have used DIA approaches to quantify lysine succinylation across the proteome, demonstrating how this method can be expanded to examine the biological regulation and function of acyl modifications on lysine residues ***(115)***.

2.6 References:

1. Olsen JV and Mann M (2013) Status of large-scale analysis of post-translational modifications by mass spectrometry. Mol Cell Proteomics 12:3444–3452

2. Olsen JV, Vermeulen M, Santamaria A, et al (2010) Quantitative phosphoproteomics reveals widespread full phosphorylation site occupancy during mitosis. Sci Signal 3:ra3

3. Wu R, Haas W, Dephoure N, et al (2011) A large-scale method to measure absolute protein phosphorylation stoichiometries. Nat Methods 8:677–683

4. Kim SC, Sprung R, Chen Y, et al (2006) Substrate and functional diversity of lysine acetylation revealed by a proteomics survey. Mol Cell 23:607–618

5. Yu BJ, Kim JA, Moon JH, et al (2008) The diversity of lysine-acetylated proteins in Escherichia coli. J Microbiol Biotechnol 18:1529–1536

6. Zhang J, Sprung R, Pei J, et al (2009) Lysine acetylation is a highly abundant and evolutionarily conserved modification in Escherichia coli. Mol Cell Proteomics 8:215–225

7. Schwer B, Eckersdorff M, Li Y, et al (2009) Calorie restriction alters mitochondrial protein acetylation. Aging Cell 8:604–606

8. Choudhary C, Kumar C, Gnad F, et al (2009) Lysine Acetylation Targets Protein Complexes and Co-Regulates Major Cellular Functions. Science 325:834–840

9. Wang Q, Zhang Y, Yang C, et al (2010) Acetylation of metabolic enzymes coordinates carbon source utilization and metabolic flux. Science 327:1004–1007

10. Zhao S, Xu W, Jiang W, et al (2010) Regulation of Cellular Metabolism by Protein Lysine Acetylation. Science 327:1000–1004

11. Yang L, Vaitheesvaran B, Hartil K, et al (2011) The fasted/fed mouse metabolic

acetylome: N6-acetylation differences suggest acetylation coordinates organ-specific fuel switching. J Proteome Res 10:4134–4149

12. Weinert BT, Wagner SA, Horn H, et al (2011) Proteome-wide mapping of the Drosophila acetylome demonstrates a high degree of conservation of lysine acetylation. Sci Signal 4:ra48

13. Simon GM, Cheng J, and Gordon JI (2012) Quantitative assessment of the impact of the gut microbiota on lysine epsilon-acetylation of host proteins using gnotobiotic mice. Proc Natl Acad Sci U S A 109:11133–11138

14. Henriksen P, Wagner SA, Weinert BT, et al (2012) Proteome-wide analysis of lysine acetylation suggests its broad regulatory scope in Saccharomyces cerevisiae. Mol Cell Proteomics 11:1510–1522

15. Lundby A, Lage K, Weinert BT, et al (2012) Proteomic analysis of lysine acetylation sites in rat tissues reveals organ specificity and subcellular patterns. Cell Rep 2:419–431

16. Foster DB, Liu T, Rucker J, et al (2013) The cardiac acetyl-lysine proteome. PLoS One 8:e67513

17. Allfrey VG, Faulkner R, and Mirsky AE (1964) ACETYLATION AND METHYLATION OF HISTONES AND THEIR POSSIBLE ROLE IN THE REGULATION OF RNA SYNTHESIS. Proc Natl Acad Sci U S A 51:786–794

18. Brownell JE, Zhou J, Ranalli T, et al (1996) Tetrahymena Histone Acetyltransferase A: A Homolog to Yeast Gcn5p Linking Histone Acetylation to Gene Activation. Cell 84:843–851

19. Shogren-Knaak M (2006) Histone H4-K16 Acetylation Controls Chromatin

Structure and Protein Interactions. Science 311:844–847

20. Neumann H, Hancock SM, Buning R, et al (2009) A method for genetically installing site-specific acetylation in recombinant histones defines the effects of H3 K56 acetylation. Mol Cell 36:153–163

21. Hebert AS, Dittenhafer-Reed KE, Yu W, et al (2013) Calorie restriction and SIRT3 trigger global reprogramming of the mitochondrial protein acetylome. Mol Cell 49:186–199

22. Rardin MJ, Newman JC, Held JM, et al (2013) Label-free quantitative proteomics of the lysine acetylome in mitochondria identifies substrates of SIRT3 in metabolic pathways. Proc Natl Acad Sci U S A 110:6601–6606

23. Sol EM, Wagner SA, Weinert BT, et al (2012) Proteomic investigations of lysine acetylation identify diverse substrates of mitochondrial deacetylase sirt3. PLoS One 7:e50545

24. Baeza J, Dowell JA, Smallegan MJ, et al (2014) Stoichiometry of site-specific lysine acetylation in an entire proteome. J Biol Chem 289:21326–21338

25. Dittenhafer-Reed KE, Richards AL, Fan J, et al (2015) SIRT3 mediates multi-tissue coupling for metabolic fuel switching. Cell Metab 21:637–646

26. Weinert BT, Iesmantavicius V, Moustafa T, et al (2014) Acetylation dynamics and stoichiometry in Saccharomyces cerevisiae. Mol Syst Biol 10:716

27. Weinert BT, Moustafa T, Iesmantavicius V, et al (2015) Analysis of acetylation stoichiometry suggests that SIRT3 repairs nonenzymatic acetylation lesions. EMBO J 34:2620–2632

28. Weinert BT, Iesmantavicius V, Wagner SA, et al (2013) Acetyl-phosphate is a

critical determinant of lysine acetylation in E. coli. Mol Cell 51:265–272

29. Henriksen P, Wagner SA, Weinert BT, et al (2012) Proteome-wide Analysis of Lysine Acetylation Suggests its Broad Regulatory Scope inSaccharomyces cerevisiae. Mol Cell Proteomics 11:1510–1522

30. Zhang Q, Gu J, Gong P, et al (2013) Reversibly acetylated lysine residues play important roles in the enzymatic activity ofEscherichia coli N-hydroxyarylamineO-acetyltransferase. FEBS J 280:1966–1979

31. Nakayasu ES, Wu S, Sydor MA, et al (2014) A method to determine lysine acetylation stoichiometries. Int J Proteomics 2014:730725

32. Kuhn ML, Zemaitaitis B, Hu LI, et al (2014) Structural, kinetic and proteomic characterization of acetyl phosphate-dependent bacterial protein acetylation. PLoS One 9:e94816

33. Schölz C, Weinert BT, Wagner SA, et al (2015) Acetylation site specificities of lysine deacetylase inhibitors in human cells. Nat Biotechnol 33:415–423

34. Svinkina T, Gu H, Silva JC, et al (2015) Deep, Quantitative Coverage of the Lysine Acetylome Using Novel Anti-acetyl-lysine Antibodies and an Optimized Proteomic Workflow. Mol Cell Proteomics 14:2429–2440

35. Elia AEH, Boardman AP, Wang DC, et al (2015) Quantitative Proteomic Atlas of Ubiquitination and Acetylation in the DNA Damage Response. Mol Cell 59:867–881

36. Tanner KG, Trievel RC, Kuo M-H, et al (1999) Catalytic Mechanism and Function of Invariant Glutamic Acid 173 from the Histone Acetyltransferase GCN5 Transcriptional Coactivator. J Biol Chem 274:18157–18160

37. Marmorstein R and Roth SY (2001) Histone acetyltransferases: function,

structure, and catalysis. Curr Opin Genet Dev 11:155–161

38. Sterner DE and Berger SL (2000) Acetylation of histones and transcription-related factors. Microbiol Mol Biol Rev 64:435–459

39. Berndsen CE, Albaugh BN, Tan S, et al (2007) Catalytic mechanism of a MYST family histone acetyltransferase. Biochemistry 46:623–629

40. Kolonko EM, Albaugh BN, Lindner SE, et al (2010) Catalytic activation of histone acetyltransferase Rtt109 by a histone chaperone. Proc Natl Acad Sci U S A 107:20275–20280

41. Albaugh BN, Kolonko EM, and Denu JM (2010) Kinetic mechanism of the Rtt109-Vps75 histone acetyltransferase-chaperone complex. Biochemistry 49:6375–6385

42. Tanner KG, Langer MR, and Denu JM (2000) Kinetic mechanism of human histone acetyltransferase P/CAF. Biochemistry 39:11961–11969

43. Lau OD, Courtney AD, Vassilev A, et al (2000) p300/CBP-associated Factor Histone Acetyltransferase Processing of a Peptide Substrate: KINETIC ANALYSIS OF THE CATALYTIC MECHANISM. J Biol Chem 275:21953–21959

44. Khochbin S, Verdel A, Lemercier C, et al (2001) Functional significance of histone deacetylase diversity. Curr Opin Genet Dev 11:162–166

45. Imai S, Armstrong CM, Kaeberlein M, et al (2000) Transcriptional silencing and longevity protein Sir2 is an NAD-dependent histone deacetylase. Nature 403:795–800

46. Fischle W, Kiermer V, Dequiedt F, et al (2001) The emerging role of class II histone deacetylases. Biochem Cell Biol 79:337–348

47. Denu JM (2003) Linking chromatin function with metabolic networks: Sir2 family of NAD(+)-dependent deacetylases. Trends Biochem Sci 28:41–48

48. Feldman JL, Baeza J, and Denu JM (2013) Activation of the protein deacetylase SIRT6 by long-chain fatty acids and widespread deacylation by mammalian sirtuins. J Biol Chem 288:31350–31356

49. Mihaylova MM and Shaw RJ (2013) Metabolic reprogramming by class I and II histone deacetylases. Trends Endocrinol Metab 24:48–57

50. Cai L, Sutter BM, Li B, et al (2011) Acetyl-CoA induces cell growth and proliferation by promoting the acetylation of histones at growth genes. Mol Cell 42:426–437

51. Morrish F, Noonan J, Perez-Olsen C, et al (2010) Myc-dependent mitochondrial generation of acetyl-CoA contributes to fatty acid biosynthesis and histone acetylation during cell cycle entry. J Biol Chem 285:36267–36274

52. Evertts AG, Zee BM, Dimaggio PA, et al (2013) Quantitative dynamics of the link between cellular metabolism and histone acetylation. J Biol Chem 288:12142–12151

53. Wellen KE, Hatzivassiliou G, Sachdeva UM, et al (2009) ATP-citrate lyase links cellular metabolism to histone acetylation. Science 324:1076–1080

54. Cai L and Tu BP (2012) Driving the Cell Cycle Through Metabolism. Annu Rev Cell Dev Biol 28:59–87

55. Friis RMN, Wu BP, Reinke SN, et al (2009) A glycolytic burst drives glucose induction of global histone acetylation by picNuA4 and SAGA. Nucleic Acids Res 37:3969–3980

56. Zhao S, Torres AM, Henry RA, et al (2016) ATP-Citrate Lyase Controls a Glucose-to-Acetate Metabolic Switch. Cell Rep 17

57. Carrer A, Parris JLD, Trefely S, et al (2017) Impact of a High-fat Diet on Tissue

Acyl-CoA and Histone Acetylation Levels. J Biol Chem 292:3312–3322

58. Lee JV, Carrer A, Shah S, et al (2014) Akt-dependent metabolic reprogramming regulates tumor cell histone acetylation. Cell Metab 20:306–319

59. Hallows WC, Lee S, and Denu JM (2006) Sirtuins deacetylate and activate mammalian acetyl-CoA synthetases. Proc Natl Acad Sci U S A 103:10230–10235

60. Schwer B, Bunkenborg J, Verdin RO, et al (2006) Reversible lysine acetylation controls the activity of the mitochondrial enzyme acetyl-CoA synthetase 2. Proc Natl Acad Sci U S A 103:10224–10229

61. Starai VJ (2002) Sir2-Dependent Activation of Acetyl-CoA Synthetase by Deacetylation of Active Lysine. Science 298:2390–2392

62. Pehar M and Puglielli L (2013) Lysine acetylation in the lumen of the ER: a novel and essential function under the control of the UPR. Biochim Biophys Acta 1833:686–697

63. Pehar M, Lehnus M, Karst A, et al (2012) Proteomic assessment shows that many endoplasmic reticulum (ER)-resident proteins are targeted by N(epsilon)-lysine acetylation in the lumen of the organelle and predicts broad biological impact. J Biol Chem 287:22436–22440

64. Ogryzko VV, Schiltz RL, Russanova V, et al (1996) The Transcriptional Coactivators p300 and CBP Are Histone Acetyltransferases. Cell 87:953–959

65. Schiltz RL, Mizzen CA, Vassilev A, et al (1999) Overlapping but distinct patterns of histone acetylation by the human coactivators p300 and PCAF within nucleosomal substrates. J Biol Chem 274:1189–1192

66. Kundu TK, Palhan VB, Wang Z, et al (2000) Activator-dependent transcription from chromatin in vitro involving targeted histone acetylation by p300. Mol Cell 6:551–561

67. McManus KJ and Hendzel MJ (2003) Quantitative Analysis of CBP- and P300-Induced Histone Acetylations In Vivo Using Native Chromatin. Mol Cell Biol 23:7611–7627

68. Yang Y-Y, Yu-Ying Y, Grammel M, et al (2011) Identification of lysine acetyltransferase p300 substrates using 4-pentynoyl-coenzyme A and bioorthogonal proteomics. Bioorg Med Chem Lett 21:4976–4979

69. Karanam B, Jiang L, Wang L, et al (2006) Kinetic and mass spectrometric analysis of p300 histone acetyltransferase domain autoacetylation. J Biol Chem 281:40292–40301

70. Stiehl DP, Fath DM, Liang D, et al (2007) Histone deacetylase inhibitors synergize p300 autoacetylation that regulates its transactivation activity and complex formation. Cancer Res 67:2256–2264

71. Wagner GR and Payne RM (2013) Widespread and enzyme-independent Nε-acetylation and Nε-succinylation of proteins in the chemical conditions of the mitochondrial matrix. J Biol Chem 288:29036–29045

72. Ghanta S, Grossmann RE, and Brenner C (2013) Mitochondrial protein acetylation as a cell-intrinsic, evolutionary driver of fat storage: Chemical and metabolic logic of acetyl-lysine modifications. Crit Rev Biochem Mol Biol 48:561–574

73. Wagner GR and Hirschey MD (2014) Nonenzymatic protein acylation as a carbon stress regulated by sirtuin deacylases. Mol Cell 54:5–16

74. Paik WK, Pearson D, Lee HW, et al (1970) Nonenzymatic acetylation of histones with acetyl-CoA. 213:513–522

75. Baeza J, Smallegan MJ, and Denu JM (2015) Site-specific reactivity of

nonenzymatic lysine acetylation. ACS Chem Biol 10:122–128

76. Hansen JC, Tse C, and Wolffe AP (1998) Structure and function of the core histone N-termini: more than meets the eye. Biochemistry 37:17637–17641

77. López-Rodas G, Brosch G, Georgieva EI, et al (1993) Histone deacetylase. A key enzyme for the binding of regulatory proteins to chromatin. FEBS Lett 317:175–180

78. Daujat S, Bauer U-M, Shah V, et al (2002) Crosstalk between CARM1 methylation and CBP acetylation on histone H3. Curr Biol 12:2090–2097

79. Hecht A, Laroche T, Strahl-Bolsinger S, et al (1995) Histone H3 and H4 N-termini interact with SIR3 and SIR4 proteins: a molecular model for the formation of heterochromatin in yeast. Cell 80:583–592

80. Yu Y, Song C, Zhang Q, et al (2012) Histone H3 lysine 56 methylation regulates DNA replication through its interaction with PCNA. Mol Cell 46:7–17

81. Struhl K (1998) Histone acetylation and transcriptional regulatory mechanisms. Genes Dev 12:599–606

82. Clark D, Reitman M, Studitsky V, et al (1993) Chromatin structure of transcriptionally active genes. Cold Spring Harb Symp Quant Biol 58:1–6

83. Dhalluin C, Carlson JE, Zeng L, et al (2002), Structure and Ligand of a Histone Acetyltransferase Bromodomain, http://dx.doi.org/10.2210/pdb1n72/pdb

84. Soutoglou E, Katrakili N, and Talianidis I (2000) Acetylation Regulates Transcription Factor Activity at Multiple Levels. Mol Cell 5:745–751

85. Park J-M, Jo S-H, Kim M-Y, et al (2015) Role of transcription factor acetylation in the regulation of metabolic homeostasis. Protein Cell 6:804–813

86. Thiagarajan D, Vedantham S, Ananthakrishnan R, et al (2016) Mechanisms of

transcription factor acetylation and consequences in hearts. Biochim Biophys Acta 1862:2221–2231

87. Tsubota T, Berndsen CE, Erkmann JA, et al (2007) Histone H3-K56 acetylation is catalyzed by histone chaperone-dependent complexes. Mol Cell 25:703–712

88. Mollapour M and Neckers L (2012) Post-translational modifications of Hsp90 and their contributions to chaperone regulation. Biochim Biophys Acta 1823:648–655

89. Reed NA, Cai D, Blasius TL, et al (2006) Microtubule acetylation promotes kinesin-1 binding and transport. Curr Biol 16:2166–2172

90. Rardin MJ, Newman JC, Held JM, et al (2013) Label-free quantitative proteomics of the lysine acetylome in mitochondria identifies substrates of SIRT3 in metabolic pathways. Proc Natl Acad Sci U S A 110:6601–6606

91. Hebert AS, Dittenhafer-Reed KE, Yu W, et al (2013) Calorie restriction and SIRT3 trigger global reprogramming of the mitochondrial protein acetylome. Mol Cell 49:186–199

92. Baeza J, Smallegan MJ, and Denu JM (2016) Mechanisms and Dynamics of Protein Acetylation in Mitochondria. Trends Biochem Sci 41:231–244

93. Baeza J, Smallegan MJ, and Denu JM (2015) Site-specific reactivity of nonenzymatic lysine acetylation. ACS Chem Biol 10:122–128

94. Michalski A, Cox J, and Mann M (2011) More than 100,000 Detectable Peptide Species Elute in Single Shotgun Proteomics Runs but the Majority is Inaccessible to Data-Dependent LC−MS/MS. J Proteome Res 10:1785–1793

95. Bruderer R, Bernhardt OM, Gandhi T, et al (2015) Extending the limits of quantitative proteome profiling with data-independent acquisition and application to

acetaminophen-treated three-dimensional liver microtissues. Mol Cell Proteomics 14:1400–1410

96. Schilling B, Rardin MJ, MacLean BX, et al (2012) Platform-independent and label-free quantitation of proteomic data using MS1 extracted ion chromatograms in skyline: application to protein acetylation and phosphorylation. Mol Cell Proteomics 11:202–214

97. Dowell JA, Frost DC, Zhang J, et al (2008) Comparison of two-dimensional fractionation techniques for shotgun proteomics. Anal Chem 80:6715–6723

98. Washburn MP, Wolters D, and Yates JR 3rd (2001) Large-scale analysis of the yeast proteome by multidimensional protein identification technology. Nat Biotechnol 19:242–247

99. Wolters DA, Washburn MP, and Yates JR 3rd (2001) An automated multidimensional protein identification technology for shotgun proteomics. Anal Chem 73:5683–5690

100. Boisvert F-M, Ahmad Y, Gierliński M, et al (2011) A Quantitative Spatial Proteomics Analysis of Proteome Turnover in Human Cells. Mol Cell Proteomics 11:M111.011429

101. Kori Y, Sidoli S, Yuan Z-F, et al (2017) Proteome-wide acetylation dynamics in human cells. Sci Rep 7:10296

102. Fan J, Baeza J, and Denu JM (2016) Investigating Histone Acetylation Stoichiometry and Turnover Rate. Methods Enzymol 574:125–148

103. Krautkramer KA, Reiter L, Denu JM, et al (2015) Quantification of SAHA-Dependent Changes in Histone Modifications Using Data-Independent Acquisition Mass

Spectrometry. J Proteome Res 14:3252–3262

104. Lin S and Garcia BA (2012) Examining histone posttranslational modification patterns by high-resolution mass spectrometry. Methods Enzymol 512:3–28

105. Rappsilber J, Mann M, and Ishihama Y (2007) Protocol for micro-purification, enrichment, pre-fractionation and storage of peptides for proteomics using StageTips. Nat Protoc 2:1896–1906

106. Bruderer R, Bernhardt OM, Gandhi T, et al (2016) High-precision iRT prediction in the targeted analysis of data-independent acquisition and its impact on identification and quantitation. Proteomics 16:2246–2256

107. Baeza J, Lawton AJ, Fan J, et al Quantifying dynamic protein acetylation using quantitative stoichiometry, http://dx.doi.org/10.1101/472530

108. Tyanova S, Temu T, Carlson A, et al (2015) Visualization of LC-MS/MS proteomics data in MaxQuant. Proteomics 15:1453–1456

109. Cox J and Mann M (2008) MaxQuant enables high peptide identification rates, individualized p.p.b.-range mass accuracies and proteome-wide protein quantification. Nat Biotechnol 26:1367–1372

110. Cox J, Neuhauser N, Michalski A, et al (2011) Andromeda: a peptide search engine integrated into the MaxQuant environment. J Proteome Res 10:1794–1805

111. Cox J and Mann M (2009) Computational principles of determining and improving mass precision and accuracy for proteome measurements in an Orbitrap. J Am Soc Mass Spectrom 20:1477–1485

112. Cox J, Michalski A, and Mann M (2011) Software lock mass by two-dimensional minimization of peptide mass errors. J Am Soc Mass Spectrom 22:1373–1380

113. Egertson JD, MacLean B, Johnson R, et al (2015) Multiplexed peptide analysis using data-independent acquisition and Skyline. Nat Protoc 10:887–903

114. Claesen J, Dittwald P, Burzykowski T, et al (2012) An efficient method to calculate the aggregated isotopic distribution and exact center-masses. J Am Soc Mass Spectrom 23:753–763

115. Meyer JG, D'Souza AK, Sorensen DJ, et al (2016) Quantification of Lysine Acetylation and Succinylation Stoichiometry in Proteins Using Mass Spectrometric Data-Independent Acquisitions (SWATH). J Am Soc Mass Spectrom 27:1758–1771

116. Still AJ, Floyd BJ, Hebert AS, et al (2013) Quantification of mitochondrial acetylation dynamics highlights prominent sites of metabolic regulation. J Biol Chem 288:26209–26219

117. Weinert BT, Satpathy S, Hansen BK, et al (2017) Accurate Quantification of Site-specific Acetylation Stoichiometry Reveals the Impact of Sirtuin Deacetylase CobB on theE. coliAcetylome. Mol Cell Proteomics 16:759–769

118. Zhou T, Chung Y-H, Chen J, et al (2016) Site-Specific Identification of Lysine Acetylation Stoichiometries in Mammalian Cells. J Proteome Res 15:1103–1113

Acknowledgements : We would like to thank Ian Lienert, Tejas Gandhi, Oliver Bernhardt, Lukas Reiter from Biognosys for the development of the software to generate the *in silico* labeled spectral library and analyze DIA MS data. This work was supported by GM65386 to J.M.D and by NIH National Research Service Award T32 GM007215 to (A.L. & J.B.)

CHAPTER 3: ACSS2 PROMOTES NUCLEAR PROTEIN ACETYLATION BEYOND HISTONES IN A TISSUE-SPECIFIC RESPONSE TO FASTING

Anastasia J. Lindahl, John R. Moffett, Aryan M. A. Namboodiri, and John M. Denu

Author contributions: A.J.L., J.R.M, A.M.M.N, and J.M.D designed research; A.J.L. and J.R.M performed experiments; A.J.L. and J.R.M. analyzed data; A.J.L., J.R.M, A.M.M.N, and J.M.D wrote and/or edited the study. A.J.L specifically made contributions to Figure 3-2 through 3-16. J.R.M made contributions to Figure 3-1, lipid analysis and RNA-sequencing and data processing.

3.1 Abstract

Post-translational modifications (PTMs) of proteins control many complex biological processes through a language of chemical modifications. Chromatin modifying enzymes utilize a variety of metabolites as co-substrates to catalyze their respective chromatin modifications, closely linking chromatin modifications and metabolism. In this study, we utilized mass spectrometry to quantitatively assess chromatin-associated protein and histone acetylation stoichiometry to examine the effects of acyl-CoA short chain synthetase family member 2 (ACSS2). ACSS2 preferentially synthesizes acetyl coenzyme A (acetyl-CoA) from free acetate and CoA and is involved in lipid synthesis and acetylation reactions in the cytoplasm. Here we demonstrate ACSS2 plays a targeted role in nuclear signaling, partially through acetylation of proteins like histones and transcription factors through local synthesis of acetyl-CoA. In the brain, ACSS2 coordinates the response to fasting through protein acetylation and transcript levels of RNA processing pathways. After glucose depletion in both tissues, ACSS2 regulates histone acetylation at H3K18 and H4, modifications catalyzed by the histone acetyltransferase p300. Overall, our results indicate ACSS2 operates through locally modulating protein acetylation in the nucleus to regulate fatty acid metabolism.

3.2 Introduction

Acetyl-CoA is the primary metabolic carbon source in all organisms. The thioester bond between the acetyl group and coenzyme A is a high energy bond facilitating acetate transfer to an enormous array of acetylation targets. Acetyl-CoA can be synthesized from many substrates including pyruvate, citrate, fatty acids, certain amino acids and ketone bodies, as well as directly from acetate. The acetate activating enzyme acyl-CoA synthetase short chain family member 2 (ACSS2) is uniquely involved in acetyl-CoA metabolism in prokaryotes and eukaryotes ***(1)***. This evolutionarily conserved enzyme catalyzes a reaction consuming ATP, acetate and coenzyme A to generate acetyl-CoA, AMP and pyrophosphate (enzyme classification; EC 6.2.1.1). The enzyme is encoded by the gene *Acss2* and has a number of other acronym aliases including ACAS, Acas1, Acs1 and AceCS1. ACSS2 was originally identified from rat liver as a cytosolic enzyme ***(2, 3)*** which participates in the synthesis of fatty acids and sterols ***(4)***. ACSS2 mRNA expression is regulated by sterol regulatory element-binding proteins further substantiating a role in lipid synthesis ***(5–7)***. Subsequently, ACSS2 was shown to be localized in both the cell nuclei and cytoplasm ***(8–10)***. More recently the enzyme has been found to shuttle rapidly between cytoplasm and nucleus over the course of two hours in hypoxic cells ***(11)***.

Radio-labeled acetate was used in the first characterized protein lysine acetylation, the acetylation of histones, which was shown to regulate transcription ***(12, 13)***. However, the mechanism and regulation of the enzymes involved in the catalysis of acetate onto chromatin have remained an open area of investigation. The basic unit of chromatin is an octamer of histone proteins (H2A, H2B, H3, and H4) wrapped by approximately 146 bp and DNA, which is packaged into larger structures and domains in the nucleus. The packaging, or structure, of chromatin is classified broadly into two domains, heterochromatin which represses transcription,

and euchromatin which is permissive to transcription. The maintenance of the domains is influenced by a host of chemical modifications, particularly on the flexible N-terminal tails of histone proteins, influencing DNA-protein and protein-protein interactions. Many of these modifications, such as methylation, acetylation, phosphorylation, and acylation, are catalyzed by chromatin-modifying enzymes utilizing secondary metabolites as co-substrates connecting nuclear processes with metabolism. The enzymes which catalyze the addition of acetyl moieties on lysine on histones, histone acetyltransferases, utilize acetyl coenzyme A (acetyl-CoA) as the co-substrate.

In contrast to the cytoplasmic and nuclear form, the mitochondrial form of the enzyme, acetyl-CoA synthetase 2 (Acas2 or AceCS2) was originally identified from ox heart and found to be expressed predominantly in heart, skeletal muscle and brown adipose tissue ***(14)***. The current accepted name for the mitochondrial form is acyl-CoA synthetase short chain family member 1 (ACSS1). ACSS1 is involved in the synthesis of acetyl-CoA for energy production via the tricarboxylic acid cycle under ketogenic conditions ***(14–16)***. Despite performing the same acetate-activating enzymatic reaction, the nuclear-cytoplasmic and mitochondrial forms of ACSS have very different functional roles and tissue distributions and are regulated by acetylation and deacetylation. The activities of ACSS2 and ACSS1 are post-translationally inhibited by enzymatic acetylation and are reactivated by NAD^+-dependent protein deacetylases known as sirtuins. Distinct sirtuins are responsible for deacetylating and activating the cytoplasmic and mitochondrial forms, with SIRT1 acting to deacetylate nuclear-cytoplasmic form, ACSS2, and SIRT3 acting to deacetylate the mitochondrial form, ACSS1 ***(16)***.

The link between acetylation and metabolism has been extensively shown in the mitochondria demonstrating a relationship between flux through metabolic pathways generating

acetyl-CoA and mitochondrial protein acetylation levels ***(24, 39)***. Acetylation in the mitochondria coordinates fuel switching across tissues in nutrient limiting conditions ***(29).*** Cytoplasmic and nuclear acetyl-CoA synthesis is distinct from mitochondrial acetylation, raising questions about the mechanism of acetyl-CoA synthesis pathways influence on acetylation in the cytoplasm and nucleus. The effects of metabolism on histone acetylation has been studied, however recent proteomics studies indicate acetylation in the nucleus extends far beyond histones and is dynamically regulated by enzymes, in contrast to non-enzymatic acetylation found in the mitochondria ***(24, 39)***. Studies into the effects of metabolism on nuclear acetylation have not used physiologically metabolic perturbations nor systems such as an animal model under fasting necessary to interrogate the influence of acetyl-CoA synthesis pathways regulation of nuclear protein acetylation. For these reasons we investigated the effects of *Acss2*$^{-/-}$ in the mouse to begin understanding the role this enzyme plays influencing protein acetylation levels either through a global concentration-dependent mechanism like the mitochondria, or alternatively through targeted local synthesis of acetyl-CoA. Our results suggest a limited role of ACSS2 in fatty acid synthesis, but a wider role in regulating protein posttranslational modifications, RNA metabolism, and metabolic pathway components.

3.3 Materials and Methods

3.3.1 Acss2 gene knockout:

Breeding pairs of *Acss2* gene (NM-019811) knockout mice were obtained from Lexicon Pharmaceuticals via Taconic Farms, New York, and they were bred in our animal facility on a C57BL background. The *Acss2* gene knockout involved standard procedures using embryonic stem cells with the 129S5 genetic background. The deleted region included approximately 3.6 kb beginning at the transcription start site.

3.3.2 Animal Breeding:

Animal care and experimental procedures were carried out in accordance with NIH guidelines and approved by the Uniformed Services University Animal Care and Use Committee. Animals were housed in an environmentally controlled room (20-23°C, ~44% humidity, 12 hour light/dark cycle, 350-400 lux, lights on at 6:00 am), with food and water available continuously. Animal handling was minimized to reduce animal stress. The homozygous *Acss2*$^{-/-}$ mice reproduced normally and therefore wild type mice and homozygous mice were bred separately for the experiments. Before use in experiments, individual genotypes were confirmed via PCR using probes designed by Lexicon Pharmaceuticals.

3.3.3 Animal Behavior:

Animal behavior in wild type, *Acss2*+/- and *Acss2*$^{-/-}$ mice was examined by open field testing. Locomotor activity was measured using an Accuscan animal activity monitor with infrared photocell system (model RXYZCM; Omnitech, Accuscan Electronics, Columbus, OH), located in a dedicated room within the animal facility. Animals were placed singly in a 40 X 40 X 30 (L x W x H) cm clear Plexiglas arena and lid with multiple 3.5 cm diameter holes placed on top of the arena. One hour of activity was monitored, and data were automatically gathered and transmitted to a computer via an Omnitech Model DCM-I-BBU Digiscan analyzer. Animals were acclimated to the arena prior to testing. Subjects included; males, 10 *Acss2*$^{-/-}$, 6 *Acss2* +/- and 5 wild type mice, females, 8 *Acss2*$^{-/-}$, 7 *Acss2* +/- and 8 wild type mice.

3.3.4 Fatty acid analysis:

Tissue homogenates were thawed and 10 µl aliquots were mixed with 50 µl of 1M NaOH

and left for 60 min at room temperature in the dark. The mixtures were then acidified with 1 M HCl to pH 3-4, 10 ng of the fatty acid internal standard mix was added and the solutions were saturated with NaCl. The mixtures were extracted with isooctane-ethyl acetate (9:1) four times and the extracts from each sample were pooled. Samples were then dried and redissolved in 65 µl of solvent B (methanol-water-ammonium acetate; 95:5:0.1%, pH 7.6). To each sample, 35 µl of solvent A was added (methanol-acetonitrile-water-ammonium acetate; 5:5:85:0.1%, pH 7.6). An aminopropyl-Strata column was conditioned with di-isopropyl ether followed by hexane, and the samples loaded. Columns were eluted with 3 ml di-isopropyl ether-formic acid (98:2). Eluates were dried and redissolved in a mixture of solvents A and B (35:65%). LC-MS was performed as previously described ***(19)***.

3.3.5 Site-Specific Acetylation Stoichiometry

3.3.5.1 Chromatin Isolation

Chromatin isolation performed as described previously ***(20)***. In brief, homogenized 40 mg of tissue in 800 µL of hypotonic lysis buffer (10 mM Tris-HCl, 10 mM NaCl, 3 mM $MgCl_2$ at pH 7.4) in a 1 mL dounce homogenizer. Cells were mechanically lysed and let to stand on ice for 5 minutes to complete hypotonic lysis. Filtered the homogenate through a cell strainer to remove debris. Centrifuged the homogenate at 800 x g for 5 minutes at 4 °C . Washed crude nuclear pellet with 2 mL cold lysis buffer and centrifuge at 800 x g for 5 minutes at 4 °C. Repeated wash steps again with lysis buffer and then PBS. Resuspended the nuclear pellet in 500 µL of nuclear lysis buffer (10 mM Tris-HCl 10 mM NaCl 3 mM $MgCl_2$ 0.2 mM EDTA at pH 7.4). Incubated for 15 minutes on ice with vortexing every 5 minutes. Centrifuged at 14,000 x g for 5 minutes. Resuspended pellet with lysis buffer, centrifuged at 3000 x g and then kept the

pellet. Resuspended chromatin pellet in 300 µL of 150 mM salt in the lysis buffer (10 mM Tris-HCl 3 mM $MgCl_2$ pH 7.4). Let stand on ice for 15 minutes with vortexing every 5 minutes. Centrifuged at 3000 x g for 5 minutes. Resuspended in 300 µL 450 mM salt in lysis buffer (10 mM Tris-HCl 3 mM $MgCl_2$ pH 7.4). Let stand on ice for 15 minutes with vortexing every 5 min. Centrifuged at 3000 x g for 5 min obtain chromatin-bound proteins in the supernatant.

3.3.5.2 Mitochondria Isolation

Mitochondrial isolation performed as described previously ***(20)***. In brief, homogenized 40 mg of tissue in 800 µL of hypotonic lysis buffer (10 mM Tris-HCl, 10 mM NaCl, 3 mM $MgCl_2$ at pH 7.4) in a 1 mL dounce homogenizer. Cells were mechanically lysed and let stand on ice for 5 minutes to complete hypotonic lysis. The homogenate was filtered through a cell strainer to remove debris and centrifuged at 800 x g for 5 minutes at 4 °C. The supernatant contained cytoplasm and mitochondria. To isolate mitochondria, the supernatant was centrifuged at 10,000 x g for 10 minutes at 4° C to pellet the mitochondria. The pellet was resuspended with 500 µL buffer and repeated centrifugation clarified the mitochondria enriched subcellular fraction.

3.3.5.3 Chemical acetylation and digestion

Chemical acetylation and digestion performed as described previously ***(20–22)***. Equal amounts of protein (20 µg) were resuspended into 25-30 µL of urea buffer (8 M urea (deionized), 500 mM ammonium bicarbonate pH = 8.0, 5 mM DTT). The sample was incubated at 60 °C for 20 minutes while shaking at 1500 RPM (Eppendorf ThermoMixer® C). Cysteine alkylation was carried out with 50 mM iodoacetamide and incubated for 20 minutes. Chemical acetylation of unmodified lysine residues was performed as previously described ***(21, 23, 24)***. Briefly, ~20 µmol of the "light" ^{12}C-acetic anhydride (Sigma) or "heavy" D_6-acetic anhydride (Cambridge Isotope

Laboratories) was added to each sample and incubated at 60 °C for 20 minutes at 850 RPM (Eppendorf ThermoMixer® C). The pH was raised to ~8 using ammonium hydroxide and visually checked with litmus paper. Two rounds of chemical acetylation were performed to ensure near-complete lysine acetylation. To hydrolyze any O-acetyl esters formed during the chemical acetylation, the pH of the sample was raised to ~8.5 and incubated at 60 °C for 20 minutes at 850 RPM (Eppendorf ThermoMixer® C). For protein digestion, the urea concentration was diluted to ~2 M by adding 100 mM ammonium bicarbonate pH = 8.0 followed by addition of trypsin (Promega) at a final ratio of 1:100. The sample was digested at 37 °C overnight while shaking at 350 RPM (Eppendorf ThermoMixer® C). The urea concentration was further diluted to ~1 M using 100 mM ammonium bicarbonate pH = 8.0 and digested with gluC (1:100) at 37 °C for 4-6 hours while shaking at 350 RPM (Eppendorf ThermoMixer® C). The sample was acidified by the addition of 15 µL of acetic acid.

3.3.5.4 Offline High pH Reverse Phase (HPRP) Prefractionation of Spectral Library Samples

Chemically acetylated peptides were resuspended into ~2mL of HPRP buffer A (100 mM Ammonium Formate pH = 10) and injected onto a pre-equilibrated Phenomenex Gemini® NX-C18 column (5µm, 110Å, 150 x 2.0mm) with 2% buffer B (10% Buffer A, 90% acetonitrile). Peptides were separated with a Shimadzu LC-20AT HPLC system using a 2% - 40% buffer B linear gradient over 30 minutes at 0.6 mL/min flow rate, collecting 24 fractions throughout the length of the gradient ***(20, 22)***. Fractions were dried down using a speedvac and pooled by concatenation into 6 final fractions as described previously ***(21)***.

3.3.5.5 LC-MS/MS Data Dependent Acquisition (DDA) Analysis of Spectral Library Samples

Our method to analyze site-specific lysine acetylation by mass spectrometry-based proteomics utilizes a Thermo Q-Exactive Orbitrap mass spectrometer coupled to a Dionex Ultimate 3000 RSLC nano UPLC with a Waters Atlantis reverse phase column (100 um x 150 mm). The mobile phases contain 0.1% formic acid in HPLC grade H_2O as solvent A and 0.1% formic acid in HPLC grade ACN as solvent B. The sample is eluted over a linear gradient of 2-40% B at a flow rate of 700 nL/minute over a 60 minute gradient. The peptides are introduced into the mass spectrometer by nanoelectrospray ionization. The mass spectrometer performs in positive mode with a survey scan with a 70,000 resolution, AGC of 1E6, max fill time 250 ms, and a scan range of 350-2000 m/z. The data-dependent MS/MS analysis is performed with a resolution of 17,500 AGC of 1E5, max fill time 100 ms, isolation window of 2.0 m/z and a loop count of 10. The voltage of the source is set at 2.3 kV and the capillary temperature is 250 °C.

3.3.5.6 LC-MS/MS DIA Data Analysis

Our method to quantify acetylation stoichiometry uses a Thermo Q-Exactive Orbitrap mass spectrometer coupled to a Dionex Ultimate 3000 RSLC nano HPLC with a Waters Atlantis reverse phase column (100 um x 150mm). The mobile phases contain 0.1% formic acid in HPLC grade H_2O as solvent A and 0.1% formic acid in HPLC grade ACN as solvent B. The sample is eluted over a linear gradient of 2-40% B at a flow rate of 700 nL/minute over a 60 minute gradient. The peptides are introduced into the mass spectrometer by nanoelectrospray ionization. The mass spectrometer performs in positive mode with a survey scan with a 70,000 resolution, AGC of 1E6, max fill time 100 ms, and a scan range of 400-1000 m/z. The survey scan was followed 30 DIA scans in profile mode with a resolution of 35,000, AGC 1E6, 20 *m/z* window, and NCE of 25 to balance the frequency of b-ions, y-ions, and the number of PSMs to gain

higher fragmentation coverage for MS2 quantitation, particularly important for site-specific quantitation of multiple lysine containing peptides. The voltage of the source is set at 2.3 kV and the capillary temperature is 250 °C.

3.3.5.7 Generating a Spectral Library

The spectral library consists of MS/MS fragmentation reference spectra resulting from data-dependent acquisition (DDA) MS runs. For our workflow, we performed DDA runs with a mixture of equal amounts of protein from all conditions which were chemically acetylated with ^{12}C-acetic anhydride, digested with trypsin and gluC, followed by HPRP prefractionation (see above). Prior to MS analysis, iRT peptides (Biognosys) were spiked into each sample following the manufacturer's guidelines. Database search was performed using MaxQuant version 1.5.4.1 using lysine acetylation and methionine oxidation as variable modifications and cysteine carbamidomethylation as a fixed modification. The MaxQuant search results were imported into Spectronaut to build the 12C-AcK library. The 12C-AcK spectral library was imported into a spectral library modifier, to create a library with all possible isotopically labeled peptide combinations, many of which may be too low in abundance to generate experimental peptide fragmentation spectra. The spectral library was completed with the corresponding precursor m/z values and fragment m/z values. The most intense fragment ions selected from the initial MS2 spectrum were cloned to the other peptide precursor versions. All peptide precursor versions will have identical retention time and hence iRT was also cloned.

3.3.5.8 DIA MS data analysis

Data from DIA-MS was analyzed using Spectronaut Pulsar version 12.0. Thermo raw files were converted to HTRMS files with the Spectronaut Raw to HTRMS converter using the default

settings and input into Spectronaut. The Spectronaut default settings for quantitation were used with a slight modification: Identification-Qvalue score was set to 0.1 and Workflow-Unify peptide peaks and force label free. With this workflow, Spectronaut will then transfer the integration boundaries of the best scoring peptide precursor to the other peptide precursors and use label free quantification for comparison of the labels in later analysis. Because all the 2^n peptide precursor versions only differ by the number of heavy instead of light acetylated lysine the retention time is expected to be identical. The spectral libraries which were completed as described above for all the light/heavy peptide precursor versions were used with this workflow. A Spectronaut output file containing all the fragment ion peak areas along with the corresponding peptide and protein identification was exported and used to compute the lysine site stoichiometry.

3.3.5.9 Quantification of Site-Specific Acetyl Lysine Stoichiometry

Data processing was performed in R v3.5.0 (http://www.r-project.org/) using an in-house made R script. The stoichiometry preprocessing pipeline consists of two major steps: quantifying fragment ion stoichiometry and natural abundance isotopic correction as previously detailed ***(20, 22)***.

3.3.5.10 Quantification of Protein with MSstats

Protein abundance summarization was performed using MSstats v3.12.0 utilizing Spectronaut output. The function "SpectronauttoMSstatsFormat" was used with the following arguments: intensity set to "PeakArea", filter_w_Qvalue set to TRUE, qvalue_cutoff set to 0.01, useUniquePeptide set to TRUE, fewMeasurements set to "remove", removeProtein_with1Feature set to FALSE, and summaryforMultipleRows set to "max". The dataProcesses function was then performed using the defaults ***(22, 25)***.

3.3.5.11 Subcellular Localization Analysis

To assign protein subcellular localization, we used the MitoCarta ***(26, 27)*** and Uniprot (http://www.uniprot.org/) databases. For "Mitochondrial" assignment of proteins, we used the Mitocarta database. Additionally, we used "Subcellular location" or "GO - Cellular component" from the Uniprot database to assign "Mitochondrial", "Nuclear", "Chromatin", "Cytoplasmic", "Endomembrane", and "Histone" protein lists. Proteins not included in these lists were noted as "No Annotation". Because many proteins can be trafficked amongst subcellular compartments, assignments were not mutually exclusive.

3.3.5.12 Quantitative Site set functional Score Analysis (QSSA)

The intersection of the KEGG pathway map ***(28)*** and proteins in the spectral library detected with < 1% FDR was used for the protein set background. Acetylation coverage for each (p) pathway was calculated as the ratio of the number of acetyl sites identified (n_{ack}) over the total number of lysines in the pathway (n_k), counted using protein sequences from Uniprot. The extent of acetylation was taken into account by summing the acetylation stoichiometry(s) across all conditions and all sites in each pathway, then the ratio of extent of acetylation was calculated for each bin or condition compared to the mean. To allow for combining acetylation coverage and stoichiometry, the standard score of each quantity was taken. The overall pathway score was then calculated as the sum of the individual z-scores ***(22, 29)***.

3.3.6 Transcriptomics Analysis

3.3.6.1 RNA sequencing analysis:

Tissue samples from normally fed (non-fasted), adult (15 to 16 weeks old) *Acss2*$^{-/-}$ and

age-matched wild type mice of the same strain were subjected to RNA-seq analysis. RNA was extracted, frozen and processed at the University of Chicago Genomics Facility. Tissue samples were collected from normally fed (non-fasted) and 48-hour fasted, adult (15 to 16 weeks old) *Acss2*$^{-/-}$ and age-matched wild type mice of the same strain. RNA quality and quantity were checked using an Agilent Bioanalyzer. RNA was processed into a cDNA library using Illumina TruSeq RNA Library Prep Kit v2 according to manufacturer protocols. Samples were run on an Illumina HiSeq4000. Tissues examined included liver (n = 5 *Acss2*$^{-/-}$ and 4 wild type) and brain (n = 3 *Acss2*$^{-/-}$ and 3 wild type).

3.3.6.2 RNA-Seq Data analysis:

RNA-seq data from brain and liver of 48-hour starved and fed WT and *Acss2*$^{-/-}$mice was aligned and analyzed with DEseq by the University of Chicago Genomics Facility. A two-tailed t-test was performed to determine statistical significant differences of *Acss2*$^{-/-}$ and WT fold changes. Ratios above 2 or below negative 2 with a p-value below 0.05 for a tissue were determined to be significant. Significant genes from all four conditions were clustered by their four fold changes using the R k means algorithm PAM clustering. The number of clusters was evaluated by mean silhouette indices. The clusters were then analyzed DAVID for GO term enrichment and network building. Cytoscape was utilized to visualize the networks with gene expression data.

3.3.7 Histone Posttranslational modifications

3.3.7.1 Histone Extraction and preparation

Tissue was homogenized in 800 µL of ice-cold buffer A (10 mM Tris-HCl, 10 mM NaCl, 3 mM $MgCl_2$, pH 7.4) with histone deacetylase and protease inhibitors (1 mM sodium butyrate, 4

μM trichostatin A, 100 μM phenylmethylsulfonyl fluoride, 10 μg/mL leupeptin, and 10 μg/mL aprotinin) in a prechilled 1 mL dounce homogenizer. Tissue was homogenized with 40 strokes and centrifuged at 800 x *g*. The crude nuclear pellet was then resuspended in 200 μL of ice-cold PBS. Histones were acid extracted, followed by two rounds of chemical derivatization using propionic anhydride and trypsinized as described ***(30, 31)***. After chemical derivatization, all N-termini and unmodified or monomethylated lysine residues were propionylated. This labeling method prevents cleavage by trypsin, which cleaves C-terminally to unmodified lysine and arginine residues, enabling the generation of consistent peptides amenable to MS analysis.

3.3.7.2 Generation of a Spectral Library

For both DDA and DIA, 1 μg of propionylated histone peptides were injected onto a Dionex Ultimate3000 nanoflow HPLC with a Waters NanoEase C18 column (100 μm × 15 cm, 3 μm) coupled to a Thermo Q-Exactive Orbitrap mass spectrometer. The mobile phases contain 0.1% formic acid in HPLC grade H_2O as solvent A and 0.1% formic acid in HPLC grade ACN as solvent B. The sample was eluted over a linear gradient of 2–35% mobile phase B over 65 min a a flow rate of 700 nL/minute. The peptides were introduced into the mass spectrometer by nanoelectrospray ionization. The mass spectrometer was operated in DDA mode with dynamic exclusion enabled (exclusion duration = 8 s) in positive mode with a survey scan with a 70,000 resolution, AGC of 1E6, max fill time 100 ms, MS2 resolution 17 500, MS2 AGC 2E5, MS2 maximum fill time 500 ms, and MS2 NCE 30. For each cycle, one full MS1 scan range, 300–1100 *m*/*z*, was followed by 10 MS2 scans using an isolation window size of 2.0 *m*/*z*.

3.3.7.3 LC-MS/MS DIA Data Analysis

In DIA, the mass spectrometer was operated with a MS1 scan resolution 35 000, AGC of

1E6, max fill time 100 ms, scan range 390–910 *m*/*z*, followed by a DIA scan with a loop count of 10. DIA settings were window size of 10 *m*/*z*, resolution 17 500, AGC of 1E6, max fill time AUTO, and NCE 30. For each cycle, one full MS1 was followed by 10 MS2 scans using an isolation window size of 10 *m*/*z*. Total cycle time for a complete scan across the whole scan range was 5.4 s.

3.3.7.4 Quantification of histone posttranslational modifications

For Skyline analysis, all MS1 and MS2 peaks were selected manually based on retention times and presence of appropriate transitions. Peak areas for all selected transitions in Skyline were combined for quantitation. All histone peptide MS1 peaks and their integration bounds were verified using the XCalibur Qual Browser (v2.2). For quantifying the percent of total for each peptide species, all peptide areas belonging to a peptide "family" were summed to obtain the total area for that family. The percent of the total for each peptide member of the family was then obtained by dividing the individual peptide area by the total family area. In cases of isobaric and co-eluting peptides, the summed area of precursor peaks was averaged among all co-eluting, isobaric members since all such members are represented by the same set of precursor peaks. All *p*-values were generated using Welch's *t*-test (biological replicates, $n = 4$). Statistical significance was determined by $p < 0.05$.

3.3.8 Metabolite Analysis

Brain cortices and liver isolated from 2-month old, 48-hour-fasted and fed WT and *Acss2*$^{-/-}$ mice (n = 5) were placed in 0.8 ml cold (20°C) 80:20 methanol:H_2O (v/v) and homogenized with a glass dounce homogenizer. The sample was centrifuged at 14,000 3x g for 10 min at 4°C. The supernatant was transferred to a new tube on ice. The pellet was re-extracted with 0.8 ml

cold (20°C) 40:40:20 methanol:ACN:H_2O (v/v) twice, and the supernatants were combined. The samples were dried under nitrogen and resuspended in H_2O for LC-MS analysis. Samples were analyzed using a Thermo Fisher Q Exactive Hybrid Quadrupole-Orbitrap Mass spectrometer coupled to a Dionex UltiMate 3000 UHPLC system. Samples are separated using a 1.7 μm C18 100mm x 2.1 mm Waters Acquity column, with the following gradient of solvent A (MeOH) and solvent B (97% H_20, 3% MeOH, 10mM TBA, pH 8.4) at a flow rate of 0.2 mL/min: 0-5min, 95% solvent B; 5-17min, linearly increase solvent A to 95%; 17-120min, isocratic 95% solvent B ; 20-25min, equilibration with 95% solvent B. Samples are introduced to the mass spectrometer by heated electrospray ionization. Settings for the ion source are: 10 aux gas flow rate, 35 sheath gas flow rate, 1 sweep gas flow rate, 3.5 kV spray voltage, 320°C capillary temperature, and 300°C heater temperature. Analysis is performed under negative ionization mode, with scan range of 85–1275 *m/z*, resolution of 70 000, maximum injection time of 40 ms, and AGC of 1E6. The results were normalized to tissue weight.

3.4 Results

3.4.1 Animal Behavior:

The importance of acetyl-CoA generation in the brain is underscored by the fact cytoplasmic-nuclear acetyl-CoA is used for lipid synthesis and histone acetylation. To assess whether disruption of acetyl-CoA synthesis through ACSS2 affects memory formation, we performed open field and novel object recognition testing. Normally fed *Acss2*$^{-/-}$, *Acss2* +/- and wild type mice were tested for open field activity. Overall movement was decreased in both male and female *Acss2*$^{-/-}$ mice, but only reached significance in females (Figure 3-1). The *Acss2*$^{-/-}$ females show a difference in total distance (Figure 3-1A) and movement time (Figure 3-1B).

(32)

Figure 3-1. Fed *Acss2*$^{-/-}$, *Acss2* +/- and wild type mice open field activity.

Overall movement was decreased in both male and female *Acss2*$^{-/-}$ mice, but only reached significance in females. The *Acss2*$^{-/-}$ females show a difference in total distance. * $p < 0.05$

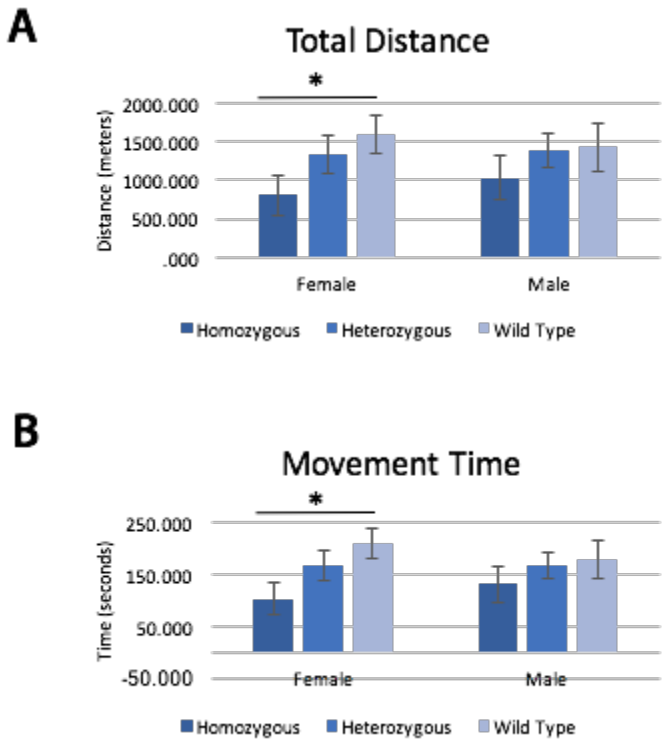

3.4.2 Lipid analysis:

To evaluate whether ACSS2 functions in fatty acid homeostasis, we performed a lipidomic analysis of the WT and *Acss2*$^{-/-}$ mice. Brain, liver and adipose tissues from non-fasted mice were analyzed for fatty acid content via mass spectrometry (n = 3). Very few significant differences were observed in fatty acid content between wild type and knockout mouse tissues. Liver eicosanoic acid (a saturated fatty acid with a 20:0) was slightly elevated in the knockout mice (KO = 1.55 μg/ml +/- 0.18, WT = 1.31 μg/ml +/- 0.15 $p < 0.054$). In the brain, oleic acid (a monounsaturated omega-9 fatty acid; 18:1 cis-9) was significantly lower in the *Acss2*$^{-/-}$ mice (KO = 1084 μg/ml +/- 121, WT = 1401 μg/ml +/- 268, $p = 0.043$). Brain stearic acid (18:0) was significantly lower in the knockout mice (KO = 773 +/- 38, WT = 884 +/- 66, $p = 0.012$). In adipose tissue myristic acid (C 14:0) was significantly higher in the *Acss2*$^{-/-}$ mice (KO = 22.2 μg/ml +/- 3.1, WT = 15.5 μg/ml +/- 4.4, $p = 0.024$). No other significant differences were noted. Together, these results indicate ACSS2 does control the levels of some fatty acids, however, the overall lack of major changes in fatty acid profiles suggests ACSS2's impact on whole-body lipid composition under fed conditions is surprisingly limited.

3.4.3 Acetylation of chromatin coordinates metabolic signaling and RNA metabolism response to fasting in ACSS2 dependent manner

We performed our site-specific acetyl-lysine stoichiometry analysis detailed in Chapter 2 on chromatin isolated proteins from brain and liver tissue to study tissue-specific and ACSS2-dependent alterations to chromatin acetylation stoichiometry and the chromatin proteome to examine targeted versus global effects of protein lysine acetylation Four wild type and *Acss2*$^{-/-}$ mice were harvested after regular feeding and a 48-hour fasting to examine the effects of the loss

of *Acss2*$^{-/-}$ in a state of lipid degradation and utilization in physiological conditions under which ACSS2 contributes to metabolism ***(4, 33)***. Absence of ACSS2 did not significantly reduce lipid synthesis in the fed state, nor change lipid composition suggesting another role of ACSS2 in regulating metabolism, such as protein acetylation. Across brain and liver, a total of 4370 acetyl sites were identified and stoichiometry of 2966 acetylation sites was quantified from 1700 chromatin-associated proteins (Figure 3-2A).

For a comparison across all four combinations of diet and genotype in both tissues, we employed data-independent acquisition (DIA) mass spectrometry based acetylation stoichiometry method ***(20, 22)*** to reduce missing values, which are commonly observed in data-dependent acquisition (DDA). In DDA obtaining peptide fragment information is determined by peptide abundance for a limited number of peptides each scan, leading to missing values between samples ***(34)***. When employing isotopic chemical labeling for stoichiometry determination, DIA based methods capture a more complete dataset, fragmenting both heavy and light peptides within each m/z window rather than based on each labeled peptide relative abundance ***(22)***. However, due to our heavy isotopic labeling scheme acetylation occupancy nearing the two extremes of 0 or 100% is impossible to directly determine. Acetylation, particularly enzyme-catalyzed acetylation, can change dramatically and may reach either 0% or 100%. Therefore, to capture extreme acetylation stoichiometries, data imputation was used. If a heavy and light fragment pair was observed in at least three animals in one condition, missing fragments were imputed as 75% the lowest observed value of the missing label in other conditions if protein abundance was unchanged. This assumes missing heavy or light peaks for these peptides were not present at a detectable level, rather than simply not observed (Figure 3-2C, D).

Global distribution of lysine acetylation stoichiometry was not altered by diet or

genotype, indicating ACSS2 does not globally alter chromatin protein acetylation through a reduction of the cytoplasmic and nuclear pool of acetyl-CoA, as has been previously suggested (Figure 3-2B). Global acetylation stoichiometry distribution across chromatin samples demonstrated higher acetylation site occupancy on average than has been determined for other subcellular compartments, specifically mitochondria. The higher levels of acetylation on chromatin suggest acetylation of chromatin-associated proteins is catalyzed and regulated by an enzyme-catalyzed mechanism, rather than low levels of acetylation through a non-enzymatic mechanism. Alterations in observed acetylation stoichiometry were primarily due to changes in acetyl occupancy rather than protein abundance, as shown by the minimal overlap of significantly changing acetylation sites and significantly changing proteins.

Analysis of biological pathways of protein acetylation was undertaken with QSSA analysis previously described ***(22, 29)***. QSSA analysis incorporates both the levels of acetylation stoichiometry and the number of identified acetylation sites into account to determine the level of enrichment across a specific pathway (Figure 3-3A, B). To look at global acetylation trends on chromatin which have not been previously explored despite higher levels of lysine acetylation and studies demonstrating targeted enzymatic regulation of acetylation, lysine acetylation stoichiometries from fed WT animals were split into 4 equal-sized bins and assessed for functional enrichment within each bin. Brain and liver had similar trends in fed wild type animals with acetylation stoichiometry of chromatin-bound proteins regulating metabolism and metabolism of protein distributed across high and low acetylation stoichiometries. Previous studies have suggested acetyl-CoA and acetylation of metabolic pathways may function as a rheostat of cellular metabolism on metabolic pathway components to coordinate carbon source usage of acetyl-CoA and metabolic flux ***(35–38)***. Alternatively, components of cellular responses

to stress, particularly the execution phase of apoptosis and associated with DNA fragmentation, are highly acetylated in the fed state suggesting these acetylation events may inhibit cell death in healthy wild type normally fed animals. Similar results were observed in a previous proteomic study for acid stress in *E.coli* where acetate metabolism drove acetylation of a stress response DNA binding factor to occlude it from binding to DNA and execute DNA fragmentation ***(39)***. Chromatin associated signaling pathways were lowly acetylated in fed animals, indicating acetylation is likely an activating modification that has not been induced. One key difference exists between brain and liver in the fed animals, where in brain acetylation of proteins associated with the immune system, particularly interferon signaling have moderate levels of acetylation (Figure 3-3A, B).

Dietary stress, such as the 48-hour fasting period used in this study, induces coordinated signaling, metabolic and transcriptional response across tissues to maintain nutrient availability. In our analysis of brain and liver chromatin acetylation stoichiometry, the median stoichiometry across the chromatin proteome was around ~7%, which was not altered in the *Acss2*$^{-/-}$ animals nor by the 48-hour fast (Figure 3-2B) indicating ACSS2 does not influence acetylation through a global concentration-dependent model. However, although the overall distribution of acetylation stoichiometry did not change, individual acetylation sites were significantly perturbed by the loss of ACSS2, the 48-hour fast, and a combination of the two challenges. Acetylation sites have two proposed mechanisms of affecting downstream protein function 1) through single acetylation sites independently moderating function of a protein such as enzymatic activity, binding, localization, or complex assembly and 2) through acetylation cooperatively moderating multiple protein components along pathway. The first is more likely to regulate protein function by larger magnitude changes in acetylation stoichiometry, whereas the second is more likely to function

through moderate changes in acetylation stoichiometry distributed across many sites. In our analysis, we see alterations in acetylation in response to fasting that fit both profiles.

Overall, the brain had a larger dynamic range of acetylation stoichiometry than liver, and the dynamic acetylation response to fasting is significantly reduced in the absence of ACSS2 (Figure 3-4). When examining acetylation sites present in all four conditions for each tissue, the brain has more significantly changing acetylation sites than liver in response to fasting, of which a subset is differentially acetylated between wild type and *Acss2*$^{-/-}$ animals (Figure 3-5). Many of the acetylation sites with the largest dynamic range affected by the loss of ACSS2 were more highly acetylated under fed conditions (Figure 3-4).

Functional differences in the brain showed higher acetylation stoichiometry in wild type compared to the loss of ACSS2 on pathways controlling metabolism, metabolism of proteins and RNA, mRNA processing, protein posttranslational modifications, and vesicle-mediated transport. Previously, in brain ACSS2 was found to be preferentially nuclear and recruited to active genes in differentiated neurons ***(32)***. Reduction of protein acetylation on mRNA processing and RNA metabolism in the absence of ACSS2 suggests ACSS2-derived acetyl-CoA regulates these acetylation sites, likely through controlling synthesis of the acetyl donor, acetyl-CoA. In the liver, acetylation stoichiometry in wild type mice was high on chromatin proteins associated with DNA fragmentation, cell senescence, and apoptosis in addition to p53 and p38 MAPK signaling. In the absence of ACSS2, the stoichiometry of many of these acetylation sites was reduced. ACSS2 has demonstrated roles in lipid metabolism, autophagy, and acetylation of histones and the transcription factor HIF-2a to respond to dietary stress ***(40–42)***. In addition, previous studies have intimately linked mitochondrial metabolism and adaptation to fasting to changes in acetylation ***(29, 43, 44)***. This is the first assessment of changing acetylation broadly moderating

chromatin-bound proteins which regulate metabolism demonstrating ACSS2-derived acetyl-CoA regulates targeted acetylation in the nucleus. The regulation by ACSS2-derived acetyl-CoA was mutually exclusive with regulation of the ACLY, an alternative acetyl-CoA generation pathway, locus by acetylation ***(42)***.

Figure 3-2. Global analysis of chromatin acetylation stoichiometry.

A) Total counts of proteins, peptides, acetyl-lysine since, and sites with quantified stoichiometry from brain and liver chromatin of *Acss2*$^{-/-}$ and WT fed and 48-hour fasted animals (n = 4 each condition). **B)** Global distribution of the mean stoichiometry for each lysine site quantified *Acss2*$^{-/-}$ and WT fed and 48-hour fasted animals. **C)** Overlap of proteins quantified from chromatin acetyl-proteomics across all four conditions. **D)** Overlap of peptides quantified from chromatin acetyl-proteomics across all four conditions.

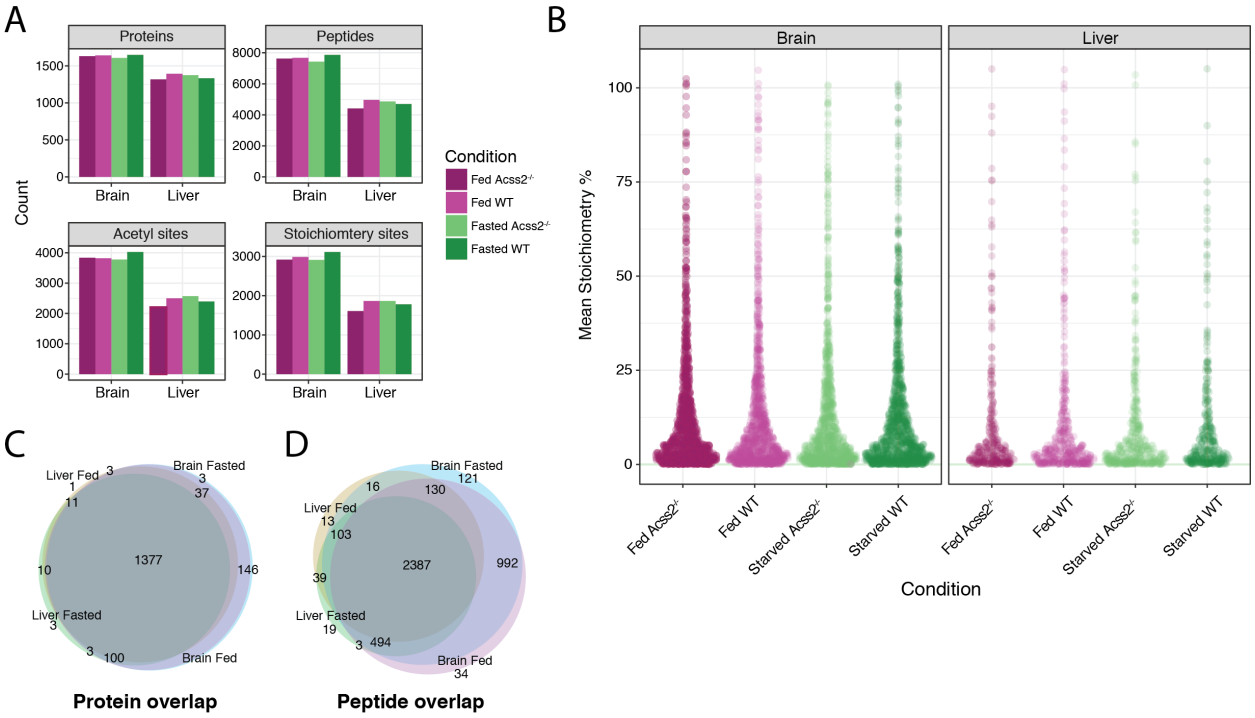

Figure 3-3. Functional QSSA analysis of acetylation distribution on chromatin during fed the state in WT animals.

A) QSSA plot of brain chromatin acetylation stoichiometries from WT fed mice. **B)** QSSA plot of liver chromatin acetylation stoichiometries from WT fed mice. **C)** Global distribution of brain chromatin acetylation stoichiometries **D)** distributed in 4 equequal-sizedns for the QSSA analysis above. **E)** Global distribution of liver chromatin acetylation stoichiometries **F)** distributed in 4 equequal-sizedns for the QSSA analysis above.

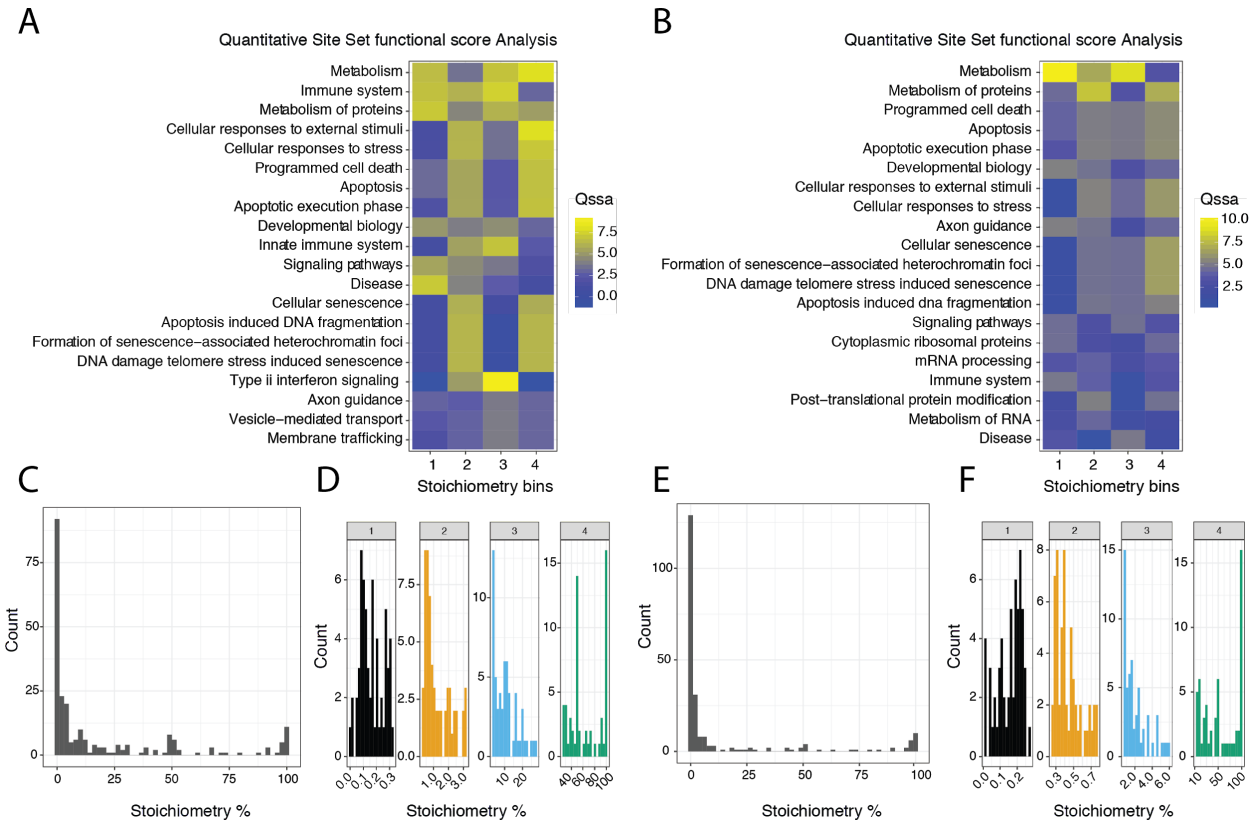

Figure 3-4. Chromatin acetylation changes across dietary conditions and tissues in *Acss2*$^{-/-}$ and WT mice.

Stoichiometry % difference plot of *Acss2*$^{-/-}$ and WT mice. Lines show magnitude of difference and stoichiometry of fed and 48-hour fasted mice and are colored by which dietary condition was higher.

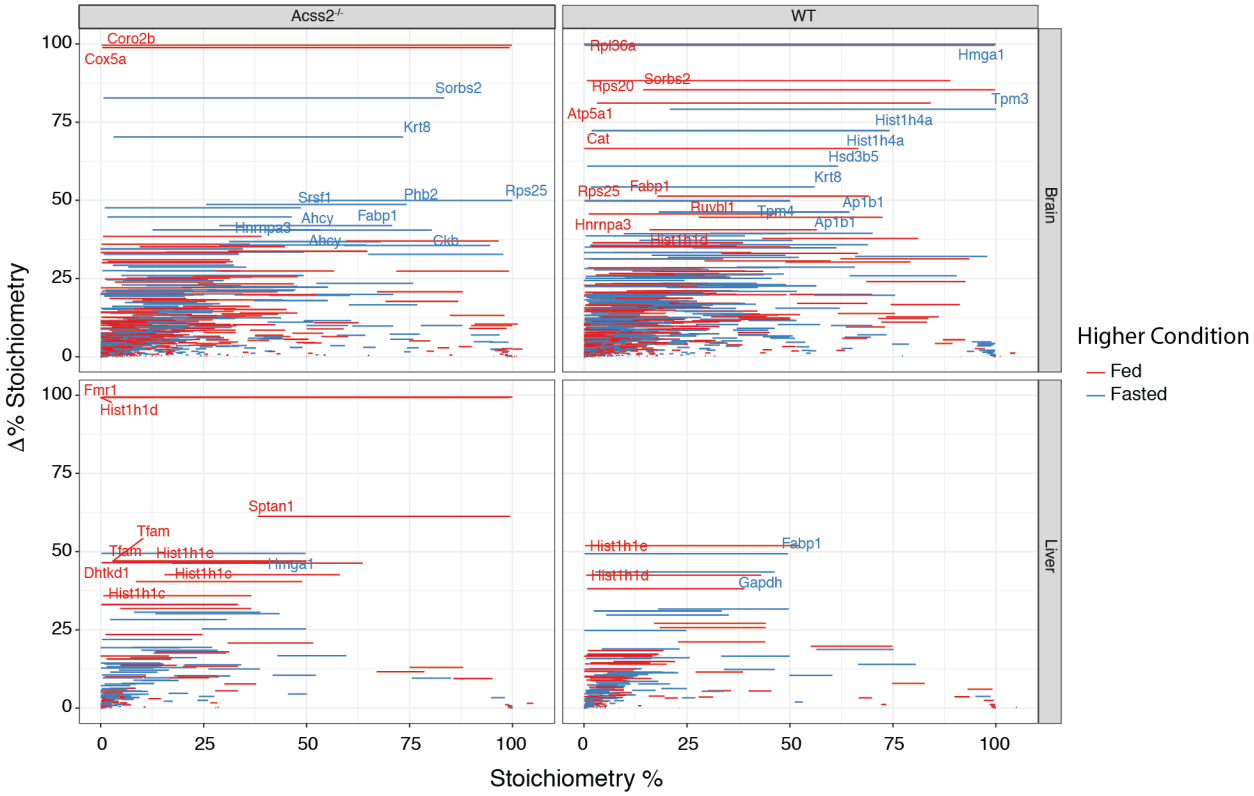

Figure 3-5. Volcano plot of acetylation changes across dietary conditions and tissues in *Acss2*$^{-/-}$ and WT mice.

Stoichiometry % difference volcano plot of *Acss2*$^{-/-}$ and WT fed and 48-hour fasted mice. P values calculated by two way ANOVA (n = 4 each condition).

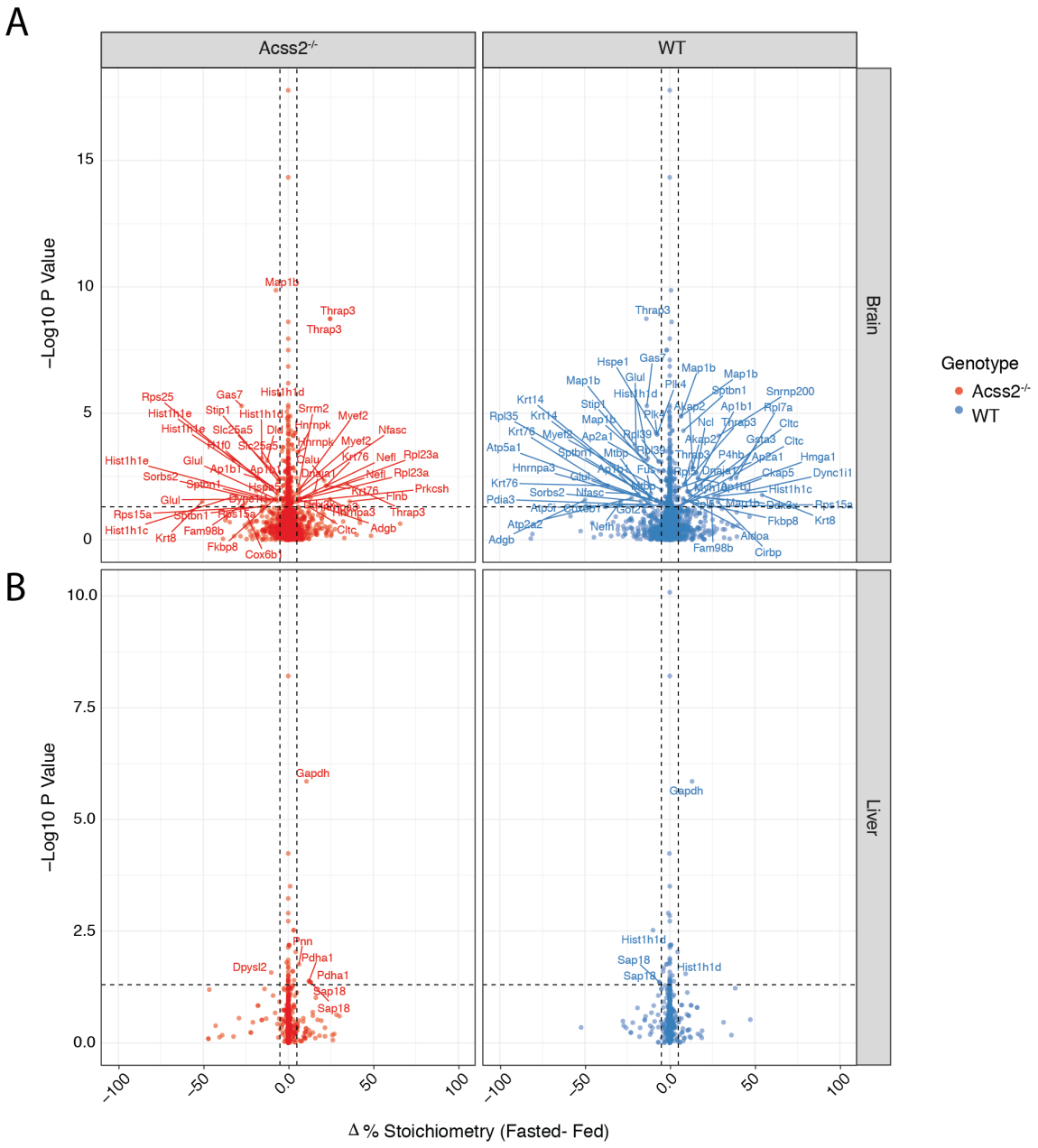

Figure 3-6. Functional QSSA analysis of brain acetylation changes on chromatin across dietary conditions in *Acss2*$^{-/-}$ and WT mice.

A) QSSA plot of brain chromatin acetylation stoichiometries fed and 48-hour fasted *Acss2*$^{-/-}$ and WT mice. **B)** Distribution of brain chromatin acetylation stoichiometries used in the bins above.

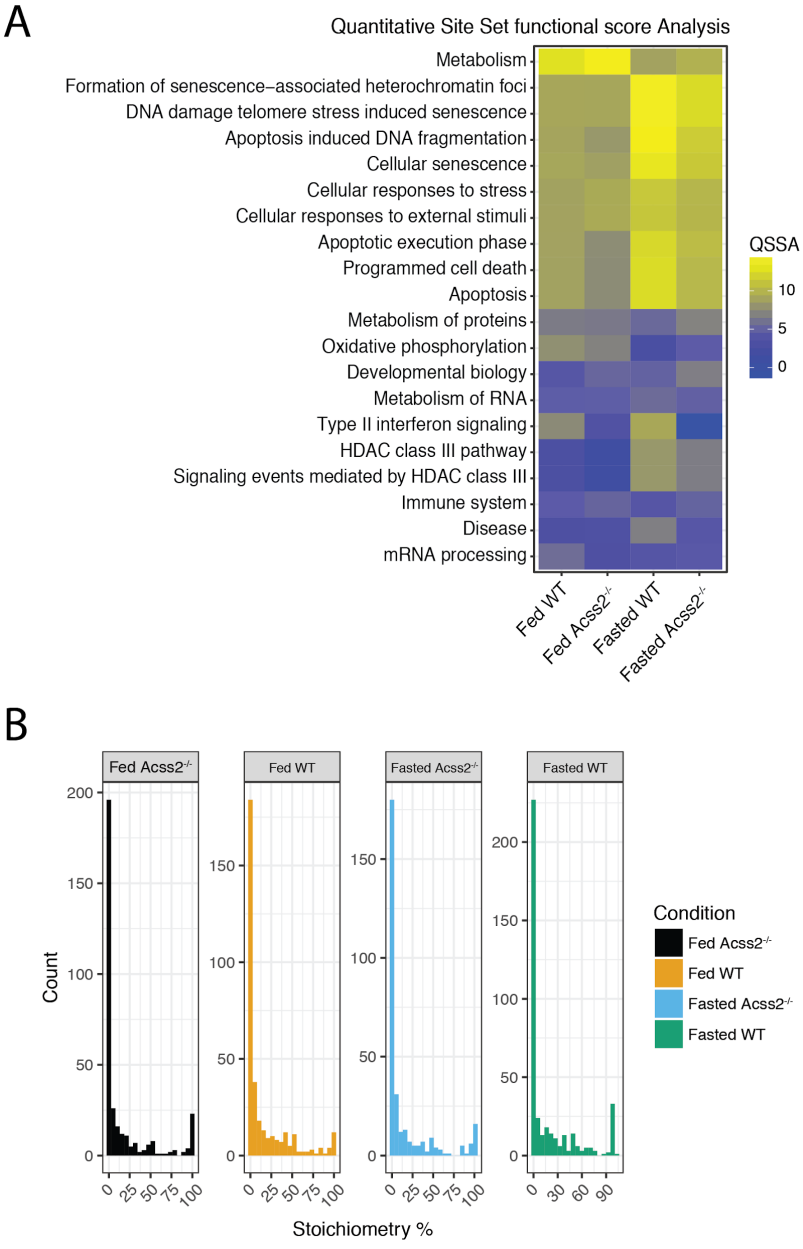

Figure 3-7. Functional QSSA analysis of liver acetylation changes on chromatin across dietary conditions in *Acss2*$^{-/-}$ and WT mice.

A) QSSA plot of liver chromatin acetylation stoichiometries fed and 48-hour fasted *Acss2*$^{-/-}$ and WT mice. **B)** Distribution of liver chromatin acetylation stoichiometries used in the bins above.

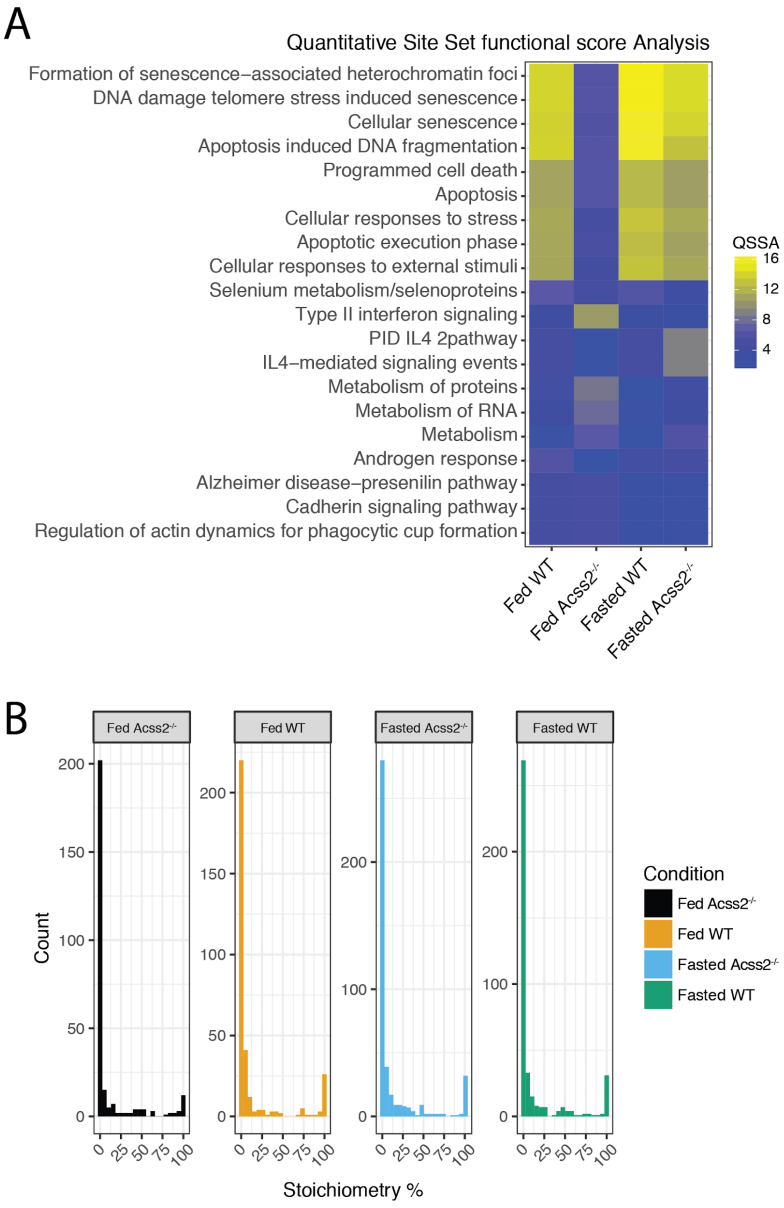

3.4.4 Limited Changes to the Chromatin Proteome of Fed and 48-hour fasted WT and Acss2$^{-/-}$ *mice*

In adapting to limited nutrient availability in fasting, chromatin protein abundance remained relatively constant in brain and liver demonstrating alterations in acetylation occurred through a direct mechanism of acetylation rather than passively through protein synthesis of degradation. A small subset of proteins were altered significantly in abundance upon 48-hour fasting (Figure 3-7A). Fewer proteins had differential abundance in the absence of ACSS2, suggesting ACSS2 moderates protein and metabolite acetylation reactions preferentially over large scale proteome changes. The pathways affected by upregulated chromatin protein abundance were associated with metabolism, particularly fatty acid metabolism, propanoate metabolism, PPAR signaling, and branched-chain amino acid metabolism (Figure 3-7 B, C). None of these pathways were significantly differentially regulated between wild type and *Acss2*$^{-/-}$ mice. In fasting conditions, liver synthesis of coenzyme A was induced through transcriptional induction of coenzyme synthesis enzymes ***(45)***. Coenzyme A and branched-chain amino acids (BCAA) synthesis pathways utilize propanoate as a precursor ***(46, 47)***. These changes in propanoate metabolism are reflected both in protein abundance and in coenzyme A synthesis metabolite abundances. Previous studies have identified integration of BCAA synthesis and ACLY activation. The kinase BDK targets ACLY for activation and inhibits BCAA synthesis in favor of lipogenesis resulting in NAFLD ***(46, 47)***. PPAR signaling is induced by fasting to coordinate fatty acid metabolism, upregulating fatty acid oxidation during the limited nutrient availability. A previous study demonstrated altered transcriptional regulation of loci linked to PPAR signaling pathway in the liver of ACSS2 deficient mice ***(48)***. These limited changes of chromatin-associated protein abundance indicate ACSS2 under fasting acts primarily through

protein acetylation instead of large scale changes to protein abundance to enable a more rapid response to alterations in nutrient availability.

Figure 3-8. Volcano plot of chromatin protein abundance changes across dietary conditions and tissues in *Acss2*$^{-/-}$ and WT mice.

A) Log2 Fold change of *Acss2*$^{-/-}$ and WT fed and 48-hour fasted mice. P values calculated by two way ANOVA (n = 4 each condition). **B)** Significance of enrichment of KEGG pathways upregulated from *Acss2*$^{-/-}$ vs WT chromatin. **C)** Fold enrichment of KEGG pathways upregulated from *Acss2*$^{-/-}$ vs WT chromatin. **D)** Overlap of *Acss2*$^{-/-}$ dependent significant changes to chromatin protein and acetylation stoichiometry.

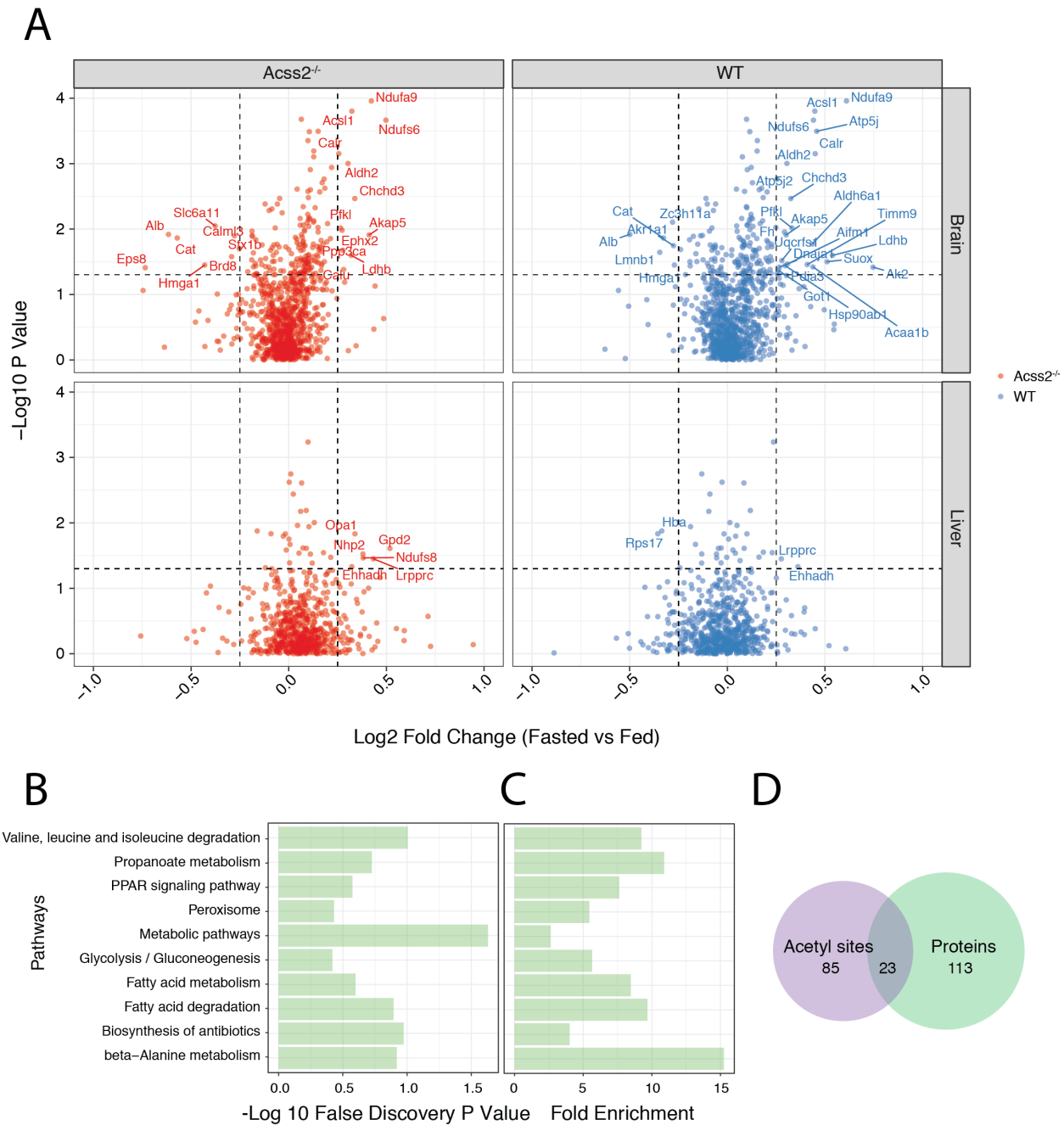
A
Acss2-/-
WT
Brain
Liver
−Log10 P Value
Log2 Fold Change (Fasted vs Fed)
Acss2-/-
WT
B
C
D
Pathways
Valine, leucine and isoleucine degradation
Propanoate metabolism
PPAR signaling pathway
Peroxisome
Metabolic pathways
Glycolysis / Gluconeogenesis
Fatty acid metabolism
Fatty acid degradation
Biosynthesis of antibiotics
beta−Alanine metabolism
-Log 10 False Discovery P Value
Fold Enrichment
Acetyl sites
85
23
Proteins
113

3.4.5 Tissue-specific alterations in transcripts coordinate fasting response ACSS2-dependent manner:

Next, we performed RNA transcription analysis to assess pathways under the control of ACSS2-derived acetyl-CoA. RNA was extracted from brain and liver tissues and RNA-seq analysis was performed. A two-tailed t-test was performed to determine statistically significant differences of the *Acss2*$^{-/-}$ and wild type mice. Log transformed fold changes between *Acss2*$^{-/-}$ and wild type mice above 2 or below negative 2 with a p-value below 0.05 for each tissue were determined to be significant. Significant genes from brain and liver were clustered by their log2 fold change using k means clustering (Figure 3-8A). We performed a DAVID functional annotation analysis ***(49)*** of the gene expression changes in the brain tissue samples from *Acss2*$^{-/-}$ mice as compared with wild type mice of the same strain to determine pathways under the control of ACSS2-derived acetyl-CoA (Figure 3-8B, C). KEGG pathway analysis of altered transcription in *Acss2*$^{-/-}$ mice tissue gave further evidence of ACSS2-derived acetyl-CoA regulating nuclear processes such as transcription factor signaling and RNA processing. The analysis of the RNA-seq data set demonstrates ACSS2 had a tissue and dietary specific role in the regulation of transcription, and loss of ACSS2 did not lead to a global loss of transcription due to reduction in acetyl-CoA leading to a global loss of histone acetylation, a mechanism previously proposed ***(9, 10, 50)***. The majority of genes showed no significant changes between *Acss2*$^{-/-}$ and wild type, suggesting the role of ACSS2 in regulating transcription is targeted, rather than a global effect through contribution to a general nuclear pool of acetyl-CoA for indiscriminate use by many histone acetyltransferases. Indeed, there were 6774 transcripts displaying significantly altered levels across tissues with the pattern of up-regulation and downregulation of the 6774 significantly changing genes having little overlap between all four

conditions (Figure 3-8A). The majority of transcripts differentially up- and down-regulated in response to fasting in an ACSS2-dependent manner were in the brain, where chromatin acetylation of RNA metabolism and mRNA processing was significantly altered in the absence of ACSS2.

Clustering of the significantly changing genes in Figure 3-9A demonstrated tissue and diet-specific response patterns, with 5 of the 7 clusters displaying similar trends in gene expression only displayed in the starvation condition in brain and liver and only 2 clusters containing overlap in the response of these two tissues. ACSS2 was required for tissue-specific transcriptional responses to fasting in the brain and liver. The brain and liver displayed dysregulated fasting response in metabolic pathways and transcriptional control pathways associated with cancer metabolism in the *Acss2*$^{-/-}$ animals. In an organism, ACSS2-dependent metabolism and signaling is important under dietary stress in addition to providing increased metabolic resources and robustness in cancers ***(41)***. The brain specifically showed downregulation of RNA transport and splicing under fasting in the *Acss2*$^{-/-}$ animals, paralleling chromatin pathways regulated by ACSS2-dependent acetylation in the brain (Figure 3-8B, C). Endocytosis, MAPK and cAMP signaling were upregulated under fasting in the absence of ACSS2 in the brain indicating ACSS2 was necessary for essential neuronal functions, such as local translation and endocytosis for neurotransmitter reuptake, implicating impairment of neurotransmitter signaling and higher cognitive functions in animals (Figure 3-8B, C) ***(32, 41)***. In the liver, the transcriptional response to fasting showed downregulation in pathways related to immune function and blood vessel function and maintenance and primary immunodeficiency disorders in the absence of ACSS2. There was little overlap of transcripts differentially regulated in response to the loss of ACSS2, however, ACSS2 regulates an overlapping transcriptional

regulatory network in a tissue-specific manner, including the p300 and CBP histone acetyltransferases (Figure 3-9A-D). ACSS2 has been co-immunoprecipitated with CBP in brain and cell lines under hypoxic conditions ***(32)***. Furthermore, the 59 transcription factors enriched in all four conditions include many known transcription factor substrates and co-activators associated with p300/CBP (Figure 3-10). Many of the proteins included in this network have roles in regulating lipid synthesis and degradation and other related metabolic pathways discussed throughout this study.

Figure 3-9. Transcriptional changes show a tissue-specific pattern, with little overlap of significantly changing genes in fed and 48-hour fasted brain and liver.

A) PAM clustering of the Log2 fold change of statistically (6774) significantly changing genes from fed and 48-hour fasted brain and liver samples from RNA-seq. **B)** Fold Enrichment and **C)** -Log 10 P-Value of KEGG pathway enrichment analysis of significantly changing genes.

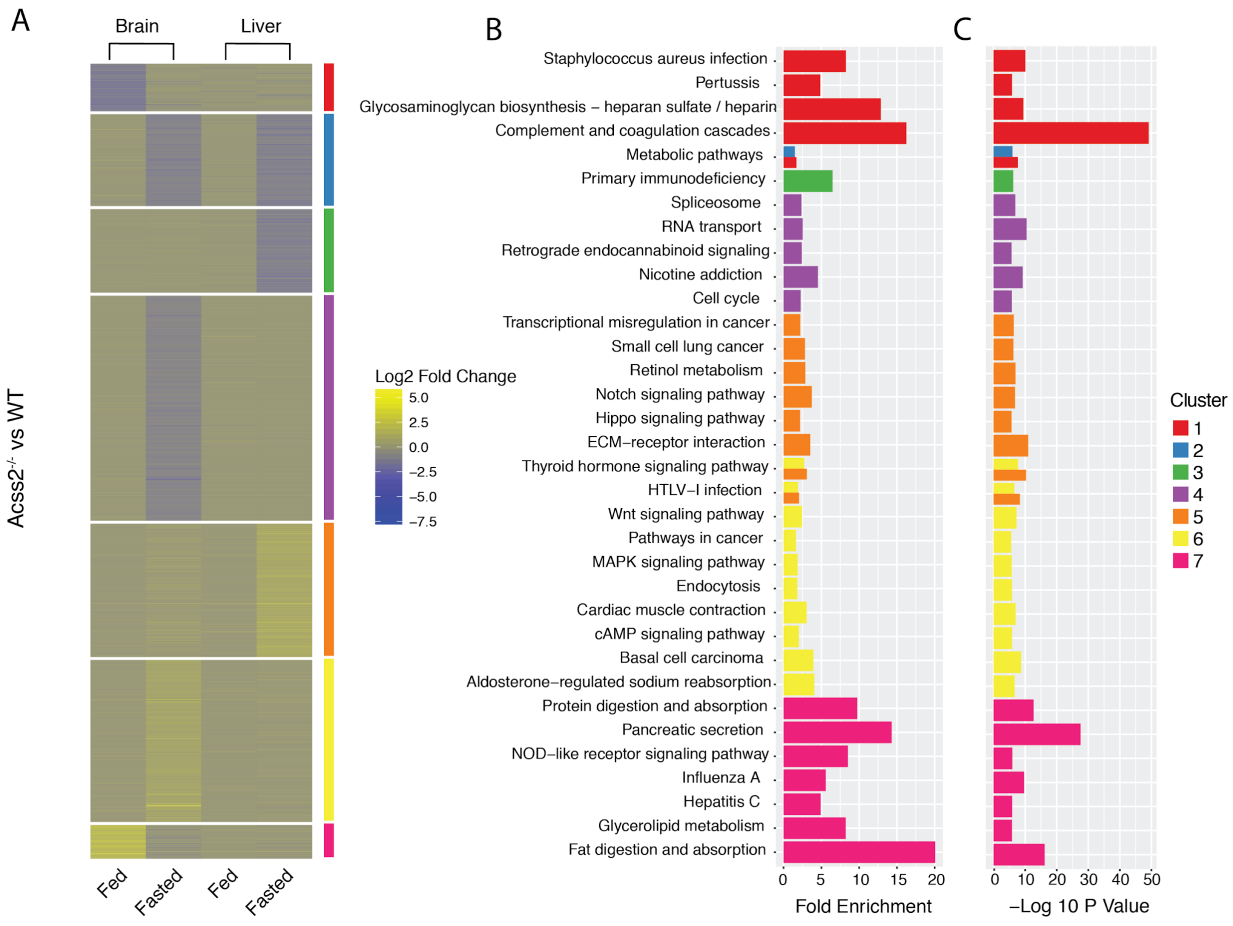

Figure 3-10. Transcriptional regulation by ACSS2 reveals tissue-specific patterns driven by overlapping transcription factors.

A) Venn diagram of all significantly changing genes in the *Acss2*$^{-/-}$ mice. B) Venn diagram of all significantly upregulated genes in the ACSS KO mice. C) Venn diagram of all significantly downregulated genes in the ACSS KO mice. D) Venn diagram of all enriched transcription factors (175) for significantly changing genes by DAVID, with an overlap of 59 transcription factors.

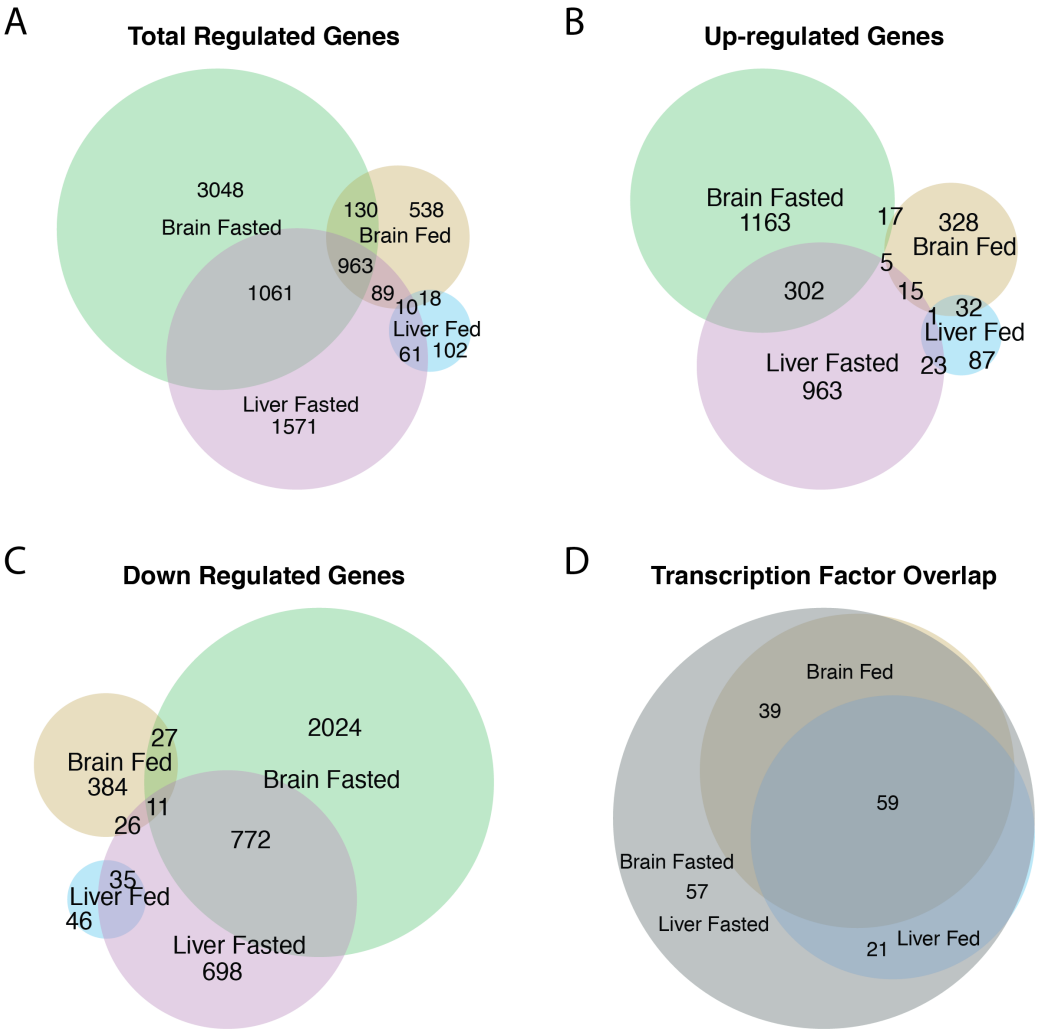

Figure 3-11. Interaction network of Transcription Factors.

Network of 59 transcriptional factors enriched across all four conditions changing transcripts from String Database, including the Histone Acetyltransferase p300 and many of its co-activators and transcription factor substrates.

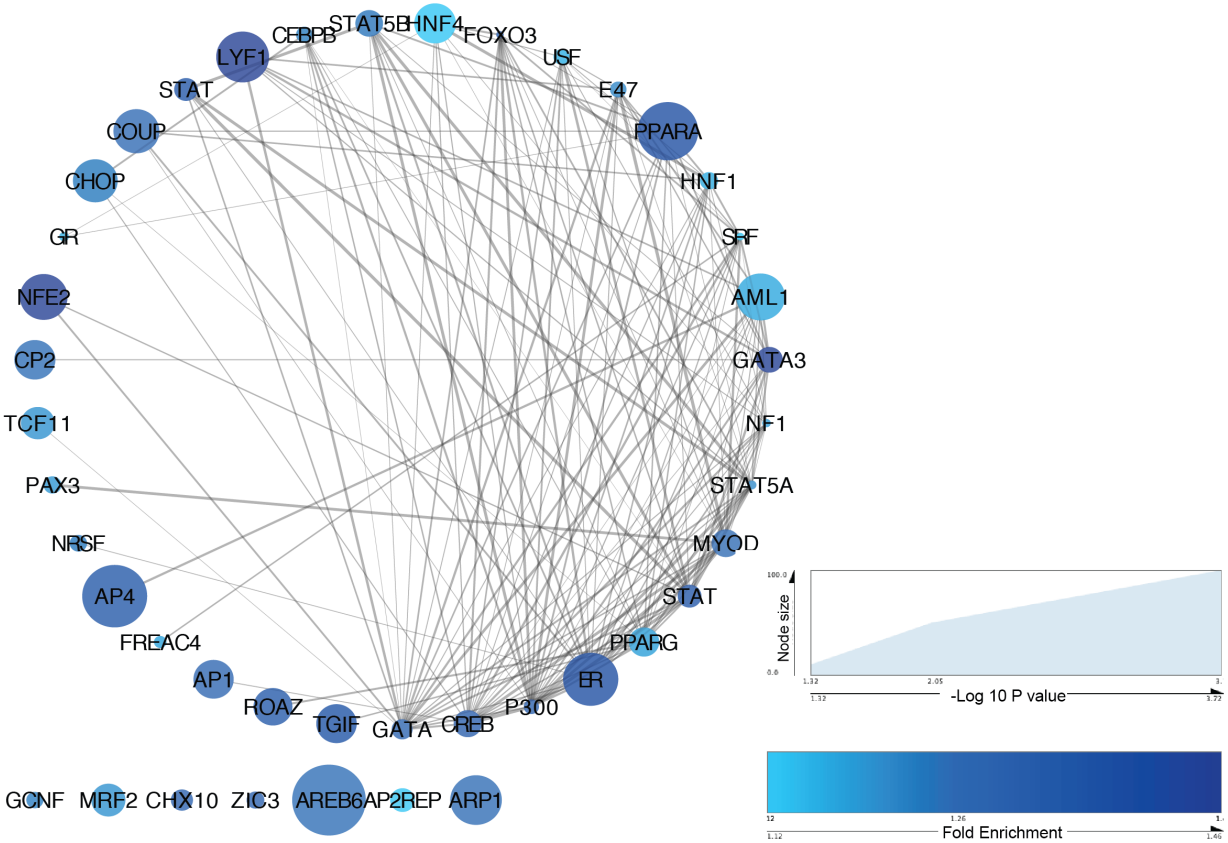

3.4.6 Mitochondria Acetyl-Proteomics Quantified in Liver of Fed and 48-hour fasted WT and Acss2$^{-/-}$ *mice*

In liver, chromatin acetylation changes were very limited, even in the absence of ACSS2 under fasting. Previous studies have indicated these animals have systemic reduction of free fatty acid circulation and likely β-oxidation of fatty acids under prolonged fasting conditions in the absence of ACSS2. To determine the downstream effect of altered fatty acid oxidation, which occurs in the mitochondria, in response to fasting by loss of ACSS2 we isolated a mitochondrion enriched fraction in our subcellular fractionation from the liver to perform our site-specific acetyl-lysine stoichiometry analysis and assess the mitochondrial proteome. Acetyl-CoA synthesis is compartmented within the cell, therefore even in the absence of chromatin acetylation changes in liver there may be alterations in the mitochondria in the absence of ACSS2. Four wild type and *Acss2*$^{-/-}$ mice were harvested after regular feeding and a 48-hour fasting to examine the effects of the loss of *Acss2*$^{-/-}$ in nutrient limiting conditions. A total of 5938 acetyl sites were identified and stoichiometry of 2918 acetylation sites was quantified from 2220 proteins in the mitochondria enriched fraction.

Global distribution of mitochondrial acetylation sites remained unchanged between the four conditions, with the median acetylation stoichiometry below 1%. Mitochondrial acetylation stoichiometry changes between fed and fasting were smaller in magnitude in relation to chromatin-associated proteins, and many acetylation sites had negligible acetylation stoichiometry in one dietary condition that changed to a low acetylation stoichiometry upon dietary adaptation. This demonstrated the acetylation stoichiometries measured in this study correlated with previously determined second-order rate constant of isolated mitochondria proteins ***(51)***. These parallels suggest a non-enzymatic mechanism of acetylation driven by

mitochondrial conditions such as high pH and altered acetyl-CoA concentrations ***(24, 51–53)***. Upon metabolic perturbation by fasting, dynamic acetylation sites were reduced, many to near 0% acetylation stoichiometry. The absence of ACSS2 reduced many of the highest magnitude dynamic changes of acetylation stoichiometry observed. This contrasts previous findings of increases in mitochondrial acetylation in response to fasting to coordinate metabolic fuel switching ***(29, 48)***. In addition, a subset of acetylation induced upon fasting were observed in the absence of ACSS2. QSSA functional analysis of differentially acetylated sites demonstrated enrichment of metabolic pathways having higher acetylation stoichiometry in the wild type in comparison to the *Acss2*$^{-/-}$ mice. Oxidative phosphorylation, amino acid metabolism, as well as lipid metabolism and adipogenesis were enriched paralleling trends of alterations in chromatin protein abundance. Similar metabolic pathways were enriched in acetylation sites differentially higher in fed liver mitochondria versus fasted, as well as regulation by p53, the TCA cycle, and the electron transport chain in agreement with previous studies ***(29)***. Metabolism of fatty acids had a very low QSSA score, indicating de-enrichment in fed conditions and higher acetylation under fasted conditions. These trends indicate ACSS2-derived acetyl-CoA coordinates cytoplasmic and mitochondrial metabolic adaptation to fasting. In the absence of ACSS2, fatty acid synthesis is not down-regulated and mitochondrial metabolism did not respond to limited nutrient availability during fasting. ACSS2 nuclear and cytosolic acetyl-CoA levels rather than mitochondria. Therefore, reduction in acetylation in the mitochondria in the absence of ACSS2 is through an indirect mechanism, such as upregulation of citrate export for ACLY-derived acetyl-CoA synthesis or inhibition of the TCA cycle.

Figure 3-12. Mitochondrial acetylation changes across dietary conditions in liver of *Acss2*$^{-/-}$ and WT mice.

A) Stoichiometry % difference plot of *Acss2*$^{-/-}$ and WT mice. Lines show magnitude of difference and stoichiometry of fed and 48-hour fasted mice and are colored by which dietary condition was higher. **B)** Functional QSSA analysis of liver acetylation changes in mitochondria across dietary conditions in *Acss2*$^{-/-}$ and WT mice. **C)** Distribution of liver mitochondrial acetylation stoichiometries used in the QSSA analysis for each condition (n = 4 for each condition).

A

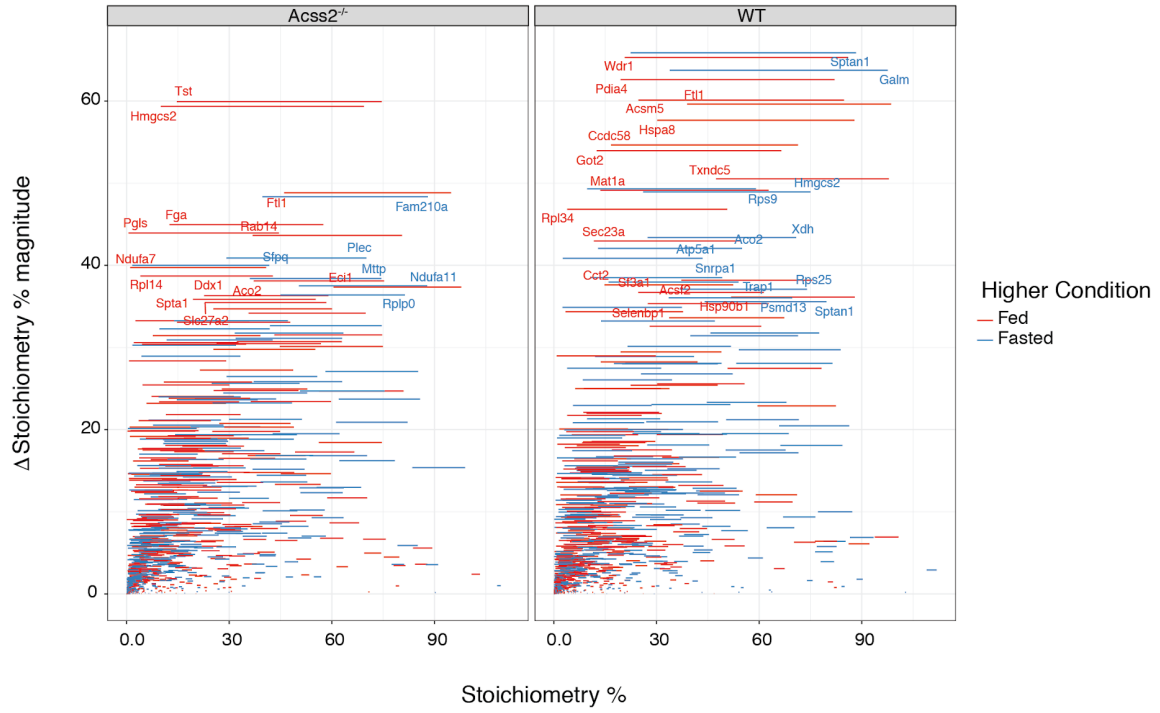
Acss2-/-
WT
ΔStoichiometry % magnitude
Stoichiometry %
Higher Condition
Fed
Fasted
Tst
Hmgcs2
Ftl1
Fam210a
Pgls
Fga
Rab14
Plec
Ndufa7
Sfpq
Mttp
Ndufa11
Rpl14
Ddx1
Aco2
Eci1
Spta1
Rplp0
Sle27a2
Wdr1
Sptan1
Galm
Pdia4
Ftl1
Acsm5
Ccdc58
Hspa8
Got2
Txndc5
Mat1a
Hmgcs2
Rps9
Rpl34
Sec23a
Xdh
Aco2
Atp5a1
Cct2
Snrpa1
Sf3a1
Acsf2
Trap1
Rps25
Selenbp1
Hsp90b1
Psmd13
Sptan1

B

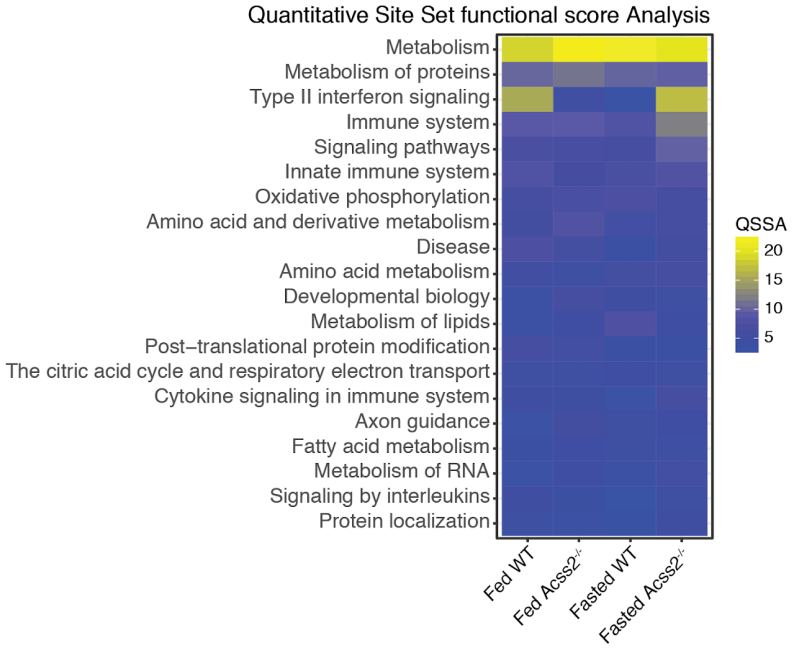
Quantitative Site Set functional score Analysis
Metabolism
Metabolism of proteins
Type II interferon signaling
Immune system
Signaling pathways
Innate immune system
Oxidative phosphorylation
Amino acid and derivative metabolism
Disease
Amino acid metabolism
Developmental biology
Metabolism of lipids
Post−translational protein modification
The citric acid cycle and respiratory electron transport
Cytokine signaling in immune system
Axon guidance
Fatty acid metabolism
Metabolism of RNA
Signaling by interleukins
Protein localization
Fed WT
Fed Acss2-/-
Fasted WT
Fasted Acss2-/-
QSSA
20
15
10
5

C

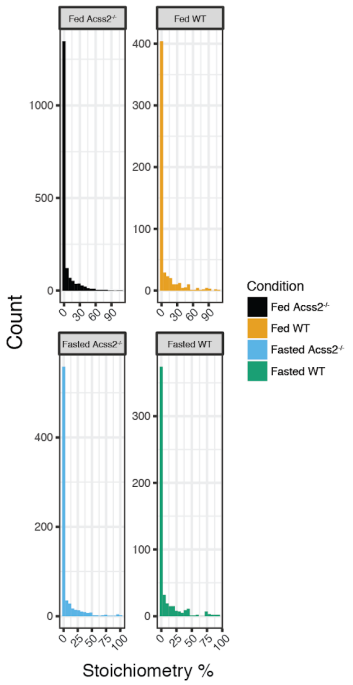
Fed Acss2-/-
Fed WT
Fasted Acss2-/-
Fasted WT
Count
Stoichiometry %
Condition
Fed Acss2-/-
Fed WT
Fasted Acss2-/-
Fasted WT

3.4.7 Alterations in the Mitochondrial Proteome of Liver of Fed and 48-hour fasted WT and Acss2$^{-/-}$ *mice*

Unlike chromatin-associated proteins, which remained relatively unchanged in abundance in response to fasting and the absence of ACSS2, mitochondrial proteins significantly changed to adapt to limited nutrient availability during fasting. These results suggest chromatin acetylation regulation by acetyl-CoA synthesis may be more targeted locally, in comparison to mitochondrial acetylation. To determine if the alterations in mitochondrial acetylation were through direct non-enzymatic acetylation or passive alteration in protein levels, we quantified changes in protein abundance. The majority of proteins were not significantly altered by fasting or the absence of ACSS2, indicating alterations in acetylation were through direct acetlyation on mitochondrial proteins rather than an alteration in protein abundance. In the limited protein response to fasting in wild type liver mitochondria, more proteins were significantly downregulated than upregulated. In contrast, of the proteins changing in the absence of ACSS2 more proteins were upregulated in response to fasting. We observed an increase in acetylation of mitochondrial p53 transcriptional regulating pathway components in fasting conditions, particularly in the absence of ACSS2, which correlate with these trends through altering protein abundance through a p53 transcriptional mechanism. Furthermore, proteins downregulated in wild type mice were enriched for mitochondrial components of glucagon signaling, AMPK signaling and fatty acid biosynthesis. AMPK and glucagon signaling promote fatty acid synthesis and systemic circulation ***(54, 55)***. Glucagon, a peptide hormone produced by alpha cells of the pancreas, also raises the concentration of glucose and fatty acids in blood ***(54)***. ACSS2 was also previously found to be necessary to coordinate systemic fatty acid circulation and utilization in the liver during extended fasting ***(48)***.

Mitochondrial pathways upregulated in the absence of ACSS2 during fasting were mitochondrial components of PPAR signaling, fatty acid metabolism, propanoate and butanoate metabolism, branched-chain amino degradation, and the peroxisome, a subcellular structure responsible for the breakdown of long-chain fatty acids before utilization in the mitochondria (Figure 3-14A, B). These pathways parallel those upregulated in chromatin protein abundance upon fasting, demonstrating a coordinated metabolic response to limited nutrient availability across subcellular compartments. In addition, BCAA breakdown has been linked to insulin insensitivity, diabetes, and fatty liver ***(46, 47)***.

Figure 3-13. Volcano plot of chromatin protein abundance changes across dietary conditions and tissues in *Acss2*$^{-/-}$ and WT mice.

Log2 Fold change of *Acss2*$^{-/-}$ and WT fed and 48-hour fasted mice. P values calculated by two way ANOVA (n = 4 each condition).

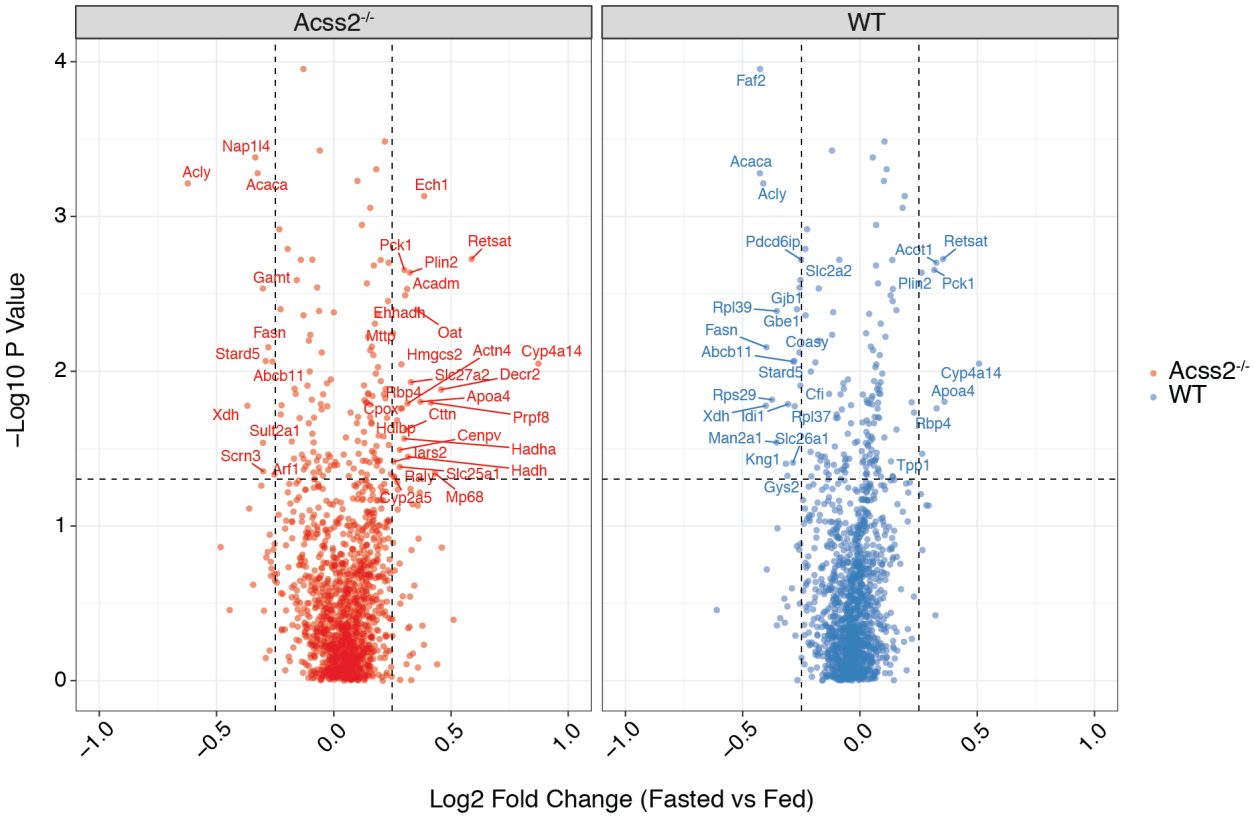

Figure 3-14. Pathway analysis of mitochondrial protein abundance changes in liver of *Acss2*$^{-/-}$ and WT fed and 48- hour mice.

A) Significance of enrichment and fold enrichment of KEGG pathways downregulated from *Acss2*$^{-/-}$ vs WT mitochondria. **B)** Significance of enrichment and fold enrichment of KEGG pathways upregulated from *Acss2*$^{-/-}$ vs WT mitochondria. **C)** Overlap of *Acss2*$^{-/-}$ dependent significant changes to mitochondrial protein and acetylation stoichiometry.

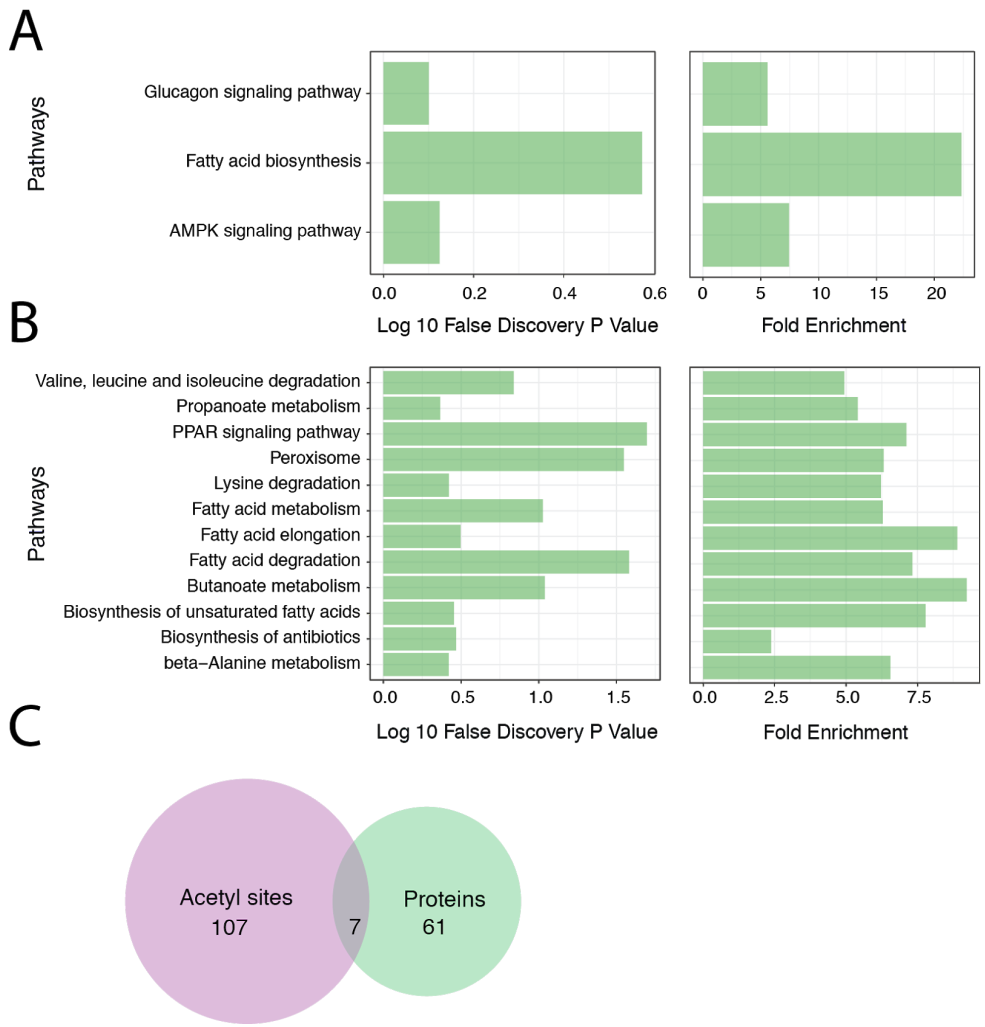

3.4.8 Histone posttranslational modifications:

We performed histone posttranslational modification analysis using mass spectrometry to determine whether ACSS2 generated acetyl-CoA was involved in tissue-specific gene expression alterations through contributions to a global pool of cytoplasmic and nuclear acetyl-CoA influencing acetylation levels on histones broadly. Histone posttranslational modification analysis of brain, and liver tissue from fed and 48-hour fasted *Acss2*$^{-/-}$ mice as compared with wild type mice of the same strain revealed alterations in histone acetylation and methylation (Figure 3-15A). ACSS2 is required for histone modification changes under nutrient stress in a tissue-specific manner between the brain and liver, highly different metabolic tissues. Under fasting conditions *Acss2*$^{-/-}$ animals do not display the increased acetylation displayed in response to the prolonged 48-hour fast. The brain, a metabolically expensive organ with a highly-coordinated response to nutrient deprivation, requires ACSS2 for the increased acetylation mediated fasting response at H3K18, an acetylation modification associated with active enhancers (Figure 3-15B, E). In the liver, the response to fasting leads to more changes in chromatin, which are blunted in the *Acss2*$^{-/-}$, indicating ACSS2 plays a role in coordinating a chromatin-based fasting response. In the liver, ACSS2 was important for the hyperacetylation of H4 in fasting as well as the methylation state of H3.3K36 (Figure 3-15C, D). These histone acetylation sites have been characterized as substrates for the p300/CBP family of histone acetyltransferases, which has previously been co-immunoprecipitated with ACSS2 ***(32, 41)***.

Histone methylation of histone 3 and the variant histone 3.3 also showed alterations in lysine 27 and lysine 36 methylation, which co-occur on the same peptide. In the brain, the methylation state of lysine 27 was significantly changing, which may be a direct effect of the increase in the H3K27 demethylase, Utx, which had upregulated gene expression in the brain of

Acss2$^{-/-}$ mice. In the liver, the alterations were driven by increased lysine 36 methylation, particularly on H3.3, which suggests increased transcription. This effect was strongly diet-dependent rather than genotype, which indicated a transcriptional response to fasting in both *Acss2*$^{-/-}$ and wild type mice. These alterations in histone posttranslational modifications described suggest ACSS2 does not control histone acetylation by contributing to a global acetyl-CoA pool that affects all acetylation reactions, but rather a more targeted mechanism. These results conflict with previously reported data, however, differences in the systems under inquiry may largely account for these differences ***(10, 32, 42, 50)***.

In this study, the response to fasting in the absence of ACSS2 has been shown to be subcellular compartment, dietary condition, and tissue-specific indicating the importance of the metabolic environment. Previous studies have been undertaken in tissue culture models with significant amounts of glucose, creating conditions where ACSS2-dependent pathways of lipogenesis, as well as other effects of changes in ACSS2-derived acetyl-CoA, would be insignificant ***(10, 42, 50)***. In tissue culture models where the effects of glucose levels would be reduced, examining acetate-dependent histone acetylation in an *Acly*$^{-/-}$ tissue culture model system, these challenges have been addressed, however questions still remain about regulation under physiological conditions***(50)***. A final study examining histone acetylation by ACSS2-derived acetyl-coA assess tissue-specific effects in the brain by introducing a virally delivered ACSS2 knockdown system in the hippocampus of mice ***(32)***. This is the closest system examined to our own, which demonstrates the greatest overlap in changes to histone acetylation.

Figure 3-15. Histone posttranslational modification changes in 2-month old *Acss2*$^{-/-}$ and WT animals from fed and 48-hour fasted mice.

A) Global analysis of Log2 fold change B) H4 acetylation, C) H3K18K23 modifications, p<0.05. D) H4 acetylation peptide modifications percent total, p <0.05. E) H3K18K23 peptide modifications percent total, p <0.05.

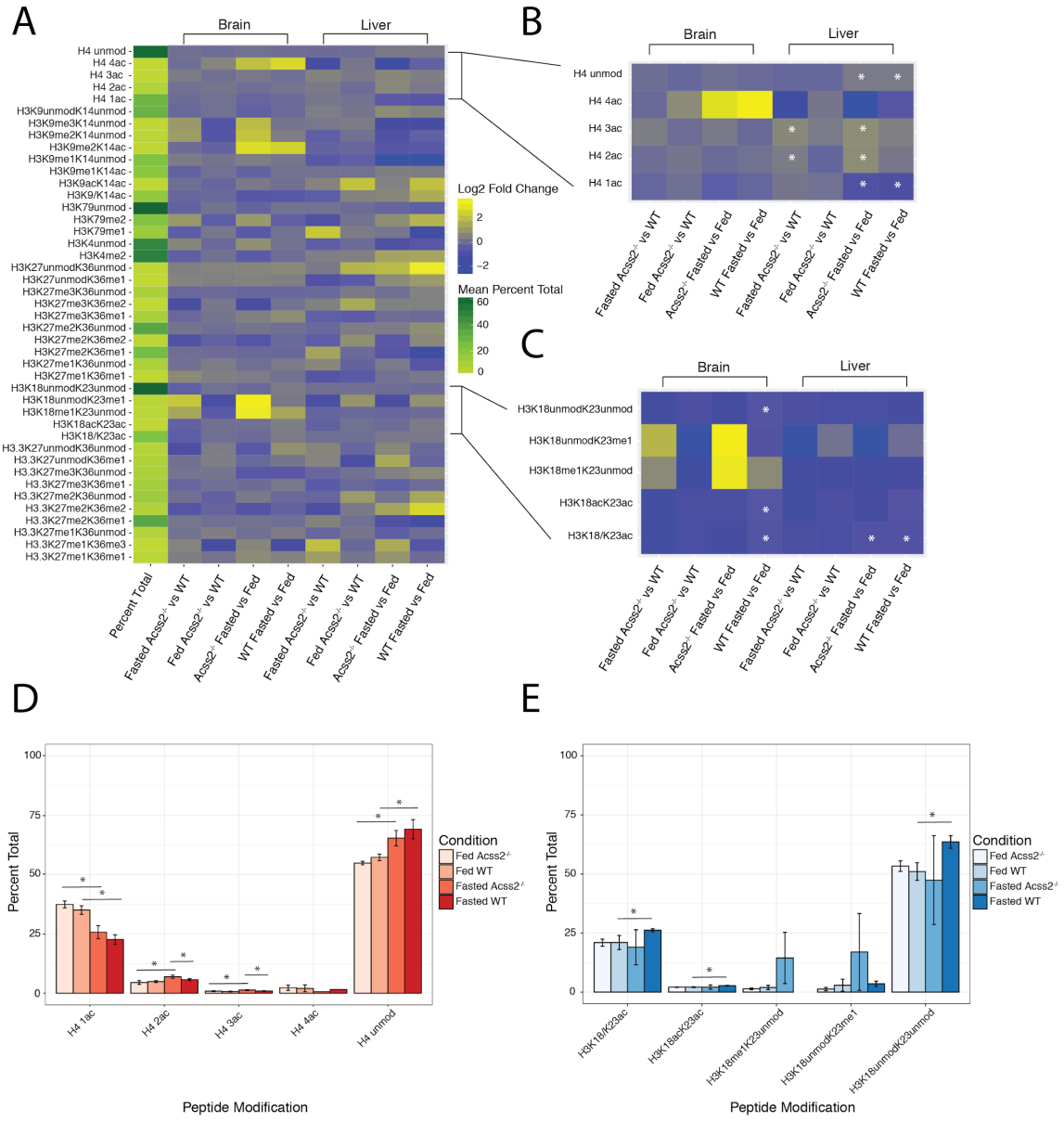

3.4.9 ACSS2 Regulates Liver Coenzyme A Synthesis and ketone body synthesis dietary stress.

Mass spectrometry-based metabolomics assessed changes in metabolism affected by ACSS2 when challenged with a 48-hour fast. Global trends indicated *Acss2*$^{-/-}$ animals have limited ability to metabolically respond to fasting. A global reduction in metabolites observed in the brain was driven by diet, however, this metabolic suppression increased in the *Acss2*$^{-/-}$, likely through decreased metabolic coupling using ketone bodies and reduction in systemic fatty acid circulation (Figure 3-16A) ***(43, 48)***. In the brain, both acetyl-CoA and coA were equally reduced during starvation and in the *Acss2*$^{-/-}$ animals. In liver, coenzyme A biosynthesis has previously shown to be upregulated during dietary stress, which we observed in fasted wild type animals ***(45)***. Acetyl-CoA and CoA were upregulated and a corresponding downregulation of CoA precursors was observed (Figure 3-16B). However, in *Acss2*$^{-/-}$ animals, this coordinated response was absent when challenged with fasting. In the absence of ACSS2, the changes in coenzyme A, citrate synthesis, fatty acid synthesis, and ketone body synthesis during fasting raises the question of ACSS2 and ACLY crosstalk regulating the balance between acetyl-CoA synthesis and acetyl-CoA consumption by ketone body synthesis and fatty acid synthesis.

Figure 3-16. Metabolomics analysis of *Acss2*$^{-/-}$ and WT animals from fed and 48-hour fasted mice found ACSS2 and fasting dependent alterations in brain and liver metabolism.

A) K means clustering of Log2 Fold changes of brain metabolites. **B)** K means clustering of Log2 Fold changes of liver metabolites. **C)** Fold changes of *Acss2*$^{-/-}$ versus WT in fed and fasted conditions in brain and liver show no significant differences in acetyl-CoA or CoA levels. (n= 5 for each condition)

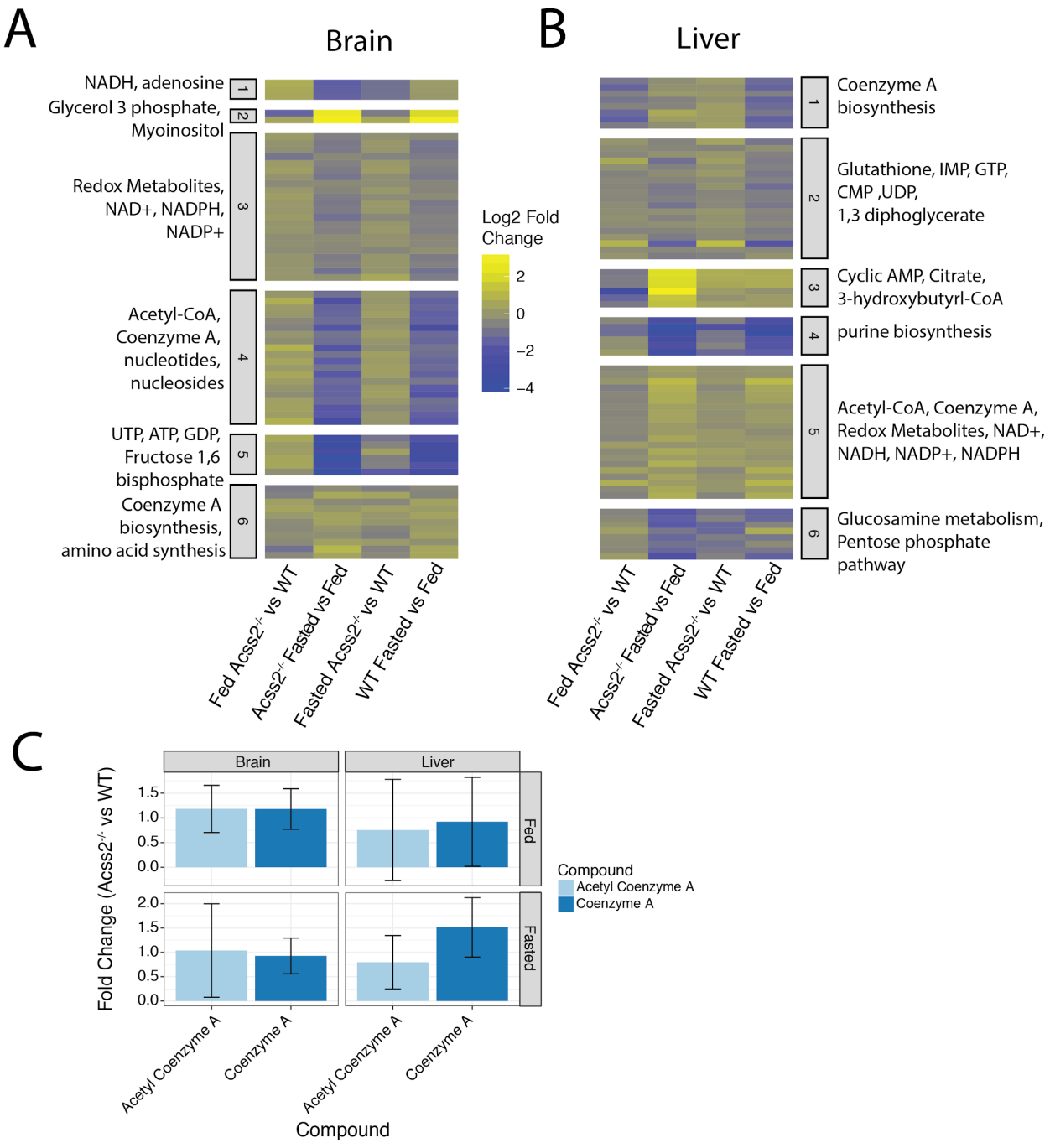
A
Brain
NADH, adenosine
Glycerol 3 phosphate,
Myoinositol
Redox Metabolites,
NAD+, NADPH,
NADP+
Acetyl-CoA,
Coenzyme A,
nucleotides,
nucleosides
UTP, ATP, GDP,
Fructose 1,6
bisphosphate
Coenzyme A
biosynthesis,
amino acid synthesis
1
2
3
4
5
6
Log2 Fold
Change
2
0
−2
−4
Fed Acss2-/- vs WT
Acss2-/- Fasted vs Fed
Fasted Acss2-/- vs WT
WT Fasted vs Fed
B
Liver
Coenzyme A
biosynthesis
Glutathione, IMP, GTP,
CMP ,UDP,
1,3 diphoglycerate
Cyclic AMP, Citrate,
3-hydroxybutyrl-CoA
purine biosynthesis
Acetyl-CoA, Coenzyme A,
Redox Metabolites, NAD+,
NADH, NADP+, NADPH
Glucosamine metabolism,
Pentose phosphate
pathway
Fed Acss2-/- vs WT
Acss2-/- Fasted vs Fed
Fasted Acss2-/- vs WT
WT Fasted vs Fed
C
Brain
Liver
Fed
Fasted
Fold Change (Acss2-/- vs WT)
1.5
1.0
0.5
0.0
2.0
1.5
1.0
0.5
0.0
Compound
Acetyl Coenzyme A
Coenzyme A
Acetyl Coenzyme A
Coenzyme A
Acetyl Coenzyme A
Coenzyme A
Compound

3.5 Discussion

Three distinct levels of acetate generation and utilization can be described including intracellular, paracellular and systemic. Intracellular acetate metabolism is associated with acetate generation and utilization within individual cells, and subcellular compartments. Paracellular acetate metabolism involves free acetate production in one cell type transferred to a neighboring cell for metabolism. Systemic acetate is generated predominantly in the liver and is released into circulation, analogous to ketone body production and metabolism.

ACSS2 enzyme activity falls in the liver upon feeding in animals, and its mRNA expression is regulated by sterols ***(7)*** associating ACSS2 with lipid synthesis across tissues. ACSS2 has been directly associated with cytoplasmic synthesis of fatty acids in cell culture models ***(33)***. ACSS2 provides an alternative pathway to ATP citrate lyase (ACLY) for acetyl-CoA generation. ACLY breaks down citrate exported by the mitochondria to acetyl-CoA in the cytosol. ACSS2 acts as an additional source of acetyl-CoA for the synthesis of fatty acids in the cytosol by scavenging cellular free acetate for re-synthesis of acetyl-CoA ***(5, 33)***. However, our findings suggest a primary role of ACSS2 may not only funnel carbon into fatty acid synthesis, but may also be directed at more specialized acetyl-CoA functions including protein and metabolite acetylation reactions.

The primary source for acetyl-CoA in the cytoplasm and nuclei of cells is through the action of the enzyme ACLY on citrate. ACSS2 is an alternative pathway that complements the action of ACLY and may be more functionally important when nutrient availability is low and the need to reutilize acetate is more critical. The yeast mitochondrial and nuclear-cytoplasmic forms of ACS are distinct and the nuclear localized enzyme is involved in the regulation of

chromatin activity via the action of histone acetyltransferases ***(9)***. The same has been shown for the mammalian forms of the enzyme ***(10)***.

In this study, we demonstrated ACSS2 is involved in lysine site-specific, subcellular compartment-specific, and tissue-specific patterns of acetylation on proteins in response to fasting. Examining the brain and liver of wild type and *Acss2*$^{-/-}$ mice demonstrated a highly tissue-specific response. In the brain, the loss of ACSS2 dynamically affects acetylation of chromatin proteins, specifically signaling, metabolic pathways, RNA metabolism, and mRNA processing. Interrogation of downstream effects by transcriptomics and metabolomics elucidated an altered transcriptional and metabolic response to fasting in the absence of ACSS2. In contrast to previous studies, ACSS2-dependent alterations to histone acetylation were limited to specific lysine sites ***(10, 50)***. In the liver, the dynamic acetylation response on chromatin proteins and histones was extremely limited. Instead, acetylation stoichiometry of liver mitochondria was significantly affected, in addition to perturbations in metabolism associated with a lack of fatty acid circulation and beta-oxidation in the absence of ACSS2.

Overall these trends demonstrated coordinated control of the metabolic response to fasting by ACSS2-derived acetyl-CoA in multiple subcellular compartments to control the switch between fatty acid synthesis and utilization in a targeted mechanism. Protein abundance alterations also supported the role of ACSS2 regulating splicing and downstream metabolic pathway component abundance beyond providing acetyl-CoA as a substrate for fatty acid synthesis.

It is difficult to determine if these alterations operate in a cell-autonomous manner, or result from metabolic coupling across tissues in response to fasting. In the absence of ACSS2,

intracellular, paracellular, and systemic acetate metabolism are likely altered. Additionally, previous studies show a systemic reduction in fatty acid circulation and beta-oxidation during fasting in the absence of ACSS2 ***(48)***. In conclusion, acetyl-CoA synthesis pathways do not appear to control global protein acetylation through a concentration-dependent mechanism. However, site and subcellular acetylation and downstream pathway function were altered in the absence of ACSS2, particularly in the fasted condition where acetate metabolism plays an important role in metabolic coupling and nutrient availability.

3.6 References

1. Ingram-Smith C and Smith KS (2007) AMP-forming acetyl-CoA synthetases in Archaea show unexpected diversity in substrate utilization. Archaea 2:95–107

2. Imesch E and Rous S (1984), Partial purification of rat liver cytoplasmic acetyl-CoA synthetase; Characterization of some properties, http://dx.doi.org/10.1016/0020-711x(84)90146-0

3. Woodnutt G and Parker DS (1978) Rabbit liver acetyl-CoA synthetase. Biochem J 175:757–759

4. Goldberg RP and Brunengraber H (1980) Contributions of cytosolic and mitochondrial acetyl-CoA syntheses to the activation of lipogenic acetate in rat liver. Adv Exp Med Biol 132:413–418

5. Luong A, Hannah VC, Brown MS, et al (2000) Molecular characterization of human acetyl-CoA synthetase, an enzyme regulated by sterol regulatory element-binding proteins. J Biol Chem 275:26458–26466

6. Ikeda Y, Yamamoto J, Okamura M, et al (2001), Transcriptional Regulation of the Murine Acetyl-CoA Synthetase 1 Gene through Multiple Clustered Binding Sites for Sterol Regulatory Element-binding Proteins and a Single Neighboring Site for Sp1, http://dx.doi.org/10.1074/jbc.m103848200

7. Sone H, Shimano H, Sakakura Y, et al (2002) Acetyl-coenzyme A synthetase is a lipogenic enzyme controlled by SREBP-1 and energy status. Am J Physiol Endocrinol Metab 282:E222–30

8. Ariyannur PS, Moffett JR, Madhavarao CN, et al (2010) Nuclear-cytoplasmic localization of acetyl coenzyme a synthetase-1 in the rat brain. J Comp Neurol 518:2952–

2977

9. Takahashi H, McCaffery JM, Irizarry RA, et al (2006) Nucleocytosolic acetyl-coenzyme a synthetase is required for histone acetylation and global transcription. Mol Cell 23:207–217

10. Wellen KE, Hatzivassiliou G, Sachdeva UM, et al (2009) ATP-citrate lyase links cellular metabolism to histone acetylation. Science 324:1076–1080

11. Xu M, Nagati JS, Xie J, et al (2014) An acetate switch regulates stress erythropoiesis. Nat Med 20:1018–1026

12. Allfrey VG, Faulkner R, and Mirsky AE (1964) ACETYLATION AND METHYLATION OF HISTONES AND THEIR POSSIBLE ROLE IN THE REGULATION OF RNA SYNTHESIS. Proc Natl Acad Sci U S A 51:786–794

13. Allfrey VG and Mirsky AE (1964), Structural Modifications of Histones and their Possible Role in the Regulation of RNA Synthesis, http://dx.doi.org/10.1126/science.144.3618.559

14. Sakakibara I, Fujino T, Ishii M, et al (2009) Fasting-induced hypothermia and reduced energy production in mice lacking acetyl-CoA synthetase 2. Cell Metab 9:191–202

15. Fujino T, Kondo J, Ishikawa M, et al (2001) Acetyl-CoA synthetase 2, a mitochondrial matrix enzyme involved in the oxidation of acetate. J Biol Chem 276:11420–11426

16. Hallows WC, Lee S, and Denu JM (2006) Sirtuins deacetylate and activate mammalian acetyl-CoA synthetases. Proc Natl Acad Sci U S A 103:10230–10235

17. Moffett JR, Arun P, Ariyannur PS, et al (2013) N-Acetylaspartate reductions in brain injury: impact on post-injury neuroenergetics, lipid synthesis, and protein acetylation.

Front Neuroenergetics 5:11

18. Mathew R, Arun P, Madhavarao CN, et al (2005) Progress toward acetate supplementation therapy for Canavan disease: glyceryl triacetate administration increases acetate, but not N-acetylaspartate, levels in brain. J Pharmacol Exp Ther 315:297–303

19. Hellmuth C, Weber M, Koletzko B, et al (2012), Nonesterified Fatty Acid Determination for Functional Lipidomics: Comprehensive Ultrahigh Performance Liquid Chromatography–Tandem Mass Spectrometry Quantitation, Qualification, and Parameter Prediction, http://dx.doi.org/10.1021/ac202602u

20. Lindahl AJ, Lawton AJ, Baeza J, et al (2019) Site-Specific Lysine Acetylation Stoichiometry Across Subcellular Compartments. Methods Mol Biol 1983:79–106

21. Baeza J, Dowell JA, Smallegan MJ, et al (2014) Stoichiometry of site-specific lysine acetylation in an entire proteome. J Biol Chem 289:21326–21338

22. Baeza J, Lawton AJ, Fan J, et al Quantifying dynamic protein acetylation using quantitative stoichiometry, http://dx.doi.org/10.1101/472530

23. Fan J, Baeza J, and Denu JM (2016) Investigating Histone Acetylation Stoichiometry and Turnover Rate. Methods Enzymol 574:125–148

24. Baeza J, Smallegan MJ, and Denu JM (2015) Site-specific reactivity of nonenzymatic lysine acetylation. ACS Chem Biol 10:122–128

25. Choi M, Chang C-Y, Clough T, et al (2014) MSstats: an R package for statistical analysis of quantitative mass spectrometry-based proteomic experiments. Bioinformatics 30:2524–2526

26. Pagliarini DJ, Calvo SE, Chang B, et al (2008) A mitochondrial protein compendium elucidates complex I disease biology. Cell 134:112–123

27. Calvo SE, Clauser KR, and Mootha VK (2016) MitoCarta2.0: an updated inventory of mammalian mitochondrial proteins. Nucleic Acids Res 44:D1251–7

28. Merico D, Isserlin R, Stueker O, et al (2010) Enrichment map: a network-based method for gene-set enrichment visualization and interpretation. PLoS One 5:e13984

29. Hebert AS, Dittenhafer-Reed KE, Yu W, et al (2013) Calorie restriction and SIRT3 trigger global reprogramming of the mitochondrial protein acetylome. Mol Cell 49:186–199

30. Krautkramer KA, Reiter L, Denu JM, et al (2015) Quantification of SAHA-Dependent Changes in Histone Modifications Using Data-Independent Acquisition Mass Spectrometry. J Proteome Res 14:3252–3262

31. Lin S and Garcia BA (2012) Examining histone posttranslational modification patterns by high-resolution mass spectrometry. Methods Enzymol 512:3–28

32. Mews P, Donahue G, Drake AM, et al (2017) Acetyl-CoA synthetase regulates histone acetylation and hippocampal memory. Nature 546:381–386

33. Bulusu V, Tumanov S, Michalopoulou E, et al (2017) Acetate Recapturing by Nuclear Acetyl-CoA Synthetase 2 Prevents Loss of Histone Acetylation during Oxygen and Serum Limitation. Cell Rep 18:647–658

34. Gillet LC, Navarro P, Tate S, et al (2012) Targeted data extraction of the MS/MS spectra generated by data-independent acquisition: a new concept for consistent and accurate proteome analysis. Mol Cell Proteomics 11:O111.016717

35. Menzies K and Auwerx J (2013) An acetylation rheostat for the control of muscle energy homeostasis. J Mol Endocrinol 51:T101–13

36. LaBarge S, Migdal C, and Schenk S (2015) Is acetylation a metabolic rheostat

that regulates skeletal muscle insulin action? Mol Cells 38:297–303

37. Yucel N, Wang YX, Mai T, et al (2019) Glucose Metabolism Drives Histone Acetylation Landscape Transitions that Dictate Muscle Stem Cell Function. Cell Rep 27:3939–3955.e6

38. Wang Q, Zhang Y, Yang C, et al (2010) Acetylation of metabolic enzymes coordinates carbon source utilization and metabolic flux. Science 327:1004–1007

39. Castaño-Cerezo S, Bernal V, Post H, et al (2014) Protein acetylation affects acetate metabolism, motility and acid stress response in Escherichia coli. Mol Syst Biol 10:762

40. Mariño G, Pietrocola F, Eisenberg T, et al (2014) Regulation of autophagy by cytosolic acetyl-coenzyme A. Mol Cell 53:710–725

41. Chen R, Xu M, Nagati JS, et al (2015), The Acetate/ACSS2 Switch Regulates HIF-2 Stress Signaling in the Tumor Cell Microenvironment, http://dx.doi.org/10.1371/journal.pone.0116515

42. Gao X, Lin S-H, Ren F, et al (2016) Acetate functions as an epigenetic metabolite to promote lipid synthesis under hypoxia. Nat Commun 7:11960

43. Dittenhafer-Reed KE, Richards AL, Fan J, et al (2015) SIRT3 mediates multi-tissue coupling for metabolic fuel switching. Cell Metab 21:637–646

44. Ghanta S, Grossmann RE, and Brenner C (2013), Mitochondrial protein acetylation as a cell-intrinsic, evolutionary driver of fat storage: Chemical and metabolic logic of acetyl-lysine modifications, http://dx.doi.org/10.3109/10409238.2013.838204

45. Leonardi R, Rehg JE, Rock CO, et al (2010) Pantothenate kinase 1 is required to support the metabolic transition from the fed to the fasted state. PLoS One 5:e11107

46. White PJ, McGarrah RW, Grimsrud PA, et al (2018) The BCKDH Kinase and Phosphatase Integrate BCAA and Lipid Metabolism via Regulation of ATP-Citrate Lyase. Cell Metab 27:1281–1293.e7

47. White PJ, Mcgarrah RW, Grimsrud PA, et al (2018), Integration of BCAA and Lipid Metabolism by the BCKDH Kinase and Phosphatase, http://dx.doi.org/10.2337/db18-1874-p

48. Huang Z, Zhang M, Plec AA, et al (2018) ACSS2 promotes systemic fat storage and utilization through selective regulation of genes involved in lipid metabolism. Proc Natl Acad Sci U S A 115:E9499–E9506

49. Huang DW, Sherman BT, and Lempicki RA (2009), Systematic and integrative analysis of large gene lists using DAVID bioinformatics resources, http://dx.doi.org/10.1038/nprot.2008.211

50. Zhao S, Torres A, Henry RA, et al (2016) ATP-Citrate Lyase Controls a Glucose-to-Acetate Metabolic Switch. Cell Rep 17:1037–1052

51. Wagner GR and Hirschey MD (2014) Nonenzymatic protein acylation as a carbon stress regulated by sirtuin deacylases. Mol Cell 54:5–16

52. Tanner KG, Langer MR, and Denu JM (2000) Kinetic mechanism of human histone acetyltransferase P/CAF. Biochemistry 39:15652

53. Wagner GR and Mark Payne R (2013), Widespread and Enzyme-independentNϵ-Acetylation andNϵ-Succinylation of Proteins in the Chemical Conditions of the Mitochondrial Matrix, http://dx.doi.org/10.1074/jbc.m113.486753

54. Jiang G and Zhang BB (2003), Glucagon and regulation of glucose metabolism, http://dx.doi.org/10.1152/ajpendo.00492.2002

55. Mihaylova MM and Shaw RJ (2011) The AMPK signalling pathway coordinates cell growth, autophagy and metabolism. Nat Cell Biol 13:1016–1023

CHAPTER 4: CONCLUSIONS, ONGOING STUDIES, AND FUTURE DIRECTIONS

4.1 Overall conclusions from research

Posttranslational modifications of proteins control complex biological processes across the cell using a language of chemical modifications. Early proteomics profiles of acetylation across the cell highlighted acetylation on proteins involved in mitochondrial metabolism. Proteomics studies over the past decade have heavily focused on metabolic regulation of mitochondrial acetylation. More recent studies have demonstrated that lysine acetylation is a wide-spread and dynamic modification in the nucleus beyond histones, however many questions remain on the regulation and downstream effects. The goal of my Ph.D. research was to advance mass spectrometry assessment of chromatin, to assess the acetylation stoichiometry of chromatin proteins using data-independent acquisition mass spectrometry, and to determine the regulation of nuclear acetylation by metabolism and acetyl-CoA synthesis pathways.

The largest challenge to proteomic assessment of chromatin was the reduction of contamination from other subcellular compartments. The endoplasmic reticulum and mitochondria of the cell are attached to the nuclear envelope. Subcellular fractionation of chromatin requires removal of these attached subcellular compartments. Early proteomics studies of chromatin using up to 1M urea or stringent salt washes still contained only 40% of proteins from chromatin, with the majority of the sample containing other subcellular compartments ***(1, 2)***. I was able to use salt fractionation to remove the nuclear envelope, pellet chromatin, remove loosely bound proteins and separate chromatin-bound proteins from histones to increase chromatin coverage from 40% to 75% of the sample. Combining this method with offline prefractionation resulted in deep coverage of chromatin acetylation in a spectral library for follow-up data-independent acquisition (DIA) based acetylation stoichiometry assessment. Finally, I demonstrated the utility of a deep spectral library for DIA sample analysis. With a deep

spectral library, offline prefractionation of the experimental samples was not necessary when performing final DIA analysis. The main bottleneck in the depth of peptide identification is the generation of the spectral library. Utilizing subcellular fractionation in conjunction with DIA analysis allows for a single injection of chromatin to rival coverage of chromatin proteins in an offline prefractionation sample. Avoiding utilization of offline prefractionation reduces the variance in protein and peptide quantification, a pitfall of using offline prefractionation in quantitative mass spectrometry techniques, and also bypasses the obstacles of chromatographic draft of deuterated acetyl peptides during offline prefractionation.

My research provided a useful method for assessing the regulation of lysine acetylation within cellular organelles, in particular, the differences between enzymatic and nonenzymatic acetylation in the nucleus, cytoplasm, and mitochondria. I utilized this mass spectrometry method to quantitatively assess chromatin-associated protein and histone acetylation stoichiometry to examine the effects of acyl-CoA short chain synthetase family member 2 (ACSS2). This is the first assessment of changing acetylation moderating chromatin-bound proteins that regulate lipid metabolism. I demonstrated ACSS2 plays a specific role in signaling within the nucleus, partially through acetylation of proteins like histones and transcription factors. My results suggest a limited role in fatty acid synthesis in the fed state, but a wider role for ACSS2 in protein posttranslational modification, adaptation to fasting and coordinating intracellular and systemic fatty acid metabolism.

Assessment of chromatin lysine acetylation stoichiometry determined ACSS2 controlled acetylation on proteins regulating metabolism, metabolism of proteins and RNA, mRNA processing, protein posttranslational modifications, and vesicle-mediated transport. My findings confirmed ACSS2 had a role in regulating lipid metabolism, and acetylation of histones, RNA

processing, and transcription factors in response to dietary stress ***(3–5)***. I determined the absence of ACSS2 reduced mitochondrial acetylation in response to fasting in contrast to previous findings ***(6, 7)***. Previous studies have intimately linked mitochondrial metabolism and adaptation to fasting to increases in mitochondrial acetylation ***(6, 8, 9)***. Reduction in acetylation in the mitochondria is likely through an indirect mechanism or lack of signaling to the mitochondria in the absence of ACSS2. In conclusion, my data suggests that ACSS2 effects protein acetylation beyond histones through targeted acetyl-CoA synthesis. Others have proposed ACSS2 effects metabolism through passing acetyl-CoA to HATs at specific loci, functioning as a transcriptional co-activator to influence metabolism ***(10-12)***. I propose ACSS2 moderates protein acetylation more broadly on proteins in its local environment in a targeted mechanism to affect metabolism.

4.2 Ongoing Projects

Section 4.2 of this chapter focuses on current ongoing projects and additional future directions to aid in our understanding of the role of nuclear acetylation in metabolism. This section is broken into two subsections examining the regulation of nuclear acetylation by ACSS2, and its overlapping and mutually exclusive targets with ACLY to regulate fatty acid metabolism. The first subsection will focus on examining the role of ACSS2 in an ACLY-deficient tissue culture model to elucidate the mechanism of ACSS2 influence on nuclear protein acetylation. The second subsection will discuss the asses the role of ACLY on nuclear acetylation in a mouse model and implications on intracellular protein acetylation and systemic fatty acid metabolism.

4.2.1 Acly $^{-/-}$ Mefs ACSS2-dependent chromatin acetylation

Evidence from our study, as well as others has demonstrated ACSS2 is important for

regulating protein acetylation during fasting ***(5, 10)***. Our study demonstrated ACSS2-dependent changes in nuclear acetylation, but did not give direct evidence of a mechanism. Utilizing a mouse model for this study enabled us to investigate tissue-specific effects of the systemic loss of ACSS2 and metabolically perturb mice through fasting. However, this system is limited in the ability to assess the direct mechanism of ACSS2-dependent changes in protein acetylation. To address these gaps, a tissue culture model is needed. Previous studies indicated ACSS2 does not play an important role in metabolism or metabolic regulation in cell lines without hypoxia or extreme metabolic perturbations such as severe serum or glucose deprivation ***(4, 10–12)***. Cell lines are heavily glycolytic and depend on ACLY for a large portion of their acetyl-CoA synthesis from glucose rich media ***(13)***. These metabolic conditions pose significant challenges, including balancing sufficient metabolic stress and not inducing cell death. Therefore, we hypothesized an ACLY-deficient tissue culture system would better enable these studies. ACLY-deficient cells result in a switch from glucose to acetate based acetyl-CoA synthesis and ACSS2 is translocated to the nucleus upon the loss of ACLY.

I performed subcellular fractionation followed by acetylation stoichiometry analysis on ACLY-deficient mouse embryonic fibroblasts (MEFs) previously described ***(14)***. Wild type and *Acly*$^{-/-}$ cells were cultured in fresh DMEM with 10% dialyzed FBS and 1mM glucose for a 24 hour pre-treatment, before switching into either DMEM with 10% dialyzed FBS and 10 mM glucose or 100 μM glucose with acetate supplementation for 6 hours before harvesting. Cells were fractionated into chromatin and a cytoplasmic and mitochondrial fraction, as has been previously described ***(15)***.

In the absence of ACLY, low glucose with acetate supplementation resulted in higher levels of protein acetylation in the cytoplasm, mitochondria, and nucleus, possibly through an

ACSS2-dependent mechanism (Figure 4-1). Additionally, there were chromatin acetylation sites that were glucose-dependent in the absence of ACLY, suggesting an alternate mechanism of glucose-dependent acetylation (Figure 4-2B). There was also a subset of sites in all cellular compartments that were ACLY- and glucose-dependent (Figure 4-2A). The cytoplasm and mitochondria of the MEFs were affected to a higher degree, however limited chromatin protein yields in a cell line and media dependent manner in the *Acly*$^{-/-}$ MEFs with 10 mM glucose may indicate the 24-hour acetate deprivation pretreatment was too severe (Fig 4-3A, B). *Acly*$^{-/-}$ MEFs require exogenous acetate for viability, indicating a shorter period of pre-treatment or a metabolic labeling approach is needed ***(14)***. Protein level data also indicated the proteome in the absence of ACLY and acetate supplementation is altered in the conditions used, making it difficult to compare protein acetylation across conditions (Fig 4-3A, B).

QSSA analysis of the changes in acetylation showed nuclear protein acetylation on signaling pathways, metabolism of proteins, ribosomal proteins, and chromatin modifying enzymes including HATs and DNA nucleotide excision repair were enriched in WT cells with glucose (Figure 4-4A) ***(6)***. *Acly*$^{-/-}$ cells maintained acetylation on the metabolism of proteins pathway and ribosomal proteins with acetate supplementation, but this was lost completely in the *Acly*$^{-/-}$ cells without acetate. In the cytoplasm and mitochondria, metabolism, and specifically protein metabolism, were the only pathways highly enriched for higher levels of acetylation stoichiometry (Figure 4-4B). In the absence of ACLY, the metabolism of proteins was not enriched for acetylation, suggesting without acetate ACLY deficient cells were metabolizing proteins as a carbon source even in the presence of sufficient glucose. These results indicate acetate-driven nuclear protein acetylation in *Acly*$^{-/-}$ cells, which are a viable model for future studies on the mechanism of ACSS2-dependent acetylation.

Figure 4-1. Acetylation changes across subcellular compartments in *Acly*$^{-/-}$ MEFs and WT cells with altered levels of glucose and acetate.

A) Stoichiometry % difference plot of *Acly*$^{-/-}$ and WT MEFs in 10 mM glucose across subcellular compartments. Lines down magnitude of difference and stoichiometry of *Acly*$^{-/-}$ and WT cells. **B)** Stoichiometry % difference plot of *Acly*$^{-/-}$ MEFs in 10 mM glucose (Glucose) or 1 mM glucose with 100 μM acetate (Acetate) across subcellular compartments. Lines down magnitude of difference and stoichiometry of *Acly*$^{-/-}$ MEFs in 10 mM glucose (Glucose) or 1 mM glucose with 100 μM acetate (Acetate) (n = 3 each condition).

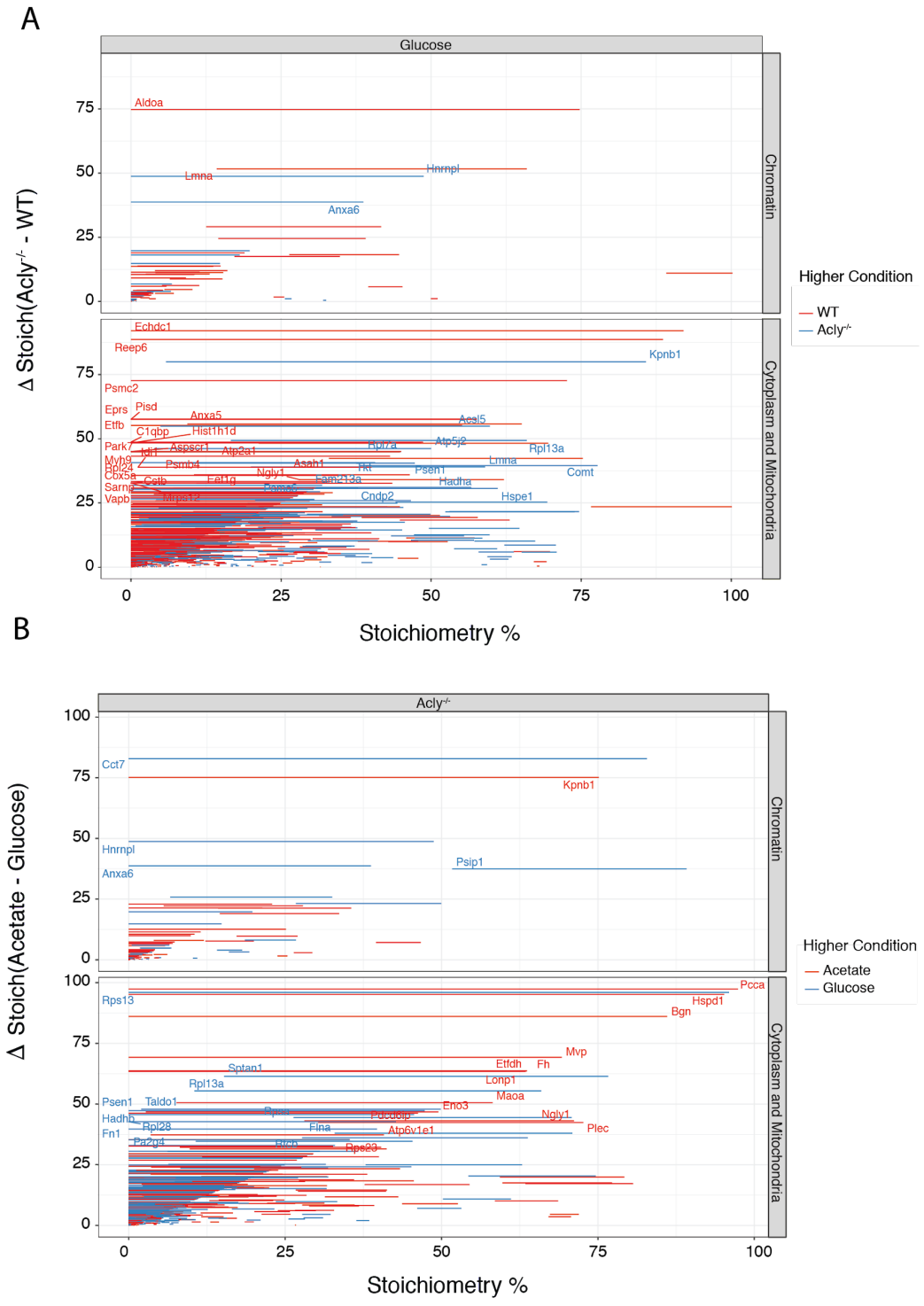
A
Glucose
Chromatin
Cytoplasm and Mitochondria
Δ Stoich(Acly-/- - WT)
Stoichiometry %
Higher Condition
WT
Acly-/-
Aldoa
Lmna
Hnrnpl
Anxa6
Echdc1
Reep6
Kpnb1
Psmc2
Eprs
Pisd
Etfb
Anxa5
C1qbp
Hist1h1d
Park7
Idh1
Aspscr1
Atp2a1
Rpl7a
Atp5j2
Rpl13a
Myh9
Rpl24
Psmb4
Aoah
Hrt
Lmna
Psen1
Comt
Cox5a
Setb
Eef1g
Fam213a
Hadha
Sarnp
Vapb
Cndp2
Hspe1
B
Acly-/-
Chromatin
Cytoplasm and Mitochondria
Δ Stoich(Acetate - Glucose)
Stoichiometry %
Higher Condition
Acetate
Glucose
Cct7
Kpnb1
Hnrnpl
Anxa6
Psip1
Pcca
Rps13
Hspd1
Bgn
Mvp
Etfdh
Fh
Sptan1
Rpl13a
Lonp1
Maoa
Psen1
Taldo1
Eno3
Hadhb
Ngly1
Fn1
Rpl28
Fina
Atp6v1e1
Plec
Pa2g4
Rps23

Figure 4-2. Volcano plot of acetylation changes across subcellular compartments in *Acly*$^{-/-}$ MEFs and WT cells with altered levels of glucose and acetate.

A) Stoichiometry % difference volcano plot of *Acly*$^{-/-}$ and WT MEFs in 10 mM glucose across subcellular compartments. P values calculated by one way ANOVA **B)** Stoichiometry % difference volcano plot of *Acly*$^{-/-}$ MEFs in 10 mM glucose (Glucose) or 1 mM glucose with 100 μM acetate (Acetate) across subcellular compartments. P values calculated by one way ANOVA (n = 3 each condition).

A

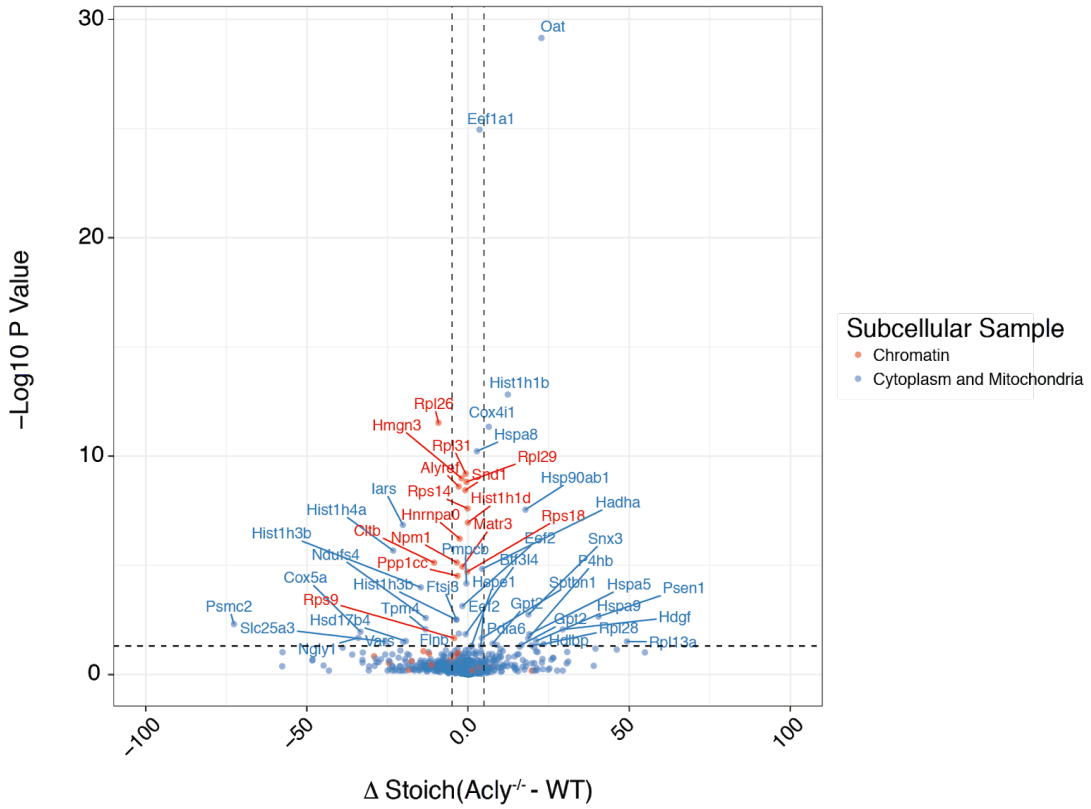
−Log10 P Value
30
20
10
0
−100
−50
0.0
50
100
Δ Stoich(Acly-/- - WT)
Oat
Eef1a1
Hist1h1b
Rpl26
Cox4i1
Hmgn3
Hspa8
Rpl31
Rpl29
Alyref
Srsf1
Hsp90ab1
Iars
Rps14
Hist1h1d
Hadha
Hist1h4a
Hnrnpa0
Matr3
Rps18
Hist1h3b
Cltb
Npm1
Pmpcb
Eef2
Snx3
Ndufs4
Ppp1cc
Rtf3l4
P4hb
Cox5a
Hist1h3b
Ftsj3
Hspa1
Sptbn1
Hspa5
Psen1
Psmc2
Rps9
Tpm4
Eef2
Gpi2
Hspa9
Hsd17b4
Slc25a3
Pdia6
Rpl28
Hdgf
Vars
Eif3i
Hdlbp
Rpl13a
Ngly1
Subcellular Sample
Chromatin
Cytoplasm and Mitochondria

B

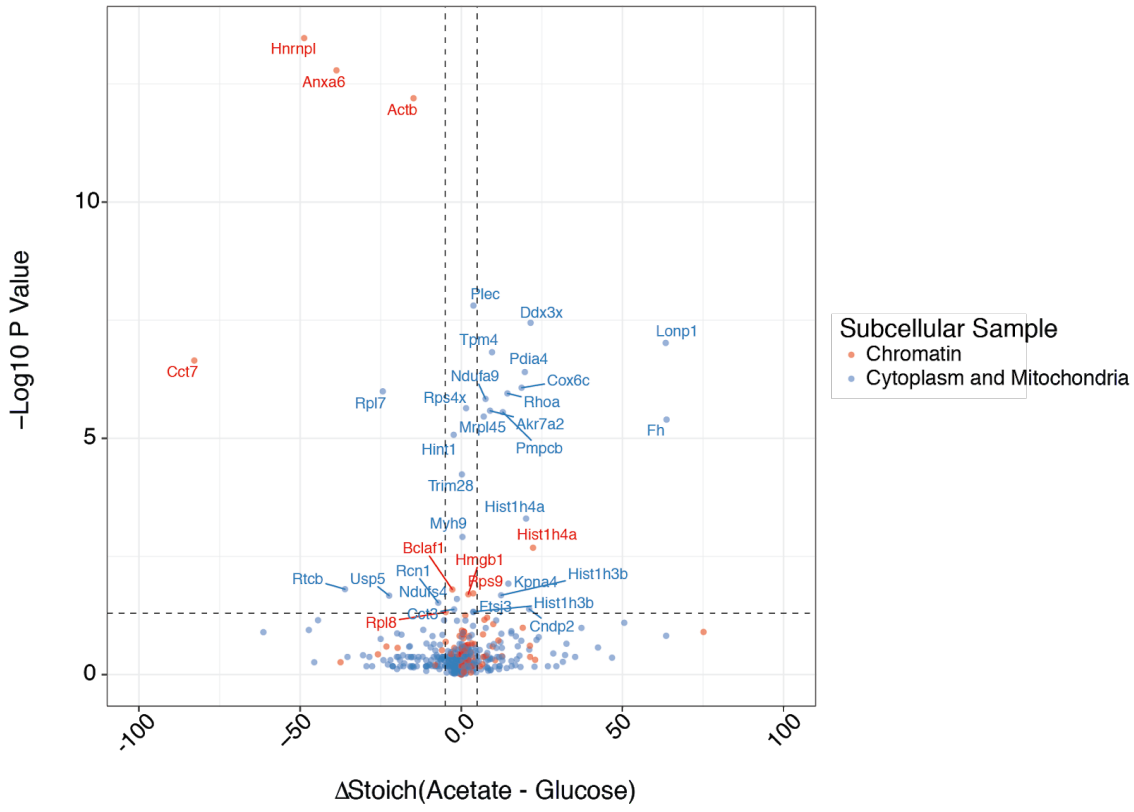
−Log10 P Value
10
5
0
-100
−50
0.0
50
100
ΔStoich(Acetate - Glucose)
Hnrnpl
Anxa6
Actb
Plec
Ddx3x
Lonp1
Tpm4
Pdia4
Cct7
Ndufa9
Cox6c
Rpl7
Rps4x
Rhoa
Mrpl45
Akr7a2
Fh
Hint1
Pmpcb
Trim28
Hist1h4a
Myh9
Hist1h4a
Bclaf1
Hmgb1
Rtcb
Usp5
Rcn1
Rps9
Kpna4
Hist1h3b
Ndufs4
Ftsj3
Hist1h3b
Rpl8
Cox5a
Cndp2
Subcellular Sample
Chromatin
Cytoplasm and Mitochondria

Figure 4-3. Volcano plot of protein abundance changes across subcellular compartments in *Acly*$^{-/-}$ MEFs and WT cells with altered levels of glucose and acetate.

A) Log2 fold change volcano plot of *Acly*$^{-/-}$ and WT MEFs protein abundances in 10 mM glucose across subcellular compartments. P values calculated by one way ANOVA **B)** Log2 fold change volcano plot of *Acly*$^{-/-}$ MEFs protein abundances in 10 mM glucose (Glucose) or 1 mM glucose with 100 μM acetate (Acetate) across subcellular compartments. P values calculated by one way ANOVA (n = 3 each condition).

A

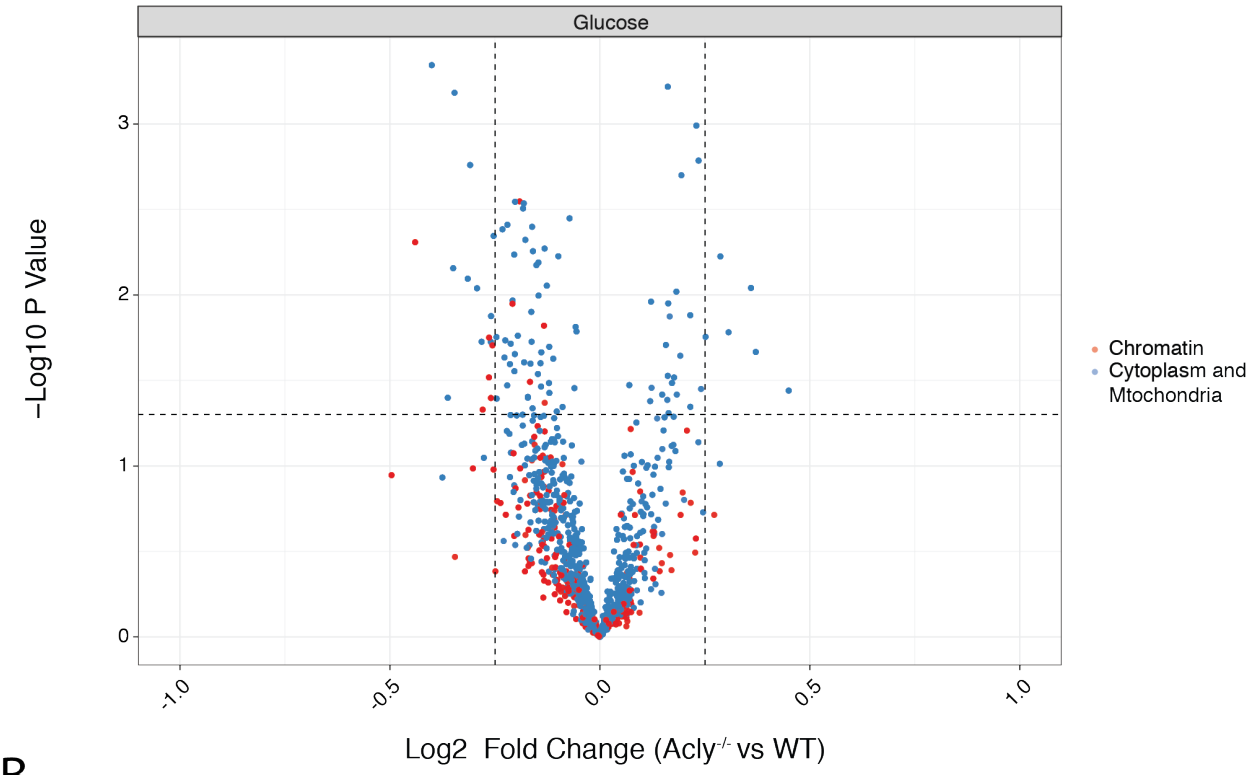
Glucose
−Log10 P Value
3
2
1
0
-1.0
-0.5
0.0
0.5
1.0
Log2 Fold Change (Acly-/- vs WT)
Chromatin
Cytoplasm and Mtochondria

B

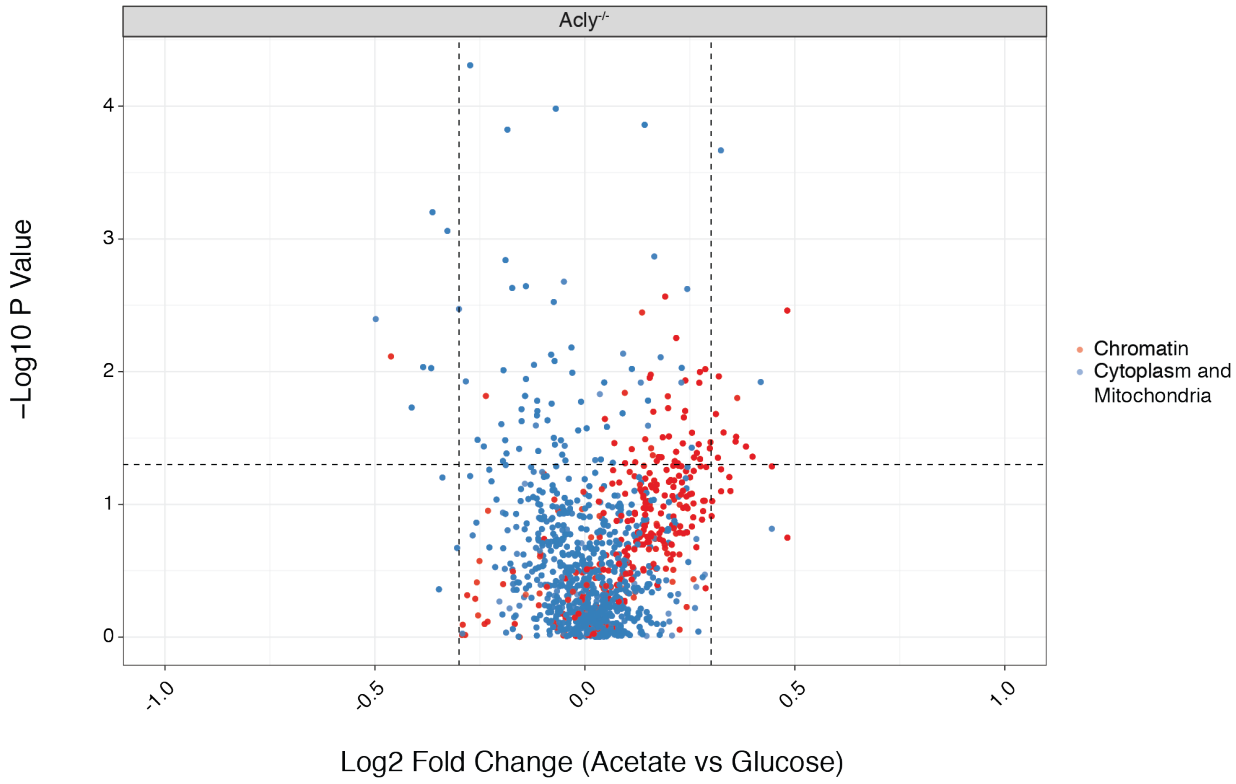
Acly-/-
−Log10 P Value
4
3
2
1
0
-1.0
-0.5
0.0
0.5
1.0
Log2 Fold Change (Acetate vs Glucose)
Chromatin
Cytoplasm and Mitochondria

Figure 4-4. Functional QSSA analysis of acetylation enrichment across pathways and subcellular compartments in *Acly*$^{-/-}$ MEFs and WT cells with altered levels of glucose and acetate.

A) QSSA plot of chromatin from WT MEFs acetylation stoichiometries in 10 mM glucose, *Acly*$^{-/-}$ MEFs acetylation stoichiometries in 10 mM glucose, and *Acly*$^{-/-}$ MEFs acetylation stoichiometries in 1 mM glucose and 100 μM acetate. **B)** QSSA plot of cytoplasmic and mitochondrial acetylation from WT MEFs acetylation stoichiometries in 10 mM glucose, *Acly*$^{-/-}$ MEFs acetylation stoichiometries in 10 mM glucose, and *Acly*$^{-/-}$ MEFs acetylation stoichiometries in 1 mM glucose and 100 μM acetate (n = 3 each condition).

A

Chromatin

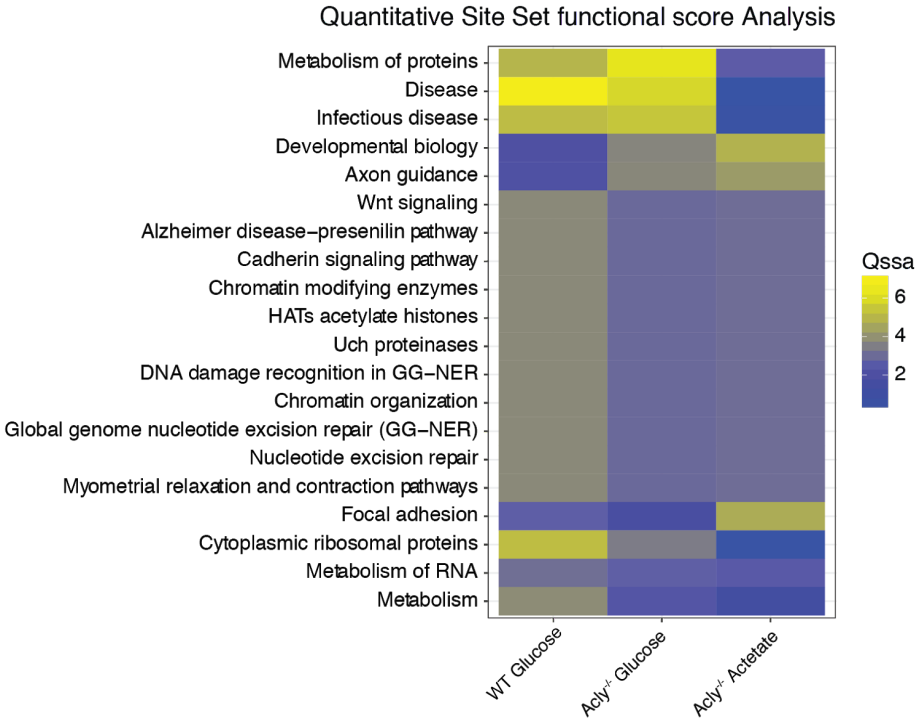

B

CYtoplasm and Mitochondria

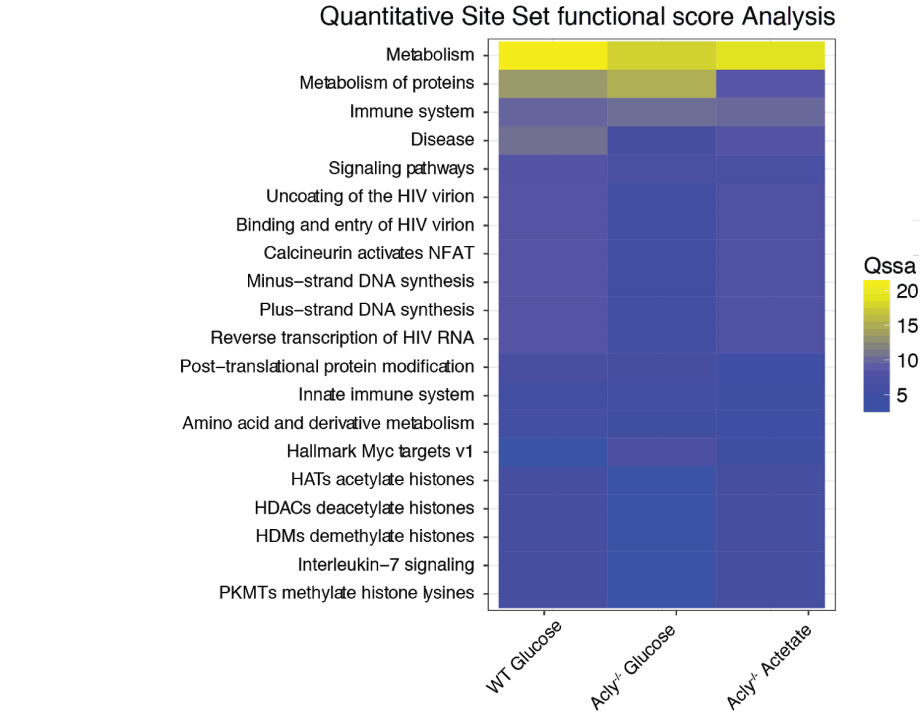

4.2.2 Elucidating the mechanism of ACSS2-dependent nuclear protein acetylation

The preliminary data with the *Acly*$^{-/-}$ MEFs suggests ACSS2-dependent acetylation can be driven in a tissue culture system even in the presence of glucose. However, 24-hour deprivation of acetate appears to be too long a period for viability. For future studies I propose to use a shorter pre-treatment and utilize metabolic labeling of acetate to provide direct evidence of ACSS2-dependent acetylation.

In these studies I propose the use of metabolically labeled acetate in a pulse-chase approach sampling over a time course. Metabolic perturbations of acetylation demonstrate pathway level trends, however these large scale responses to metabolic perturbations often mask the ability to determine primary versus secondary effects and our ability to assess mechanisms of acetylation directly. Metabolic labeling with a pulse-chase experimental approach allows for direct observation of acetate incorporation onto proteins. This experimental approach enables the determination of immediate versus cumulative effects over time from accumulation of labeled acetate into other metabolic pathways. Furthermore, analysis of amino acids and other metabolites with metabolomics can directly track and quantify incorporation of the metabolic label through indirect mechanisms.

This experimental approach can assess large scale changes in protein acetylation stoichiometry as well as ACSS2-directed changes in acetylation directly, providing a unique tool to probe upstream regulation of ACSS2 and ACLY-dependent acetylation and regulatory crosstalk. I propose to identify the acetyltransferase catalyzing ACSS2-dependent acetylation by using a small molecule inhibitor (A485) in the metabolically labeled pulse-chase experiment proposed above ***(16)***. I hypothesize p300/CBP is the acetyltransferase involved in ACSS2-

dependent acetylation for three reasons. First, our data in *Acss2*$^{-/-}$ animals showed loss of acetylation of p300/CBP histone substrates and downregulation of p300/CBP target genes. Secondly, previous studies have immunoprecipitated CBP with ACSS2 in both a tissue culture model and a mouse model ***(4, 17)***. Finally, profiles of p300/CBP substrates have found substrates broadly beyond histones ***(18)***.

Additionally, future studies may be undertaken in the *Acly*$^{-/-}$ tissue culture system to examine regulatory crosstalk affecting ACSS2 and ACLY, which have been found to be reciprocally regulated, using metabolically labeled acetate and glucose ***(14, 18, 19)***. However, one difficulty in this system will be the ability to synthesize acetate from the dehydrogenation of pyruvate when needed linking acetate synthesis to glucose ***(20)***. Metabolomics to quantify glucose derived acetate in this system will need to be undertaken. Kinase inhibitors of known regulators of ACLY (BDK, Akt) and screening for inhibition of the phosphorylation of ACSS2 can be used to determine upstream regulators of the "glucose-to-acetate" switch that has been previously described ***(14, 21, 22)***.

4.2.3 Liver ACLY-dependent chromatin acetylation

In our previous data, I demonstrated ACSS2 had limited effects on liver nuclear and mitochondrial acetylation, even during fasting which contrasts previous studies. This could indicate a defect in systemic fatty acid metabolism during fasting in the absence of ACSS2 ***(7)***. Alternatively, ACSS2 may not play an important role in liver metabolism even during fasting. Loss of ACLY in liver protects mice from steatosis, or fatty liver, on a high fat and high sugar diet ***(23)***. Studies looking at fatty liver and diabetes found altered branched chain amino acid metabolism dependent on the phosphorylation of ACLY by BDK, connecting branched chain

amino acid and fatty acid metabolism in liver ***(22)***.

To examine the role of ACLY in chromatin protein acetylation in the liver and its effect on metabolism we performed subcellular fractionation and acetylation stoichiometry assessment of chromatin. I used the methods previously described on $Acly^{Liver-/-}$ mice fed normal chow or a high fructose diet, which has been shown to induce fatty liver ***(15, 24)***. Chromatin protein acetylation was affected by the loss of ACLY and a high fructose diet (Figure 4-5, 4-6). QSSA analysis of chromatin protein acetylation demonstrated enrichment of acetylation on cell senescence, HDAC class III regulated signaling (sirtuin proteins), p38 mediated signaling, pathways as well as mRNA processing in wild type mice (Figure 4-7). Acetylation of cell senescence and cellular responses to stress and external stimuli remained high and relatively unchanged across conditions as seen in our $Acss2^{-/-}$ mouse model. In the absence of ACLY on a normal diet, acetylation HDAC class III regulated signaling (sirtuin proteins) and p38 mediated signaling pathways was lost. High fructose diet led to significantly altered acetylation on chromatin, with high levels of acetylation on IL-4 signaling pathway components and a reduction of acetylation of p38 mediated signaling, and HDAC class III regulated signaling (sirtuin proteins) pathways. In the absence of ACLY, acetylation on chromatin did not respond to the high fructose diet, suggesting the acetylation pattern driven by the high fructose diet results from ACLY-dependent synthesis of acetyl-CoA. Instead, in the absence of ACLY under high fructose conditions, the pattern of acetylation mirrors that of wild type mice on a chow diet, indicating these acetylation events are likely regulated through another mechanism, or compensation for the loss of ACLY through an alternative pathway such as ACSS2 has occurred and this pathway is fructose insensitive. There are two exceptions to this trend, p38 mediated signaling and mRNA were not restored to WT levels, suggesting this may be only an ACLY-dependent substrate for

acetylation. Additionally, DNA replication was enriched in acetylation in the absence of ACLY under a high fructose diet, suggesting this may be a specific substrate of an alternate pathway compensating for ACLY loss.

Figure 4-5. Liver chromatin acetylation changes in *Acly*$^{Liver-/-}$ and WT mice fed chow or high fructose diet.

Stoichiometry % difference plot of *Acly*$^{Liver-/-}$ and WT mice fed chow or high fructose diet. Lines represent a single acetylation site and start at a measured stoichiometry in one diet and end at the measured stoichiometry of the other diet. The length of line shows magnitude of difference of stoichiometry of *Acly*$^{Liver-/-}$ and WT mice. The color indicates which condition had higher acetylation stoichiometry, with sites higher in the chow diet in red and sites higher in the high fructose diet in blue.

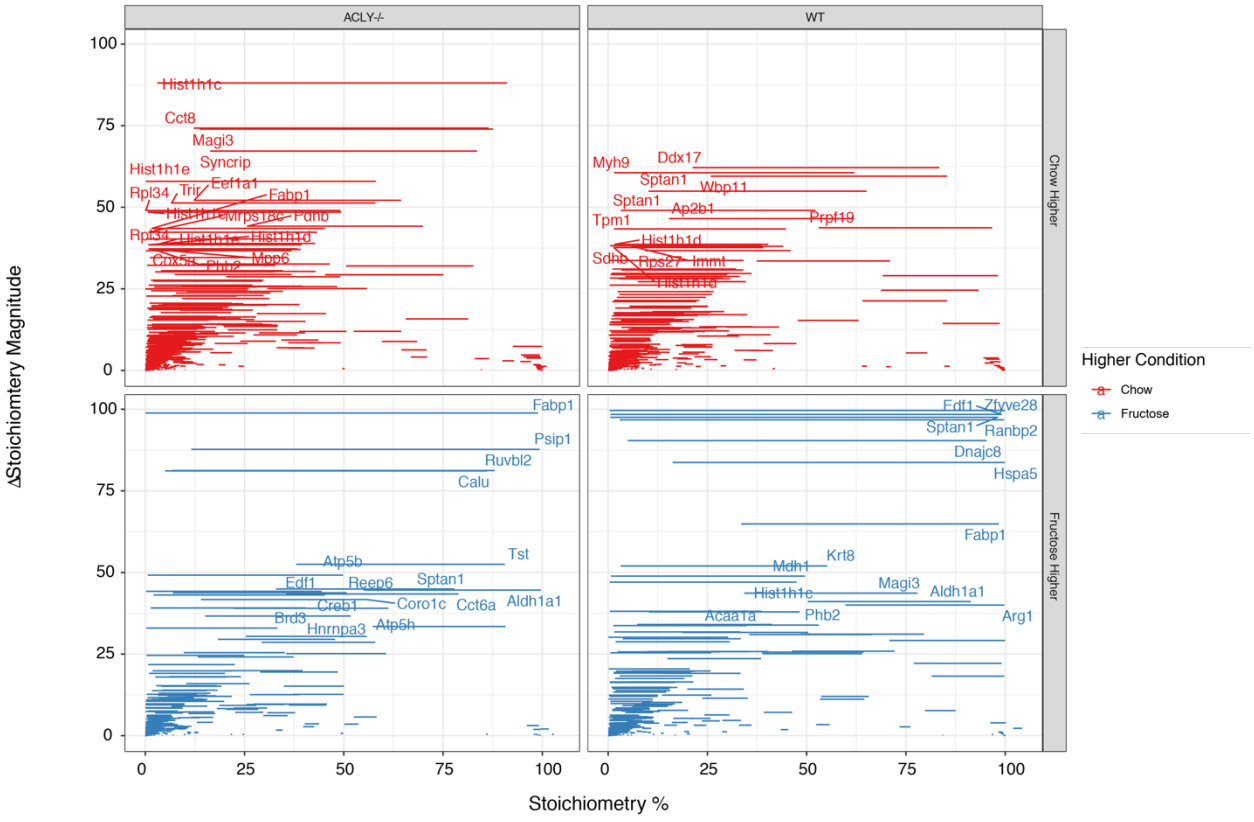

Figure 4-6. Significance of liver chromatin acetylation changes in *Acly*$^{Liver-/-}$ and WT mice fed chow or high fructose diet.

Stoichiometry % difference volcano plot of *Acly*$^{Liver-/-}$ and WT mice fed chow or high fructose diet. P values calculated by two way ANOVA.

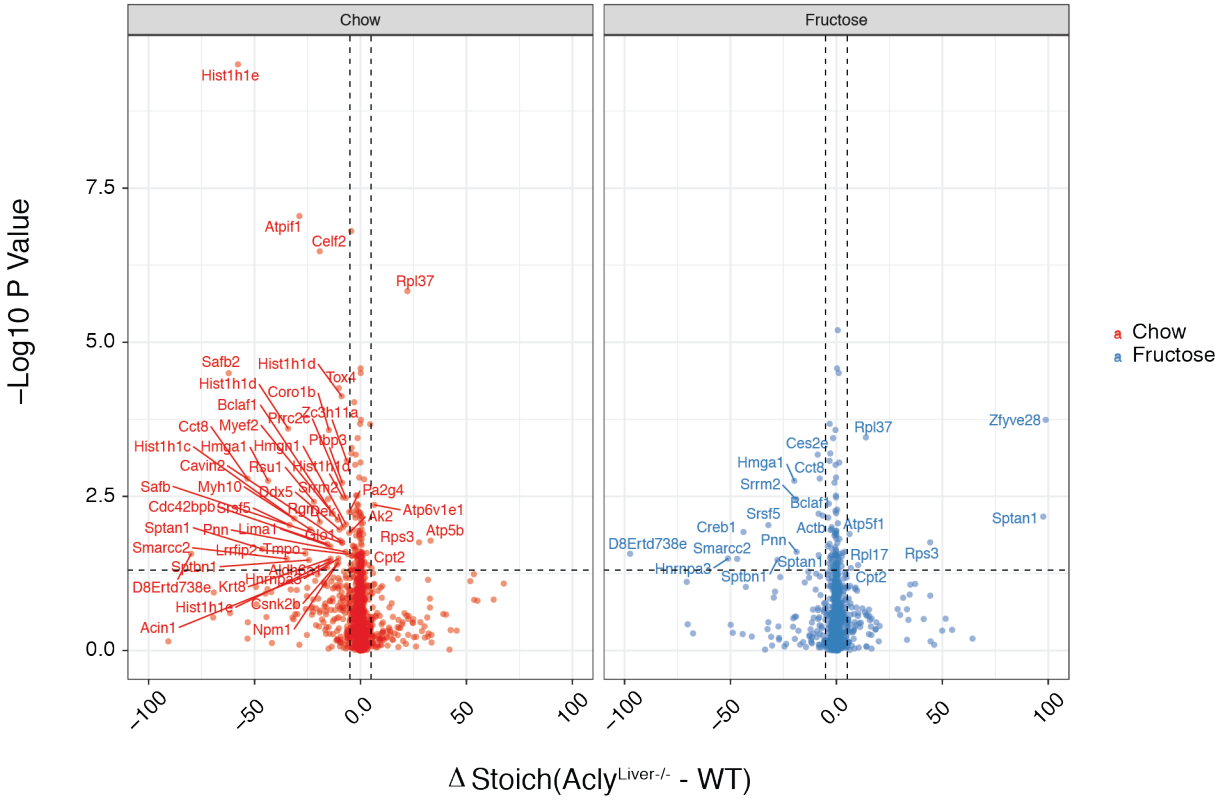

Figure 4-7. Functional QSSA analysis of acetylation enrichment across pathways Acly$^{Liver-/-}$ and WT mice fed chow or high fructose diet.

A) QSSA plot of chromatin from Acly$^{Liver-/-}$ and WT mice fed chow or high fructose diet. **B)** Log2 fold change volcano plot or protein abundances of Acly$^{Liver-/-}$ and WT mice fed chow or high fructose diet. P values calculated by two way ANOVA

A

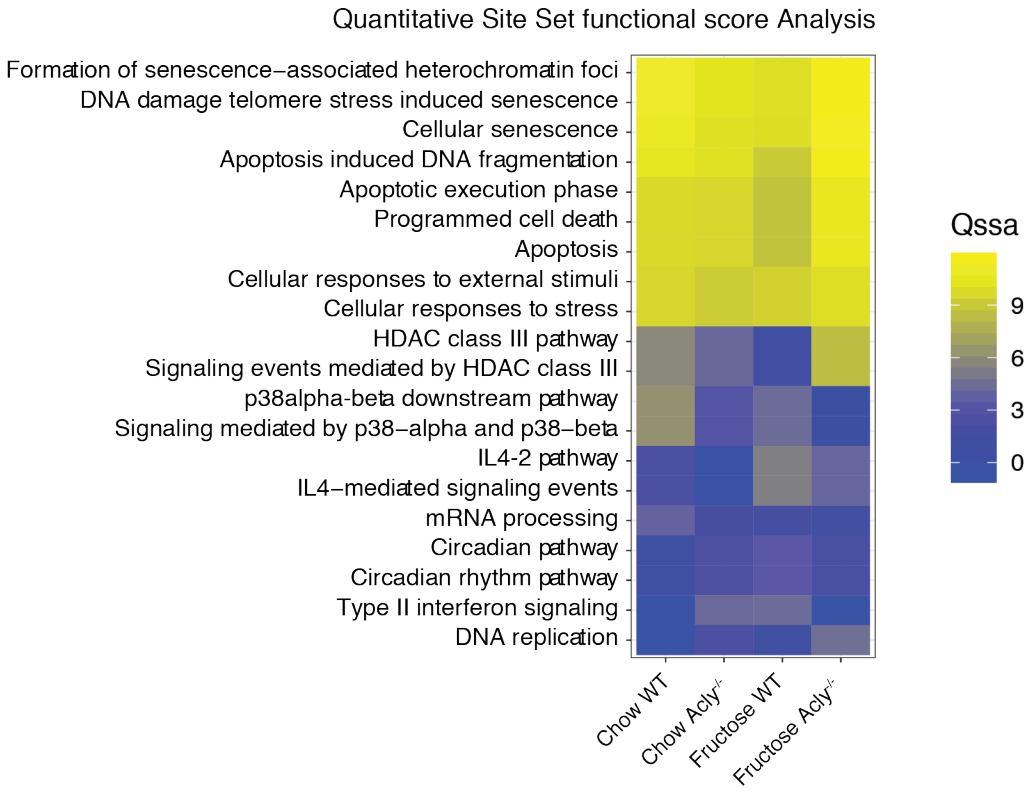
Quantitative Site Set functional score Analysis
Formation of senescence–associated heterochromatin foci
DNA damage telomere stress induced senescence
Cellular senescence
Apoptosis induced DNA fragmentation
Apoptotic execution phase
Programmed cell death
Apoptosis
Cellular responses to external stimuli
Cellular responses to stress
HDAC class III pathway
Signaling events mediated by HDAC class III
p38alpha-beta downstream pathway
Signaling mediated by p38–alpha and p38–beta
IL4-2 pathway
IL4–mediated signaling events
mRNA processing
Circadian pathway
Circadian rhythm pathway
Type II interferon signaling
DNA replication
Chow WT
Chow Acly-/-
Fructose WT
Fructose Acly-/-
Qssa
9
6
3
0

B

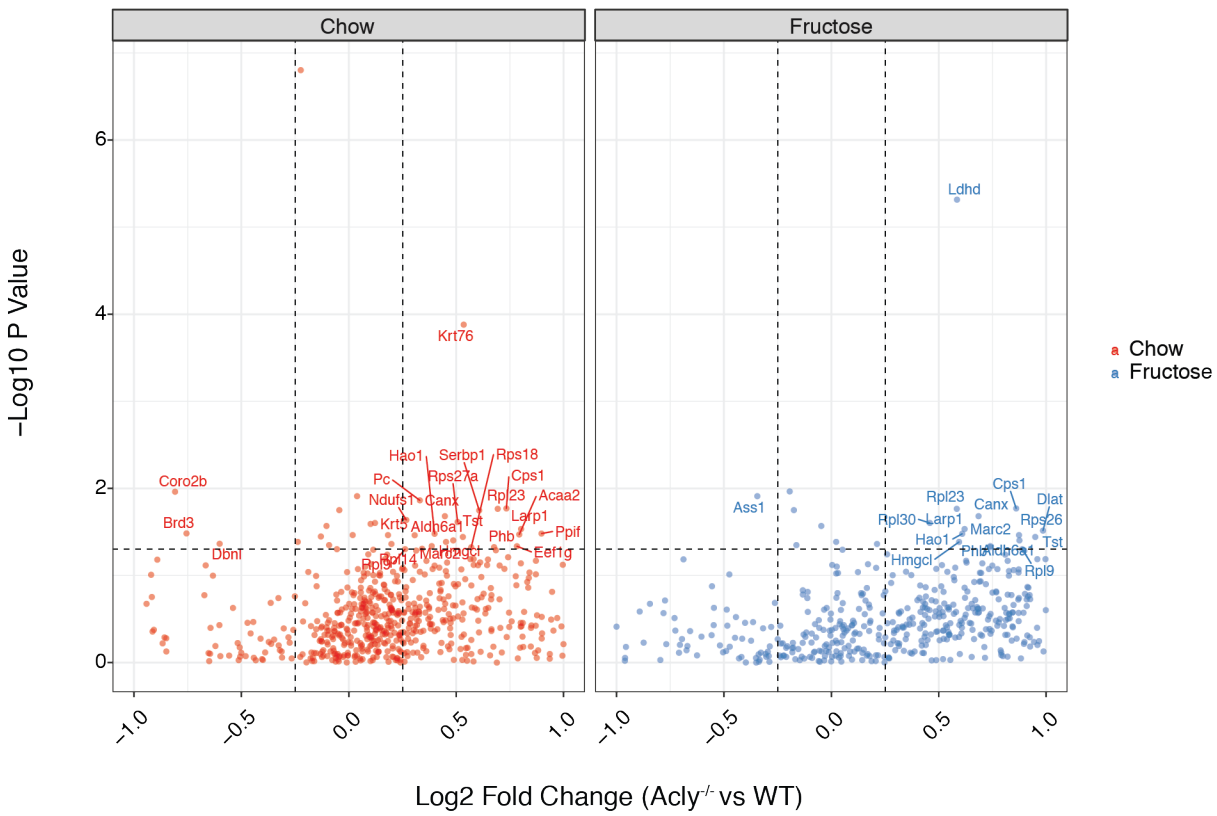
Chow
Fructose
−Log10 P Value
6
4
2
0
Krt76
Hao1
Serbp1
Rps18
Coro2b
Pc
Rps27a
Cps1
Ndufs1
Canx
Rpl23
Acaa2
Brd3
Krt5
Aldh6a1
Tst
Larp1
Ppif
Phb
Ddnt
Marh2gc1
Eef1g
Rpl9
Rpl14
Ass1
Ldhd
Cps1
Rpl23
Canx
Dlat
Rpl30
Larp1
Marc2
Rps26
Hao1
Tst
Hmgcl
Aldh6a1
Rpl9
−1.0
−0.5
0.0
0.5
1.0
Log2 Fold Change (Acly-/- vs WT)
Chow
Fructose

4.2.4 Liver ACLY-dependent mitochondrial acetylation

I hypothesize based on these results ACSS2 reduced liver mitochondrial acetylation through a systematic alteration of metabolism rather than an intracellular mechanism. In contrast ACLY affects acetylation of proteins through an intracellular mechanism. I hypothesize ACLY mediates nuclear, cytoplasmic, and mitochondrial metabolic crosstalk in liver based upon previous studies and the direct relationship ACLY has with mitochondrial metabolism through generation of citrate ***(22)***. I propose to assess acetylation stoichiometry in $Acly^{Liver\text{-}/\text{-}}$ mice fed normal chow or a high fructose diet in other subcellular compartments. I hypothesize in the absence of ACLY mitochondrial metabolism and protein acetylation will be unaffected by the high fructose diet. The observed alterations in nuclear protein acetylation and likely mitochondrial acetylation may play a role in blocking fatty acid synthesis and steatosis in $Acly^{Liver\text{-}/\text{-}}$ mice.

4.3 Impact

Metabolism and protein acetylation have been intimately tied in the mitochondria, however the relationship of metabolism and protein acetylation in other subcellular compartments has been poorly understood. Early studies looking at metabolic regulation of protein acetylation outside of the mitochondria focused on histones proteins, which are highly acetylated. These studies found histone acetylation to be dynamically regulated by metabolism, however the mechanism of metabolic influence on histone acetylation has been under active investigation and debate. The profiling of ACSS2- and ACLY-dependent acetylation in the nucleus demonstrates metabolism influences chromatin proteins broadly rather than only on histones. Furthermore, these findings indicate acetyl-CoA synthesis pathways influence protein

acetylation of proteins in their local environment rather than as a loci-specific transcriptional co-activator. Chromatin modifications more broadly and their links to metabolism are of interest to understanding how metabolism influences gene expression and other metabolic pathways connected to important cofactors may operate through a similar mechanism.

4.4 References

1. Monte E, Chen H, Kolmakova M, et al (2012) Quantitative analysis of chromatin proteomes in disease. J Vis Exp

2. Torrente MP, Zee BM, Young NL, et al (2011) Proteomic interrogation of human chromatin. PLoS One 6:e24747

3. Mariño G, Pietrocola F, Eisenberg T, et al (2014) Regulation of autophagy by cytosolic acetyl-coenzyme A. Mol Cell 53:710–725

4. Chen R, Xu M, Nagati JS, et al (2015), The Acetate/ACSS2 Switch Regulates HIF-2 Stress Signaling in the Tumor Cell Microenvironment, http://dx.doi.org/10.1371/journal.pone.0116515

5. Gao X, Lin S-H, Ren F, et al (2016) Acetate functions as an epigenetic metabolite to promote lipid synthesis under hypoxia. Nat Commun 7:11960

6. Hebert AS, Dittenhafer-Reed KE, Yu W, et al (2013) Calorie restriction and SIRT3 trigger global reprogramming of the mitochondrial protein acetylome. Mol Cell 49:186–199

7. Huang Z, Zhang M, Plec AA, et al (2018) ACSS2 promotes systemic fat storage and utilization through selective regulation of genes involved in lipid metabolism. Proc Natl Acad Sci U S A 115:E9499–E9506

8. Dittenhafer-Reed KE, Richards AL, Fan J, et al (2015) SIRT3 mediates multi-tissue coupling for metabolic fuel switching. Cell Metab 21:637–646

9. Ghanta S, Grossmann RE, and Brenner C (2013), Mitochondrial protein acetylation as a cell-intrinsic, evolutionary driver of fat storage: Chemical and metabolic logic of acetyl-lysine modifications, http://dx.doi.org/10.3109/10409238.2013.838204

10. Bulusu V, Tumanov S, Michalopoulou E, et al (2017) Acetate Recapturing by Nuclear Acetyl-CoA Synthetase 2 Prevents Loss of Histone Acetylation during Oxygen and Serum Limitation. Cell Rep 18:647–658

11. Schug ZT, Peck B, Jones DT, et al (2015) Acetyl-CoA synthetase 2 promotes acetate utilization and maintains cancer cell growth under metabolic stress. Cancer Cell 27:57–71

12. Chen R, Xu M, Nagati J, et al (2017) Coordinate regulation of stress signaling and epigenetic events by Acss2 and HIF-2 in cancer cells. PLoS One 12:e0190241

13. Wellen KE, Hatzivassiliou G, Sachdeva UM, et al (2009) ATP-citrate lyase links cellular metabolism to histone acetylation. Science 324:1076–1080

14. Zhao S, Torres A, Henry RA, et al (2016) ATP-Citrate Lyase Controls a Glucose-to-Acetate Metabolic Switch. Cell Rep 17:1037–1052

15. Lindahl AJ, Lawton AJ, Baeza J, et al (2019) Site-Specific Lysine Acetylation Stoichiometry Across Subcellular Compartments. Methods Mol Biol 1983:79–106

16. Lasko LM, Jakob CG, Edalji RP, et al (2017) Discovery of a selective catalytic p300/CBP inhibitor that targets lineage-specific tumours. Nature 550:128–132

17. Mews P, Donahue G, Drake AM, et al (2017) Acetyl-CoA synthetase regulates histone acetylation and hippocampal memory. Nature 546:381–386

18. Weinert BT, Narita T, Satpathy S, et al (2018) Time-Resolved Analysis Reveals Rapid Dynamics and Broad Scope of the CBP/p300 Acetylome. Cell 174:231–244.e12

19. Sivanand S, Rhoades S, Jiang Q, et al (2017) Nuclear Acetyl-CoA Production by ACLY Promotes Homologous Recombination. Mol Cell 67:252–265.e6

20. Liu X, Cooper DE, Cluntun AA, et al (2018) Acetate Production from Glucose

and Coupling to Mitochondrial Metabolism in Mammals. Cell 175:502–513.e13

21. Covarrubias AJ, Aksoylar HI, Yu J, et al (2016) Akt-mTORC1 signaling regulates Acly to integrate metabolic input to control of macrophage activation. Elife 5

22. White PJ, McGarrah RW, Grimsrud PA, et al (2018) The BCKDH Kinase and Phosphatase Integrate BCAA and Lipid Metabolism via Regulation of ATP-Citrate Lyase. Cell Metab 27:1281–1293.e7

23. Wang Q, Jiang L, Wang J, et al (2009) Abrogation of hepatic ATP-citrate lyase protects against fatty liver and ameliorates hyperglycemia in leptin receptor-deficient mice. Hepatology 49:1166–1175

24. Baeza J, Lawton AJ, Fan J, et al Quantifying dynamic protein acetylation using quantitative stoichiometry, http://dx.doi.org/10.1101/472530